Treatments and Analysis of C-sp^2 nanomaterials

Sergi Claramunt Ruiz

FACULTAT DE FÍSICA

Departament d'Electrònica

MEMÒRIA DE TESI DOCTORAL PRESENTADA PER OPTAR AL TÍTOL DE DOCTOR EN FÍSICA

Treatments and Analysis of C-sp^2 nanomaterials

Sergi Claramunt Ruiz

Directors: Dr. Albert Cirera Hernández

Dr. Albert Cornet Calveras

Barcelona, Setembre 2013

Programa de Doctorat en Física

Treatments and Analysis of C-sp^2 nanomaterials

Tesi que presenta Sergi Claramunt Ruiz

per optar al títol de Doctor per la Universitat de Barcelona

Directors de la Tesi:

Dr. Albert Cirera Hernández

Prof. Dr. Albert Cornet Calveras

Departament d'Electrònica

Grup de Micro-Nanotecnologies i Nanoscòpies per Dispositius Electrònics i Fotònics (MIND)

Institut de Nanociència i Nanotecnologia (IN^{2}UB)

A la meva Estrella Polar.

Contents

1. Introduction

The new carbon technology

Some time ago, someone said: “Optimists say we are entering a carbon age. Even pessimists argue only that the impact will be somewhat less”. This “someone” was the Nobel laureate Andre Gueim, that along his colleague Konstanin Novoselov, discovered graphene in 2004 [1]. This material, hidden in plain sight in graphite, is one of the lasts wonders of carbon. From buckyballs to carbon nanotubes, carbon has been revealed as a perfect platform for either study new types of physics [2] or for create new devices [3].

Applications of carbon nanostructures seem endless. Electronic researchers see these nanostructures as one of the ways to continue the Moore’s Law. In this sense, we are living exciting times. During the writing of this thesis has been just presented the first computer that use exclusively carbon nanotube based transistors [4]. Now, all the “potential” applications of these transistors are a reality. Although still there is work to do to make this kind of computers commercially available, the technology is not science fiction anymore.

In spite of all the good new, the reality is that the society hardly has been benefit of all the wonders of carbon nanomaterials. Carbon nanotubes and nanofibres have been used only in composite materials, like polymers or paints that take advantage of only few of all the superior properties of this material. Graphene applications has not even reached any commercial stage. This situation is because the scalable production process and implementation is not straightforward and even are not fully understood. For example, the properties and possible

applications of graphene were discovered using samples obtained from the mechanical cleavage of graphite [1], a hand-made technique that is impossible to scale to the industry. Because that, great efforts have been invested in the research of a scalable method to synthesise graphene at large scale. Up to no, is possible to obtain polycrystalline graphene sheets of meters square of area by chemical vapour deposition (CVD) [5,6], although its electrical properties may be impaired for this polycristanility. The chemical route has similar problems but at higher extent, as the material obtained is not even graphene but reduced graphene oxide (rGO) [7,8], a material with higher resistivity but easier to manipulate. Carbon nanotubes, in spite to have more history than graphene, also have their own problems. One of the main concerns is the difficulty to synthesise only one type of nanotubes, as usually there

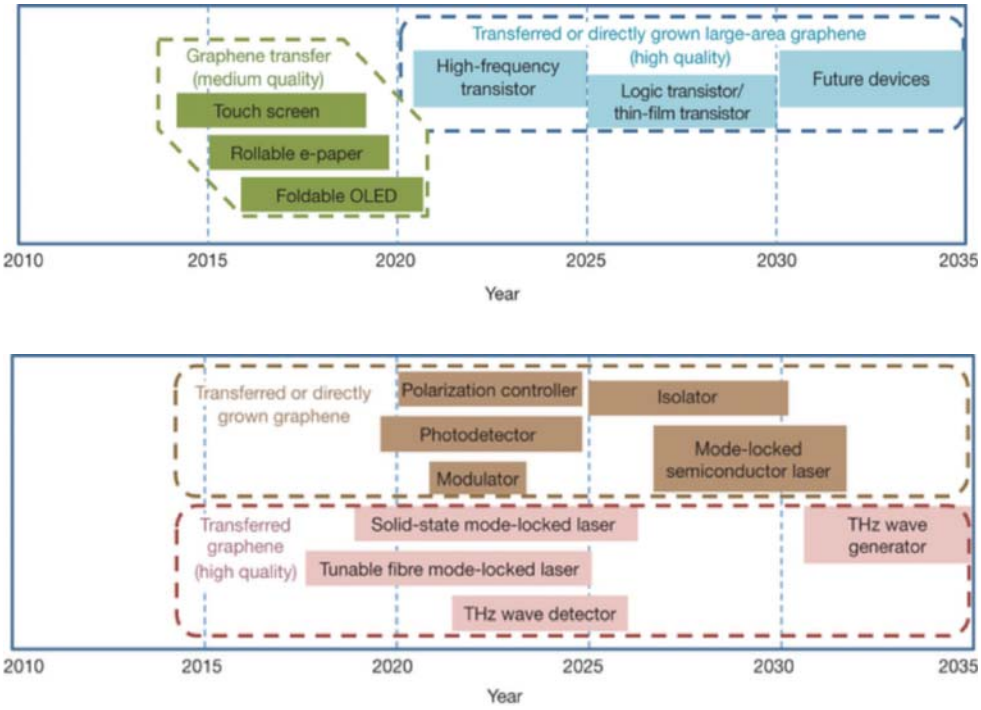

Figure 1. Future graphene based applications that could appear in the next years. Adapted from [9].

is a mix of metallic and semiconductor nanotubes.

The future applications of carbon are impressive. From biotechnology to gas sensors, one only need to see the list that Novoselov presented for graphene [9] and one can get an idea of what there is ahead (Fig. 1). But although the current industrial production of carbon nanostructures is ready for cover the supply for these new applications the truth is there is still a gap in the implementations of these nanostructures on the devices, and more research is needed in this aspect.

1.2. Motivations

The synthesis of carbon nanostructures is somewhat controlled and commercial products have been in the market for years. But now there is a necessity to use these new materials beyond laboratory applications and use it in commercial viable applications.

So, a part of the analysis of the new devices, there is a special interest in study the modification and integration processes of these carbon nanostructures, as well the study of its final quality after the integration process.

This thesis focuses in the analysis of these aspects in the area on gas sensing. It has been used three types of materials: carbon nanofibers, graphene oxide and reduced graphene oxide. The main objectives can be divided in two main areas:

- Carbon nanofibers

  - Detailed study of the surface properties evolution during a purification process: gas sensing applications relies on the properties of the surface of the nanomaterials. For this reason is important to know what changes experiments the carbon nanofibers during its purification process, both chemical and structural.
  - Decoration process: as is well known, carbon nanostructures like carbon nanotubes need to be decorated with metal nanoparticles in order to gain sensitivity and selectivity towards a given gas. In the case of carbon nanofibers we expect the same, and it will be studied its decoration process with noble metal nanoparticles.
  - Sensor fabrication: the integration of the carbon nanofibers over the metal pads of the sensor is a critical issue in order to obtain a good response signal. In this work has been applied a new deposition strategy with a modified electrospray process. Using this strategy, the responses of the new sensors (with bare nanofibers and decorated) have been studied.

- Graphene oxide and reduced Graphene Oxide

  - Detailed Raman analysis: graphene oxide and its reduction products are a promising candidate for generate graphene at industrial scale. In the other hand, Raman spectroscopy is the ideal technique for analysing it in a quality control process. In spite of that, still the Raman spectrum of this material is not fully understood. The Raman spectrum of graphene oxide and reduced graphene oxide is carefully studied and compared with models of other materials chemically similar in order to find a new approach for analyse its Raman spectrum.
  - Reduction process of graphene oxide: the reduction process of graphene oxide also has been studied using the new Raman approach developed early.

1.3. Outline of the thesis

I started my PhD in 2010 under the supervision of Dr.Albert Cirera Hernández and Dr. Albert Cornet Calveras, and the main findings and innovations developed during this research period are written down in this thesis that is divided in 6 chapters:

- Chapter 1: Introduction

  The current chapter, there is a small tease of the future of carbon-based applications as well the motivations for the realization of this thesis and its structure.

- Chapter 2: Properties of carbon materials

  In this chapter a state of the art of the carbon nanomaterials is presented. From its physical properties to its application in gas senors, the intention of this chapeter is to give to the reader a general view of the state of carbon nanomaterias until this date.

- Chapter 3: Experimental section

  Here will be discussed the different synthesis and modification processes of all the carbon nanomaterials used (carbon nanofibers, GO and rGO) as well the techniques used for its characterization. Moreover, the depostion techniques also will be discussed.

- Chapter 4: Carbon nanofibers

  This chapter will focus in the superficial analysis of the carbon nanofibers as well its metal decoration process. The effect of this decoration at the gas sensor signal is also discussed.

- Chapter 5: Analysis of GO and its reduction process

  In this chapter the Raman analysis of graphene oxide will be widely discussed. After that the reduction process of GO will be analysed.

- Chapter 6: Main conclusions and critic review

References

[1] K.S. Novoselov, a K. Geim, S. V Morozov, D. Jiang, Y. Zhang, S. V Dubonos, et al., Electric field effect in atomically thin carbon films., Science. 306 (2004) 666–9.

[2] K.S. Novoselov, Z. Jiang, Y. Zhang, S. V. Morozov, H.L. Stormer, U. Zeitler, et al., Room-Temperature Quantum Hall Effect in Graphene, Science (80-.). 315 (2007) 1379.

[3] Z. Sun, T. Hasan, F. Torrisi, D. Popa, G. Privitera, F. Wang, et al., Graphene Mode-Locked Ultrafast Laser, ACS Nano. 2 (2010) 803–810.

[4] M.M. Shulaker, G. Hilla, N. Patil, H. Wei, H.-Y. Chen, H.-S. Philips Wong, et al., Carbon nanotube computer, Nature. 501 (2013) 526–530.

[5] H. Yamaguchi, G. Eda, C. Mattevi, H. Kim, M. Chhowalla, Highly uniform 300 mm wafer-scale deposition of single and multilayered chemically derived graphene thin films., ACS Nano. 4 (2010) 524–8.

[6] M. Wang, S.K. Jang, W.J. Jang, M. Kim, S.Y. Park, S.W. Kim, et al., A Platform for Large-Scale Graphene Electronics – CVD Growth of Single-Layer Graphene on CVD-Grown Hexagonal Boron Nitride, Adv. Mater. 25 (2013) 2746–2752.

[7] H. Varela-Rizo, I. Rodriguez-Pastor, C. Merino, I. Martin-Gullon, Highly crystalline graphene oxide nano-platelets produced from helical-ribbon carbon nanofibers, Carbon N. Y. 48 (2010) 3640–3643.

[8] B. Martín-Medina, M.M. Velázquez, F. Rossella, V. Bellani, E. Diez, J.L.G. Fierro, et al., Functionalization of Reduced Graphite Oxide Sheets with a Zwitterionic Surfactant, ChemPhysChem. 13 (2012) 3682–3690.

[9] K.S. Novoselov, V.I. Fal'ko, L. Colombo, P.R. Gellert, M.G. Schwab, K. Kim, A roadmap for graphene, Nature. 490 (2012) 192–200.

2. Properties and applications of carbon nanomaterials

2.1 Characteristics of carbon nanostructures.

Carbon can be found in different arrangements, each one with its own and unique characteristics. In this way, generally, the carbon materials can be classified in graphite, diamond, fullerenes and amorphous carbon (Fig. 1). Both graphite and diamond are ordered structures and can be found in nature, but the atom arrangement is

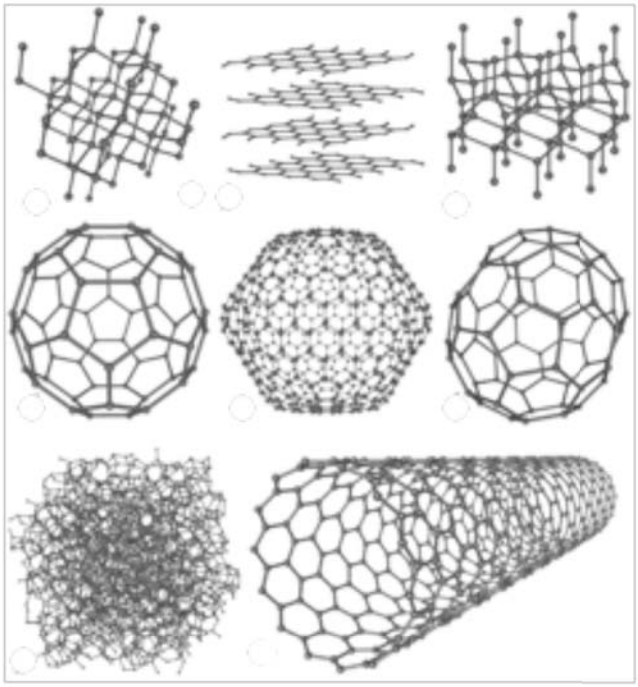

Fig. 1 Different allotropes of carbon

somewhat different. In diamond the bonding of the carbon atoms is because the sp^3 hybridization, meanwhile in graphite is because the sp^2 hybridization. So, this difference in the hybridization of the carbons atoms makes that the diamond structure is a purely 3D structure, meanwhile the graphite one is composed by 2D layer of carbon atoms

(graphene) stacked in an AB sequence as a result of a weak van der Walls interaction produced by a delocalized π-orbital [1]. On the other hand, the fullerenes are also ordered structures that include buckyballs (like C_{60}), carbon nanotubes or nanofibers. At last, there is the amorphous carbon, as like the name indicates are arrangements of carbon atoms with no crystal structure [2].

2.1.1 Graphite

Because its ordered structure, graphite has been an ideal laboratory for studying the properties of carbon materials and for the development of new carbon based nanomaterials.

A perfect graphite crystal has a layered structure with the atoms

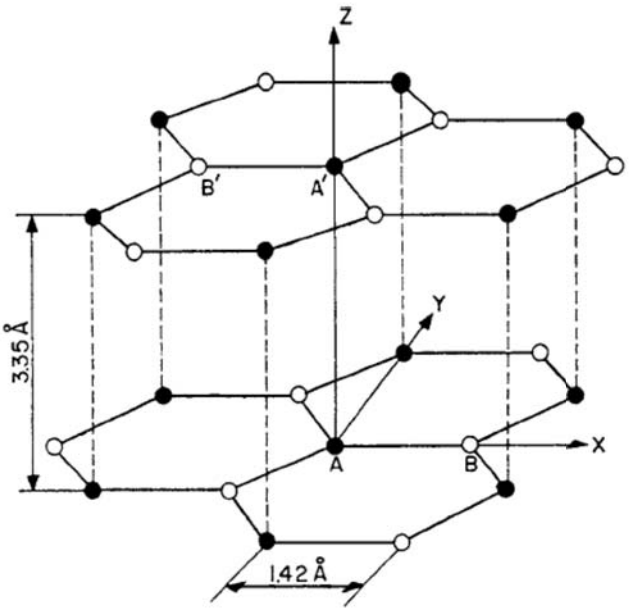

Fig. 2. Crystal structure of graphite. Adapted from [1].

of each layer forming a hexagonal structure (Fig 2), with a separation between layers of 3.35 Å [1]. This is because the bounds between carbon atoms are due a σ-bonding caused by the overlapping of three sp^2 hybridized orbitals (2s, $2p_x$ and $2p_y$) directed 120ºC apart on a layer plane. On the other hand, the $2p_z$ electron forms a delocalized orbital of π symmetry stabilizing the in-plane carbon bonding, that is stronger that the C-C covalent bond. In the c-direction, the carbon layers are bound by weak van der Waals forces, making graphite an anisotropic material that has different physical properties for in-plane and c-axis crystallographic directions.

Another possibility of bonding of the carbon atoms is the sp^3 hybridization. In this case, the four valence electrons are all assigned to a thetrahedally directed sp^3 orbital. In the case of diamond, all the carbon atoms are bonded with a sp^3 type bonding, forming a full 3D structure with different physical properties than the ones of graphite. For the case of graphite, the existence of sp^3 bonding indicates that the crystal is not perfect and there are some defects in the structure. These defects can be qualitatively measured by different techniques, although the technique where the amount of sp^2 and sp^3 bonds is more clearly seen is Raman spectroscopy. This was shown first by Tunstria and Koening [3], that found that the Raman spectra of graphite is composed basically by two peaks, one corresponding to the defects or the sp^3 hybridization (called D peak) and other corresponding to the sp^2 bounds, called G peak (Fig. 3a). This somewhat simple spectrum is due the crystal structure of graphite that only allows the vibrations of the Eg_2 mode that corresponds to the G peak in a perfect and infinite crystal structure, but the existence of defects allows a breathing mode that corresponds to the D peak (Fig. 3b). Is accepted that the intensity

(or area) of the G and D peaks give information about the amount of bounds of each type [3], being the ratio between the intensities the correspondence between the ratio of sp^2 and sp^3 bonds, or in other words, the grade of order of the sample. On the other side, there is also 2^{nd} order features around 2700 cm^{-1}, called 2D peak [4], that will be explained in detail in the following sections, but have a capital importance in graphene.

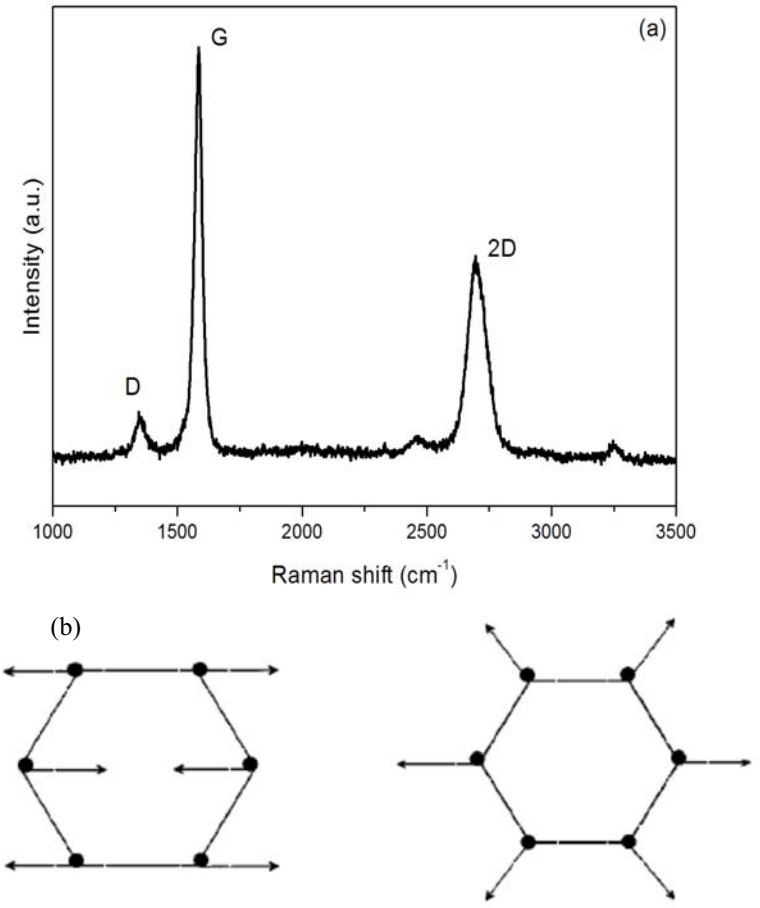

Fig. 3. (a) Raman spectrum of graphite and (b) vibratonial modes permitted in the crystal. Adapted from [2].

The structure of graphite is very interesting, as its layers are the building blocks of different carbon nanostructures depending of how is warped or configured (Fig. 4) [5]. So, these flat layers without any modification is the structure called graphene isolated by A.K Gueim and K. Novoloselov in 2004 [6]. If this layer is wrapped forming a cylinder, a carbon nanotube is created. This structure was first reported by Ijima in 1994 [7]. Also is possible to obtain carbon nanofibers, where the graphene layers are wrapped or placed with its basal plane not parallel with the axis of the tube [8]. Finally, the graphene layer can be closed on itself forming a sphere, called fullerenes [9]. Each nanostructure has its own properties and synthesis methods that will be reviewed in the following sections.

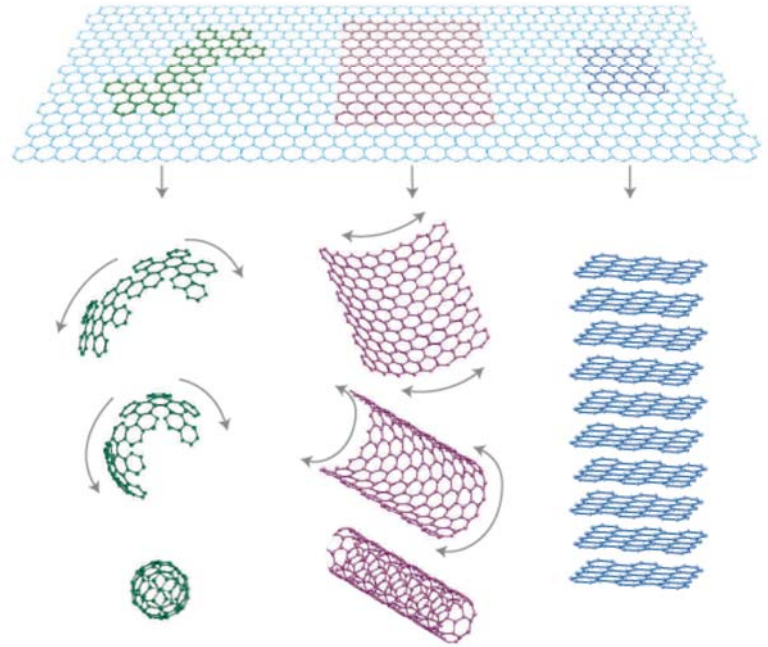

Fig. 4. Different structures obtained from a graphene layer. Adapted from [5].

2.1.2 Carbon nanotubes

Carbon nanotubes can be described as a wrapped graphene layer forming a cylinder. Can be composed by only one graphene layer [10], in this case called Single-Walled Carbon Nanotube (SWCNT) or also could be composed by two or more graphene layers [11], as in the case of Multi-Walled Carbon Nanotubes (MWCNT). Moreover, the ends of the SWCN have the possibility or being closed by a fullerene semisphere. Also is important the way the graphene layer is wrapped along the longitudinal axis, obtaining different configurations called

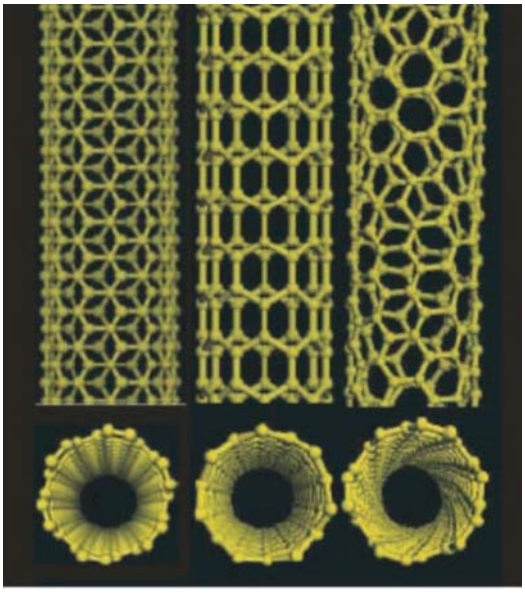

Fig. 5. Different configurations of carbon nanotubes. Adapted from [12].

armchair, zigzag or chiral [12] (Fig. 5). These configurations are important, as it will determine if the nanotube will behave as a metal or a semiconductor. For example, all the armchair type CNT will have a metallic behaviour.

Carbon nanotubes can be synthesised in different ways. In the first place Iijima discovered these nanostructures using the carbon-arc discharge method [7], but also laser ablation of carbon [13] or chemical vapour deposition [14] techniques has been used to obtain carbon nanotubes, being the last one the dominant technique to obtain industrial quantities of this material. The usual diameters of CNT can range from 2 nm to 50 nm, and in the case of MWCNT it can reach diameters of 100 nm.

The almost one-dimensional structure gives to carbon nanotubes interesting properties that differ from diamond or graphite. For example, for the case of metallic CNT the electronic transport occurs without scattering (ballistically) over long nanotube lengths [15]. This allows to these nanostructures transport high currents with no eating effects. The thermal conductivity also is greater in carbon nanotubes than diamond or the basal plane of graphite [16]. The mechanical characteristics also are impressive as it has been found that for the CNT with smaller diameters the Young Modulus is an order of magnitude higher than the one of steel [17].

2.1.3. Carbon nanofibers

Carbon nanofibers are also a nanostructure derived from graphene layers, but in contrast to carbon nanotubes [18,19], these layers have an orientation not parallel to the nanofiber axis . Because this, have been identified different families of carbon nanofibers [20]:

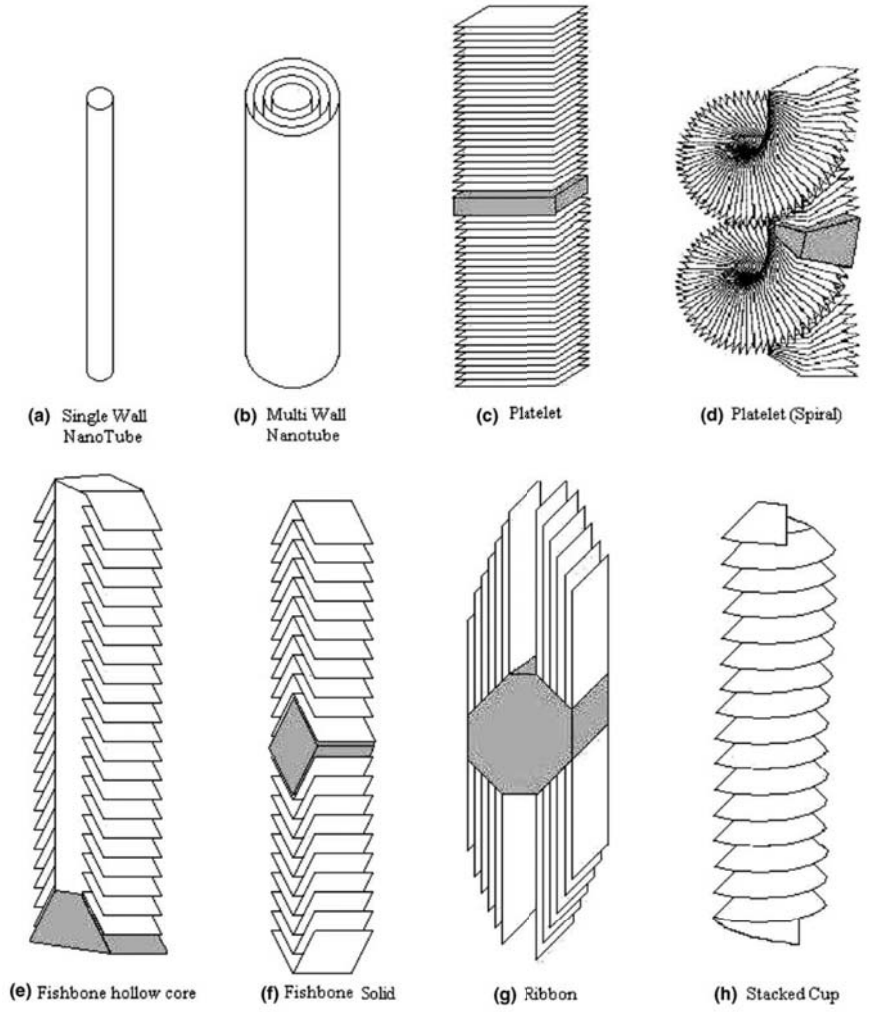

Fig. 6. Differnet types of wrapped carbon arrangements. Adapted from [20].

- Platelet: in this case, the graphene layers are stacked perpendicularly to the nanofiber axis. The seed particle can be found at the centre of the fibre, allowing the bidirectional

growing [21]. This kind of arrangement also permits the growing forming a spiral axis [22].

- Fishbone: in this family of carbon nanofibers, the graphene layers are inclined respect the axis of the nanofiber, similarly to a fishbone [23]. This structure can have a polygonal, squared or hexagonal section, and can have a hollow core or a solid one [24].
- Ribbon: in this kind of nanofibers the graphene layers are parallel to the nanofiber axis but without forming a cylinder [25].
- Stacked-cup: in this case, the graphene layers are rolled forming a spiral [20].

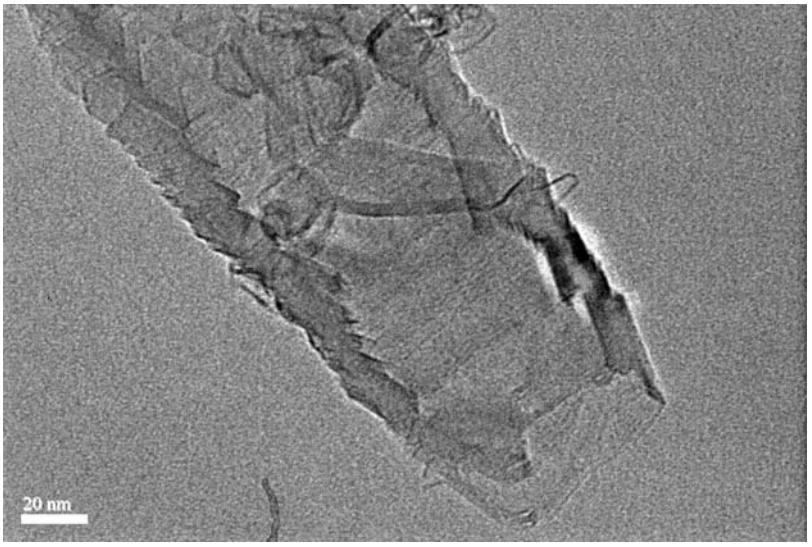

Fig. 7. TEM image of a stacked-cup carbon nanofiber obtained at the CCiTUB installations.

The last kind of nanofiber is maybe the most interesting. Its continuous structure, in contrast with the other family types, means that the structural properties depends mostly in the sp^2 bonds of the graphene layers, meanwhile the continuous nature of the spiral

promotes a very high conductivity. It is interesting to note that the idea of a continuous structure for the stacked-cup structure was not clear until recently. When were observed for first time by Endo et al [26] in 2002, the carbon nanofibers were described like truncated conical graphene layers stacked vertically, obtaining a carbon nanofibers with a hollow core. Successive characterizations and molecular simulations suggested that this vision may be incorrect, and the actual configuration of the graphene layers is a wrapped helix. Finally, Vera-Agulló et al [19] proved the actual structure of the stacked-cup carbon nanofibers using TEM, as they found some nanofibers with an unrolled graphitic layer coming out of its ends in a spiral fashion. Using these filaments as a reference they found that the measures of the hypothetical truncated cone obtained match perfectly with the diameters of the carbon nanofibers.

The physical properties of these nanofibers also are different to

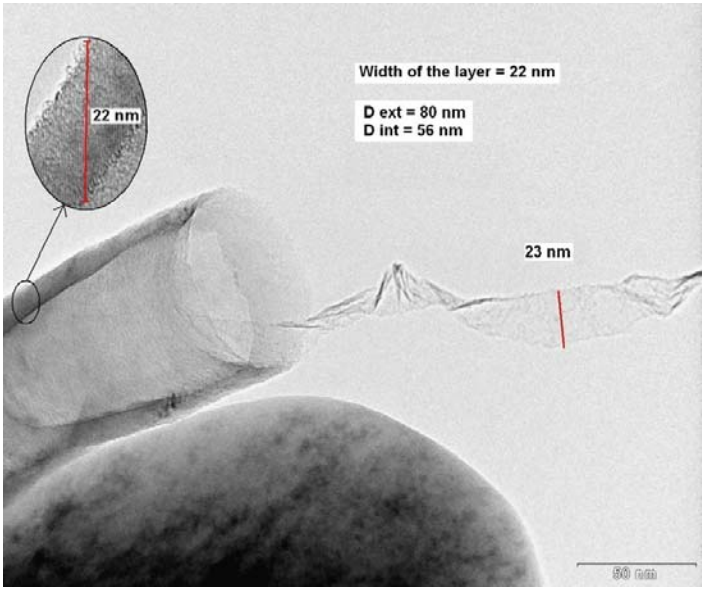

Fig. 8. Unrolled graphitic layer coming out of a stacked-cup carbon nanofiber. Adapted from [19].

graphite and carbon nanotubes. All these properties are summarised in the following table, adapted from M. H. Al-Saleh [18]:

Property	**VGCNF**	**SWCNT**	**MWCNT**	**CF**
Diameter (nm)	50-200	0.6-1.8	5-50	7300
Length (μm)	50-100			3200
Aspect ratio	250-2000	10-10000	100-10000	440
Density (g/cm^3)	2	~1.3[4]	~1.75	1.74
Thermal conductivity (W/mK)	1950	3000-6000	3000-6000	20
Electrical resistivity (Ωcm)	$1x10^{-4}$	$1x10^{-9}$-$1x10^{-4}$	$2x10^{-9}$-$1x10^{-4}$	$1.7x10^{-3}$
Tensile strength (GPa)	2.92	50-500	10-60	3.8
Tensile modulus (GPa)	240	1500	1000	227

Table 1. Several physical properties of different carbon nanostructures. Adapted from [18]. VGCNF: Vapour Grown Carbon Nanofibers. SWCNT: Singlewall Carbon Nanotubes. MWCNT: Multiwall Carbon Nanotubes. CF: Carbon Fibers.

These values are approximate, as in the case of the carbon nanofibers (especially of the vapour grown ones), the physical properties depend on the synthesis method and post-treatment techniques. In spite of that, usually these values fall between the properties of graphite and carbon nanotubes, that could be useful for different applications. As we will explain in detail later, the main

advantage of the carbon nanofibers is that the edges of the graphene layers are exposed, in contrast with carbon nanotubes that the only exposed edges are in the end of the tubes. This permits to the carbon nanofibers be more reactive to the environment [27], and for example, be useful for create composites materials and be more stable in solution [28].

2.1.4. Graphene

The building block of the different carbon materials and nanomaterials, graphene has been considered during years a theoretical entity [29]. Although it was clear that graphene layers composed graphite it was supposed that these layers were unstable independently and only can exist as part of a 3D structure. Andre Geim and Konstantin Novoselov [6] isolated a graphene layer for the first time in 2004 and were able to measure its electric characteristics. Quickly, the

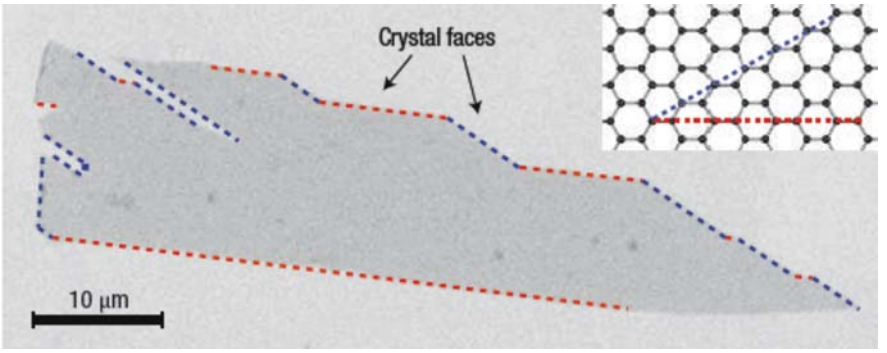

Fig. 9. SEM image of a graphene crystal. Adapted from [6].

scientific community became aware of the impressive potential of this

new material and the research papers involving graphene increased in the following years. Because the discovery of graphene, A. Geim and K. Novoselov were awarded with the Nobel Prize of Physics in 2010.

It is interesting to note that graphene crystals, and in general 2D extracted crystals, become stable due a gentle crumpling in the third dimension [30]. This crumpling results in the increase of elastic energy but suppresses the thermal vibrations, which above a given temperature can minimize the total free energy. Traditionally, graphene was obtained by micromechanical cleavage of bulk graphite [6], obtaining graphene crystallites up to 100μm and only 1 atom thick. This process is not perfect as leaves a very low quantity of perfect graphene crystals, making almost impossible to locate it in a $1cm^2$ substrate with techniques for studying atomically thin materials. Only because graphene is optically visible in a substrate of Si with a SiO_2 thickness of 300 nm this material has been discovered using standard optical methods. Another method that can be useful for locate and evaluate graphene crystallites is Raman spectroscopy. As it is mentioned in section 2.1.1, Raman spectrum of the different types of carbons (graphite, C_{60}, carbon nanotubes…) has similar features, and graphene is not an exception. But in this case, as graphene is an atom thick carbon layer, have some exceptional features. The most prominent one is that the intensity of the 2D peak around 2700 cm^{-1} is boosted and become more intense than the G peak [31]. This unique feature permits the direct identification of graphene among other carbon materials [32]. On the other hand, the shape of the 2D band also can identify the number of layers exactly . This also gives us a tool to differentiate the limit between that can be considered a 2D layer and a 3D structure. It is shown that the Raman spectra of graphene evolve to the graphite one

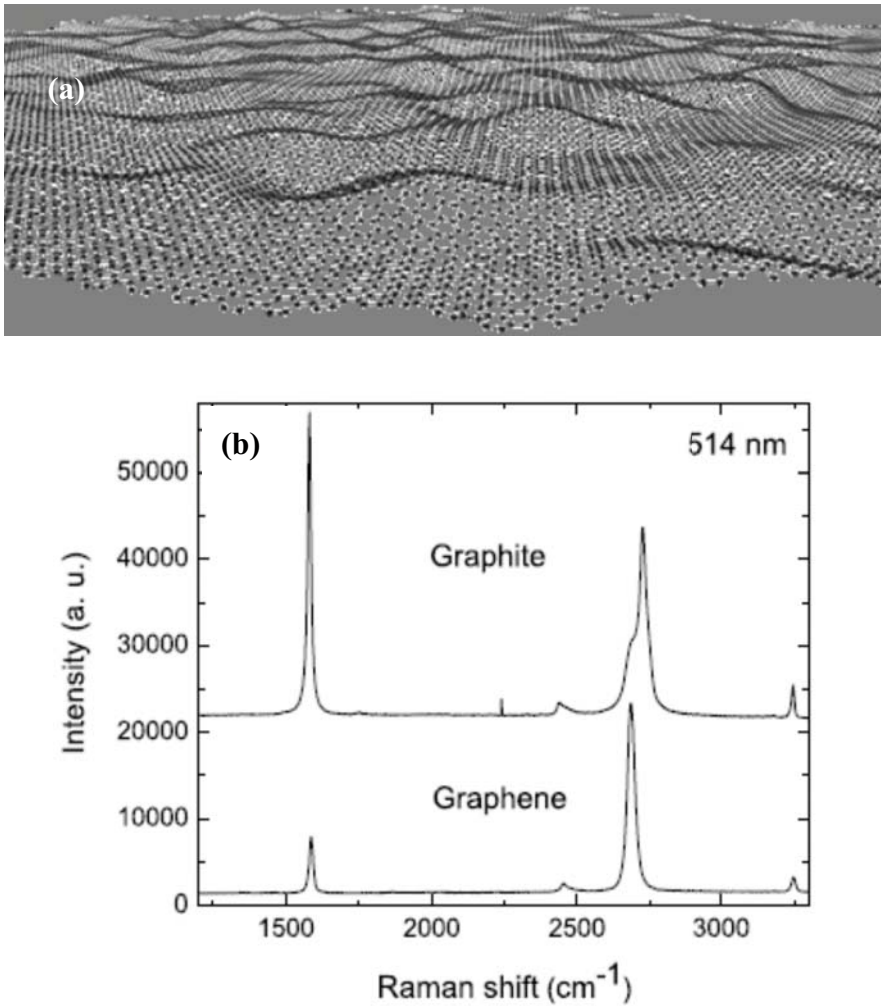

Figure 10. (a) Artistic representation of the crumpling of a isolated graphene layer. Adapted from [30] (b) Comparison between the graphite and graphene Raman spectrum. Adapted from [4].

when the number of layers is 10 or more. These results are in accordance with the calculations of Partpens et al. [33] that found that the electronic structure of graphene tends to the graphite electronic structure when the number of layers also is 10 or more, meaning that for graphene there is a precise limit where we can talk of a 2D crystal or a 3D structure.

The physical properties of graphene are outstanding, and could be used in a wide range of new applications. Like in the case of carbon nanotubes, the transport of electrons is ballistic, meaning that the electrons can move through the lattice structure of graphene without any opposition [34]. Another feature is because the layer of graphene is 1 atom thick the electrons movement is restricted in 2 dimensions, arising novel interesting properties like the anomalous Hall effect [35] or the Klein tunnelling [36,37]. On the other side, graphene is a prefect thermal conductor, being its thermal conductivity superior to graphite, diamond and also carbon nanotubes [38]. Mechanically, graphene also exhibits incredible properties [39]. The most impressive is that is a very hard material (harder than diamond) but at the same time very stretchable, being possible to stretch graphene up to 20% of its initial length. Graphene, although is one of the thinnest material ever made (1 atom thick) it absorbs up to 2.3 % of the incident light per graphene layer [40]. This make possible to seeing graphene with the naked eye in an air environment. Moreover, this visibility can be enhanced by depositing the graphene layer over a silicon substrate with a 300 nm thick silicon dioxide layer [5], creating an interference effect between these three layers (graphene, SiO_2 and Si) and changing the contrast and colours of the graphene, depending of the thickness of graphene and silicon dioxide layers.

2.1.5. Graphene oxide

Graphene oxide is, as the name suggest, oxidized graphene layers. Usually this material is obtained as a part of the synthesis of graphene layers during the oxidation of graphite [41]. After this process, the graphene layer has oxygen functional groups attached to the basal plane and the edges [42]. These groups can be carboxylic, carbonil, ketones, etc. Because this oxidation, graphene oxide have different properties than pure graphene. For example, the presence of functional groups makes graphene oxide soluble in different solvents and easier to manipulate in solution than pure graphene that needs the aid of surfactants in order to stabilize it [43]. In spite of that, the major drawback of graphene oxide is that is an insulator material in contrast of pure graphene [44], where ballistic transport occurs. That means that is needed a reduction process to eliminate the functional groups and recover the properties of graphene [45]. This process is not trivial, as the different reduction processes proposed until now either leaves some residual functional groups or damage the crystal structure of graphene [46]. This undesired result gives us a material similar to graphene called Reduced Graphene Oxide. Obviously, the electrical properties are dampened by these impurities. Although interestingly, it can be tuned depending of the grade of reduction applied [47].

2.2 Synthesis methods

2.2.1. Carbon nanotubes and carbon nanofibers

Carbon nanotubes (SWCNT and MWCNT) and carbon nanofibers can be synthesised by different methods. One of the first techniques used was the carbon-arc discharge method [7] or laser ablation method [13]. Using these synthesis techniques is possible to obtain carbon nanotubes with a very good crystalline quality, but the fraction of amorphous carbon is very high and is needed other processes in order to obtain the pure carbon nanomaterial. Moreover, the amount of material obtained is very low (only several grams) and is very expensive to produce.

On the other hand, techniques such the Chemical Vapour Deposition (CVD) [14] can avoid these drawbacks, as is possible to obtain CNT and CNF with good crystalline quality at industrial quantities and a very low amorphous carbon fraction. In this technique a catalyst in form of metal nanoparticle is usually needed, and depending on the conditions and on the nature of the catalyst is possible to obtain different types of CNT (singlewall, multiwall, different chirality) and different families of CNF (fishbone, stacked-cup, etc). It is possible to divide the CVD techniques in two categories: substrate method and floating catalyst.

- Substrate method

In this method, the metal catalyst is deposited over a substrate [48]. Then is placed inside a reactor where the carbon precursor is pumped in (usually hydrocarbon and CO) and the temperature is raised in order to decompose these carbon precursors. Between 500ºC and 1100ºC the carbon nanostructures can grow, as the decomposed carbon diffuse through the catalyst. The synthesis temperature affects the ratio of growing of the nanofibers [11]. At low temperatures the growing of the nanofibers is slow but controllable, without the formation of amorphous carbon. In contrast, at high temperature the ratio of deposition of carbon is faster being the possibility of the formation of amorphous carbon higher.

The advantage of this method is its versatility and the selection of the final product by changing the synthesis parameters like gas flow, temperature, type of metal catalyst… For example, using Fe as a catalyst we can obtain platelet type CNF at low temperatures [49–51], meanwhile at high temperatures ribbon CNF are obtained [24]. Moreover, changing the catalyst particle to Ni fishbone CNF are synthesised [52].

In spite of this versatility and the possibility to control the amorphous fraction of carbon, this technique produces very low quantity of nanofibers and is not possible to be transferred to the industry and a new method had to be envisioned in order to produce nanofibers at industrial quantities.

- Floating catalyst method

This method was designed to obtain nanofibers at industrial level and in a continuous way [53–55]. The main characteristic of this method is that the catalyst, instead to be deposited over a substrate, is introduced continuously in the reactor in the form of a precursor simultaneously with the carbon precursor and the gas carrier. Then the mixture move through the reactor. First, the catalytic particles are formed, and then the nanofibers are grown by a similar process than in the substrate method after the carbon precursor is decomposed. Finally, at the end of the reactor the fully grown carbon nanofibers are collected.

In the floating catalyst method the time of residence of the chemical components inside the reactor is shorter, meaning that the kinetic of the reactions has to be faster than in the case of the substrate method. In order to shorten the reaction time we need to increase the temperature that usually ranges from 800 ºC to 1200 ºC. This higher temperature will promote the incontrollable formation of amorphous carbon, which can be decreased by the addition of sulphur at the mixture [20].

Like in the substrate method, the floating catalyst method also is versatile in the morphologies obtained. For example, using a Fe precursor and a temperature around 725-825 ºC, it can be obtained good quality MWCNT [56]. Using CO or methane as a carbon precursor gives stacked-cup CNF independently of the catalyst precursor used [57].

2.2.2. Graphene

Graphene was first isolated by mechanical exfoliation using simply scoth tape [6]. Although the graphene flakes obtained are of very good quality and usually big enough for being detectable by optical microscopy (under the correct conditions), this method is prohibitive in cost terms if the objective is the fabrication of graphene based devices

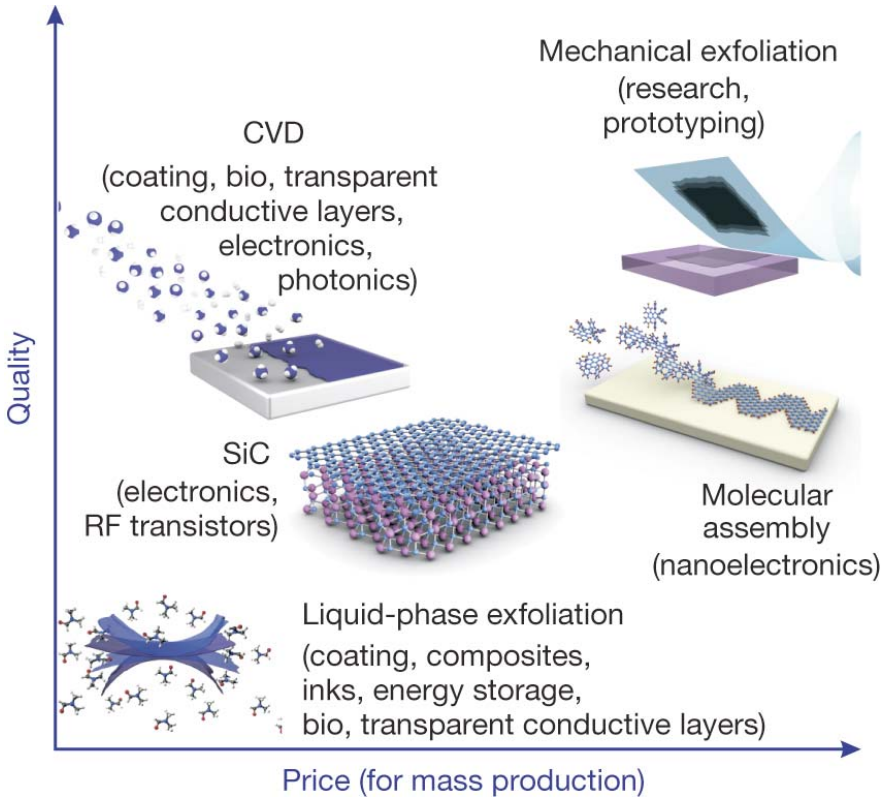

Figure 11. Different graphene síntesis methods depending its resulting quality and its price for mass production. Adapted from [57]

at industrial level [58]. So, new synthesis methods have to be envisioned and during the last years several new strategies have been proposed obtaining graphene of different quality with different costs.

- Liquid phase exfoliation

This method consists in to take advantage of the surface tension of a solvent in order to achieve the exfoliation of graphite through sonication [59,60]. This is possible because the strong interaction between the solvent and graphite reduce the exfoliation energy needed, reducing solvation. Also, the surface tension favours the increase of the total area of graphite crystallites.

Another strategy is the use of a graphite oxide route [61]. In this case graphite is strongly oxidized using sulphuric or nitric acids [62,63]. Then, as the oxygen is intercalated between graphene layers, then the graphene material can be obtained by sonication. This material then needs to be reduced to recover the properties of graphene, although it has been proved very difficult to eleminate all the oxygen, obtaining always reduced graphene oxide.

The two strategies end up with a solution of graphene/graphene oxide flakes that has to be processed (centrifugation, filtration…) in order to purify the material and be ready to use for the fabrication of coatings or composites.

- Thermal exfoliation

This case is a variation, or a continuation, of the liquid phase exfoliation. After graphite is being intercalated either by oxygen functional groups (by an oxidation process) or small molecules, instead of using a sonication process to break the graphene flakes a thermal-

shock is used. By this way, is achieved at the same time the exfoliation and the reduction [64].

- Chemical vapour deposition

With this technique is possible to synthesise continuous polycrystalline graphene sheets over different substrates [65,66]. Although the process is relatively expensive as it is needed high temperatures (around 1000ºC) to achieve the correct synthesis, the quality of the graphene films obtained and the possibility to cover large areas proves that CVD is a potential candidate for the industrial synthesis of graphene. Moreover, it have been achieved the transfer of the graphene from the original metallic surfaces to other kind of substrates [67,68], like glass or polymer. Moreover, this transfer process have been adapted to a roll-to-roll process [69], making the industrial fabrication of transparent electrodes or coatings a reality.

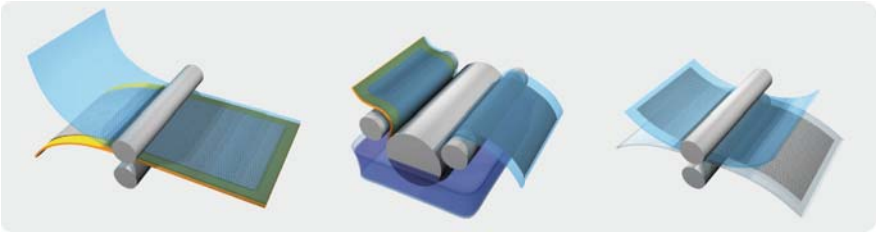

Figure 12. Example of a roll-to-roll process for the transference of CVG Brown graphene onto a polimeric substrate.

- Synthesis on SiC

In this method the starting material are wafers of silicon carbide. By heating the wafers up to 1400ºC is possible to sublimate the silicon atoms of the surface leaving a graphitized surface [70]. Also is possible

to grow graphene layers using the C-terminated face of SiC [71,72]. Nowadays can be achieved high quality graphene by this method with crystallite sizes of micrometers [73].

The major drawback with this technique is the high cost of the SiC wafers. Moreover, similarly to the CVD technique, the high temperatures needed to reach in order to synthesise the graphene layers make this technique more expensive. In spite of that, the utility of silicon carbide in high power electronics make this synthesis approach interesting for some specific applications like high frequency transistors [74].

2.3 Applications of carbon nanomaterials

2.3.1 Carbon nanotubes and nanofibers

Although the first industrial method for synthesise carbon nanofibers was envisioned in the 1980s, nuntil the past decade that the commercial applications of CNF related materials were not fully developed (Fig. 13). In 2004 the first real applications that incorporates CNT were produced, being the most famous one the bicycle of the winner of 2005 Tour de France with a CNT coated frame, allowing the fabrication of a lighter bicycle. From this same year, the industrial production of carbon nanofibers related material increased 10 times each year [75].

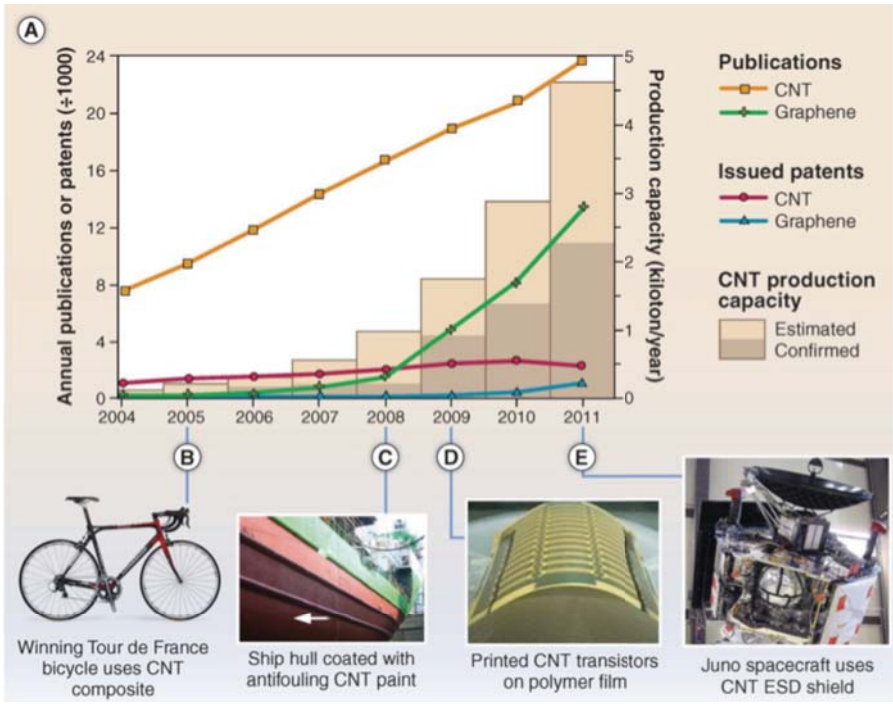

Figure 13. Evolution of CNT industrial manufacturing and CNT applications over the years, from 2004 to 2012. Adapted from [72].

The first applications of carbon nanofibers were in the area of composites materials. In fact, the addition of carbon nanotubes or nanofibers in a polymer matrix can change its physical properties, like its electrical resistance or thermal conductance [76]. This change is due mainly to the high aspect ratio of the nanostructures that allows the formation of a percolation network at concentrations as low as 0.01 wt %. For example, with loadings of MWCNT of 10 wt% conductivities of 10000 S m^{-1} has been achieved [77]. Conductive CNT plastics have been already applied in the automotive industry or in the fabrication of electromagnetic interference shielding packages. Charging polymer or resins with CNT or CNF also can change its stiffness, strength and toughness [78]. For example, the addition of MWCNT into epoxy resin enhances the stiffness by 6 and increase the fracture toughness a 23%

without affecting the rest of mechanical properties [79]. Also, this reinforcement can also increase the material damping [80], that has been applied widely to enhance sports goods like bicycle frames, tennis rackets… Nowadays it is common to find commercial premixed resins and master batches with loading between 0.1 to 20 wt%. The addition of CNT also can be used as a flame retardant of plastics [81], that could be an attractive alternative to the currently use halogenated flame retardants because environmental reasons.

Carbon nanotubes also can be used as a multifunctional coating material. For example, it have been proved that CNT paints can offer an alternative to hazardous biocide-containing paints, as applied to a ship hull reducing its biofouling [82]. Moreover, the incorporation of CNT into anticorrosion coating for metals offers an electric pathway for cathodic protection as enhance coating stiffness and strength. Another important application in coatings is the fabrication of transparent conductive films [83]. Until now, indium tin oxide (ITO) has been used as transparent conductor in displays, touch-screen devices or photovoltaics. But the increase of the demand of these products is increasing the price of indium, a scarce material. Because this is an alternative has to be found, and CNT poses as a potential candidate. The possibility of deposit the CNT from solution and pattern it by well known and cost-effective techniques, along with the compatibility with flexible substrates has attracted the attention of device developers. In spite of that, the best CNT films have a 90% transparency but a sheet resistivity of 100 ohm per square, adequate for some applications but still higher than ITO films equally transparent [84].

Great efforts have been invested in the integration of CNT in microelectronics. In fact, SWCNT are very attractive for the fabrication of transistors due its low electron scattering and bandgap that can be modified by the diameter or chirality of the nanotubes. The first CNT transistor was presented in 1998 [85], and from this point several advances were made. For example, in 2004 the first SWCNT-tunneling FET was fabricated [86], meanwhile in 2012 was achieved a SWCNT FET with a sub-10-nm channel length with a better current density than analogous silicon devices [87]. In spite of that, for now the individual placement of CNT and, specially, the synthesis of individual CNT with precise characteristics (diameter, chirality, etc) on demand are insufficient for microelectronic standards. Because this CNT mats also has been studied as a transistor components. The use of these arrays may compensate the heterogeneity of diameters and chiralities and also will produce a higher output current [88]. CNT arrays are very adequate for the fabrication of organic light-emitting diode (OLED) displays (Fig. 14) because have shown higher mobilities than amorphous silicon and that can be deposited using low temperature and nonvacuum techniques [89]. Due its particular electronic characteristics, CNT and CNF could be use as a replacement of Cu in microelectronic interconnects [90,91]. For example, recently has been demonstrated the fabrication CMOS compatible CNT inter connects with 2.8 kOhm resistance in 200 mm diameter wafers [92].

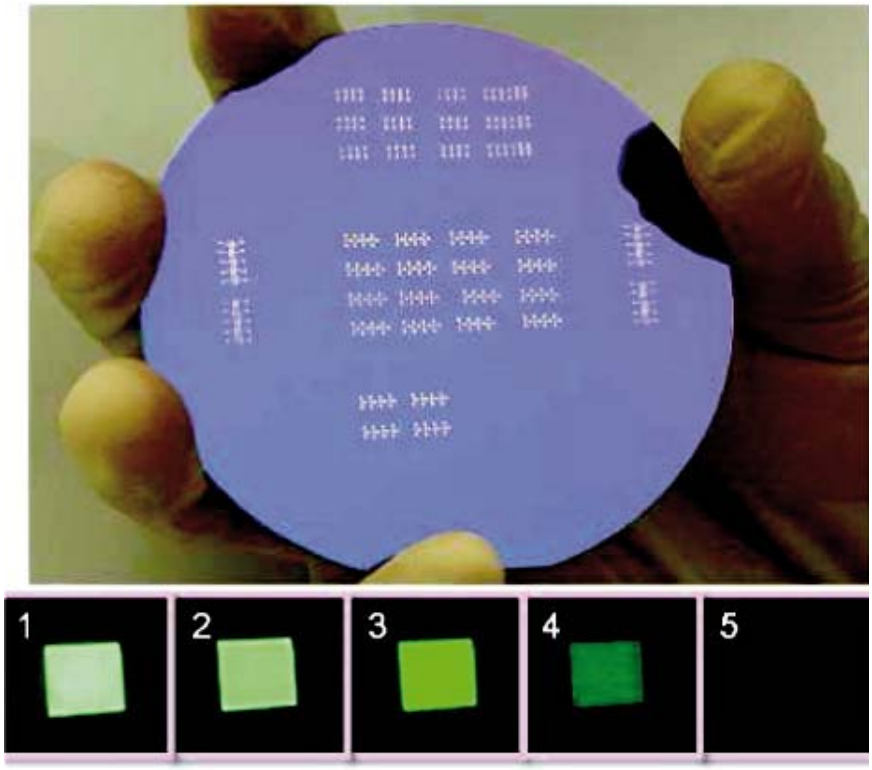

Figure 14. Application of CNT for the fabrication of OLED devices. From [82]

In the area of energy storage, carbon nanotubes have been already used as a component of lithium ion batteries for notebooks computers with great success [93,94]. Usually small quantities of MWCNT are blended with the active material ($LiCoO_2$ or graphite). This provides increased electrical conductivity and mechanical integrity, increasing its rate capability and cycle life. CNT have been also studied as a material for supercapacitors [95]. Recently a 40-F supercapactior has been build using forest grown SWCNT obtaining energy densities about 16Wh kg^{-1} and a power density of 10 $kWkg^{-1}$ with a expected lifecycle up to 16 years. On the other side, CNT and CNF also have been applied for the fabrication of fuel cells, achieving a decrease of 60% of Pt as a catalyst [96]. Finally, CNT have been

applied also in the field of photovoltaics. For organic solar cells, CNT and CNF may reduce undesired carrier recombination and enhance resistance to photooxidation [97]. Moreover, in the near future is planed the fabrication of CNT-Si heterojuntions [98] or transparent SWNT electrodes [99] will be incorporated in commercial solar cells.

Finally, CNF and CNT are also of particular interest in biotechnology research as its biocompatibility with different biomolecules, like DNA or proteins. These nanostructures are of special interest for biosensors, as CNT and CNF exhibits high changes in electrical impedance [100] and optical properties [101] depending the surrounding environment due the adsorption of molecules over the nanotubes surface. Another application of the CNT is the drug administration, as the tips of the CNT can be functionalized in order to bind the CNT to the cell membranes [102] and then achieve a transfection of a molecular cargo that could be attached to the CNT wall or encapsulated inside the nanostructure [103]. Despite the advancements in the usage of CNT or CNF in biotechnology

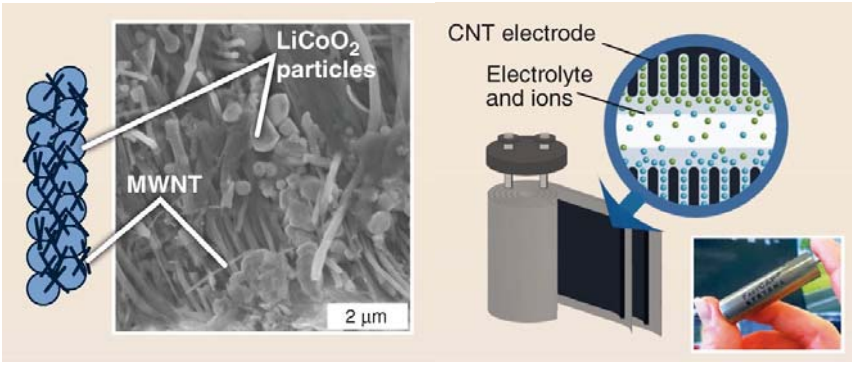

Figure 15. (a) CNT mixed with $LiCoO_2$ particles for battery applications. (b) Supercapacitors based in forest of SWCNT. From [72]

applications, it is still unsure the toxicity of these carbon nanostructures. Large quantities of MWCNT could cause asbestos like pathogenicity in mice lungs [104], but on the other hand, well dispersed SWCNT showed very little effect over the lungs [105] compared to asbestos or with air city particles. It is clear that more tests are needed to determine the immune responses towards CNT and CNF in order to achieve the medical acceptance for the commercial application of these devices.

2.3.2 Graphene

Like carbon nanofibers and carbon nanotubes, the special characteristics of graphene make this nanomaterial an ideal candidate for using it in a wide range of applications. But unlike carbon nanotubes, applications with graphene are highly restricted to the synthesis method and quality of the final product [57]:

- Mechanical exfoliation: This method may produce the higher quality graphene sheets, although the procedure is only useful for research applications.
- Chemical exfoliation: in this case we can obtain flakes between 0.1-100 μm in size that can be overlapped in order to cover a region as large as needed, obtaining charge carrier mobilites about 100 $cm^2V^{-1}s^{-1}$. This production method have proved to be easily scalable and the product could be used principally in products that is needed mix the graphene

flakes with other chemicals, like in coatings, paints, inks, composites…

- CVD: using this method, relatively large (1000 mm) policrystaline graphene continuous sheets can be obtained, with a crystallite size around 1000 μm. This policrystanility makes that the charge carrier mobility be around 10000 $cm^2V^{-1}s^{-1}$. Although this technique is more expensive that the chemical exfoliaton, great efforts are being invested in lower the price of the synthesis process. The fabrication of graphene sheets will be useful in photonics, nanoelectronics and in the fabrication of transparent conductive layers.
- SiC: although the growth of graphene layers over silicon carbide is still expensive compared to other techniques like CVD it is possible to apply this technique in the fabrication of high-frquency transistors and other electronic devices.

Besides that graphene is a very promising material is still well behind other carbon nanostructures (like CNT) in the practical application market as there is a lack of a standardized industrial method for obtaining good quality graphene that could enable the fabrication of competent electronic devices.

One of the most immediate applications will appear in the area of flexible electronics. Usually electronic products like touch screens, electronic paper or OLEDS need low sheet resistance conductive coatings combined with a transmittance above 90%. In theory, nowadays would be possible to use graphene sheets as a conductive coatings as it resistance is low as 30 ohms per square with a

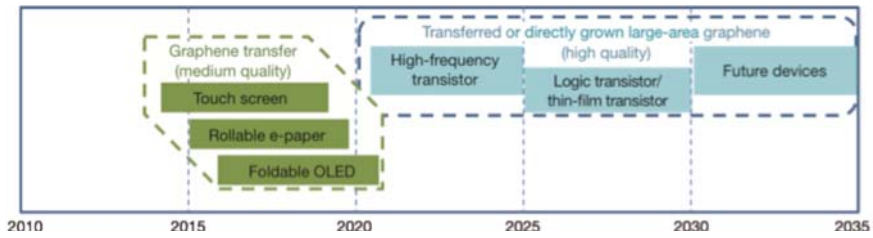

Figure 16. Future graphene-based electronic applications during the next years.

transmittance of 97.7% per layer [40] but in spite of that indium thin oxide (ITO) is still used as a standard conductive coating thanks to its better characteristics in front the current graphene layers. But this situation may change in the near future as ITO will become more expensive and the quality of the graphene layers is improving each year. Moreover, the deposition methods of graphene also are improving; meanwhile the ITO deposition nowadays is expensive in spite to being a very well know material. In addition, the different synthesis methods offer the opportunity of obtaining different conductive coating layers with different electrical properties that may be useful for certain application. For example, liquid phase exfoliation graphene flakes can be used as coatings for high mass production applications, like solar cells. Although the resulting conductive coating will have high resistances, the performance of the obtained device will be sufficient enough. On the other hand, CVD grown graphene will be applied for the fabrication of electrodes in touch screens. Again, although the sheet resistance is still a little high with respect ITO, its higher endurance and fracture strain (ten times higher than ITO) [39] make graphene an ideal candidate for being a integral component in future device, including the bendable or rollable ones.

Graphene also have the potential to be applied for the fabrication of the next generation of transistors, but before that some issues have to be solved. The most important one is the lack of bandgap, although recently have appeared different techniques that allow its generation, like the bilayer control [72,106] or chemical routes [107,108]. In spite of that, the bandgap wide is still an issue as the maximum gap obtained is around 360 meV [109], limiting the on/off ratio to 10^3, that is low compared with the 10^7 on/off ratio that can be obtained with standard CMOS technology. In order to increase the on/off ratio, some groups have used novel transistor geometries based in vertical transport through barriers [110]. On the other hand, the use of graphene nanoribbons (that have bandgap) allows the increase of the on/off ratio up to 10^5 by using ribbons with a wide lower than 10 nm [111]. Of course, is still needed more development in order to integrate these graphene devices in order to advance in the logic transistor technology.

Although the low on/off ratio is a drawback for logic transistors, a transistor with large area graphene channel may be useful for radiofrequencies applications as is not needed switch between an on – off states and could benefit from the higher mobilites from graphene channels [112]. In order to compete with more mature technologies such as compound semiconductors, based graphene high-frequency transistors have to reach a maxium oscillation frequency of f_{max}=1.2 THz and a cut-off frequency about f_T=850 GHz (values obtained with III-V materials). Nowadays is possible to reach f_T around 300Ghz that could be increased to 1 Thz in certain conditions [113]. The main concern is the maximum oscillation frequency values, as in classic graphene structures only reach 30 GHz. In order to elevate this value

two options are given: lowering the gate resistance or the source-drain conductance at pinch-off [114].

Photonic applications also are in the scope of graphene researchers. This is because graphene owns two very interesting optical properties:

1) For normal incident light below 3eV graphene exhibits a wavelength-independent absorption [40]. This is because electrons behave as massless two dimensional particles in this material.
2) In graphene there is the phenomenon of Pauli blocking, as when the optical energy is smaller than double the Fermi level mono and bilayer graphene become totally transparent [115].

These properties will allow the design of new photonic devices. One of the photonic devices more studied are the photodetectors. Because the special properties of graphene is possible to build photodetectors with characteristics that could overcome the classical semiconductors photodetectors. For example, graphene would enable the possibility to use a wider spectral range, spanning form ultraviolet to infrared. In addition, its high carrier mobility enables ultrafast extraction of photo-generated carriers, allowing an extremely high bandwidth operation. To put this in perspective, is calculated that with graphene the photodectors could have a transit-time-limited bandwidth of 1.5 Thz, that will be limited to 640 GHz because the capacitive delay [116]. This is still incredibly higher that the bandwidth obtained by semiconductors like InGaAs (150 GHz) and Ge (80 GHz). But in spite

these high bandwidth operations, graphene photodetectors still lacks of an high responsivity [116,117] that will need the design of new photodetector structures [118] or integrate the graphene with a waveguide in order to increase the light-graphene interaction length [109]. Other photonic devices studied are optical modulators [119], mode-loked lasers [120] or optical polarization controllers [121]. All of these photonic devices would benefit from the properties of graphene, but it is needed some development in order to achieve a good performance. All these photonic devices are summarized in Table 2.

A part of these devices, graphene is also studied for other kind of applications. For example, as graphene is a highly inert, the existence of techniques to synthesise large area graphene layers allows the fabrication of corrosion layers for metals [122]. Another possibility is the use of the special properties of graphene for the manufacturing of composite materials, although this approach needs more development in order to reach the properties of carbon fibers composites. From of the point of view of mechanical properties, one of the objectives is to reach a 250 GPa Young's modulus at €25 per kilogram.

Application	Drivers	Issues to be addressed
Tunable fibre mode-locked laser	Graphene's wide spectral range	Requires a cost-effective graphene-transferring technology
Solid-state mode-locked laser	Graphene-saturable absorber would be cheaper and easy to integrate into the laser system	Requires a cost-effective graphene-transferring technology
Photodetector	Graphene can supply bandwidth per wavelength of 640 GHz for chip-to-chip or intrachip communications (not possible with IV or III–V detectors)	Need to increase responsivity, which might require a new structure and/or doping control, and the modulator bandwidth must follow suit
Polarization controller	Current polarization controlling devices are bulky or difficult to integrate but graphene is compact and easy to integrate with Si	Need to gain full control of parameters of high-quality graphene
Optical modulator	Graphene could increase operating speed (Si operation bandwidth is currently limited to about 50 GHz), thus avoiding the use of complicated III–V epitaxial growth or bonding on Si	High-quality graphene with low sheet resistance is needed to increase bandwidth to over 100 GHz
Isolator	Graphene can provide both integrated and compact isolators on a Si substrate, dramatically aiding miniaturization	Decreasing magnetic field strength and optimization of process architecture are important for the products
Passively mode-locked semiconductor laser	Core-to-core and core-to-memory bandwidth increase requires a dense wavelength-division-multiplexing optical interconnect (which a graphene-saturable absorber can provide) with over 50 wavelengths, not achievable with a laser array	Competing technologies are actively mode-locked semiconductor lasers or external mode-lock lasers but the graphene market will open in the 2020s; however, interconnect architecture needs to consume low power

Table 2. Summary of different graphene-based photonic devices.

Applications in energy generations also will benefit from the optical properties of graphene [40]. The most immediate applications will be in the field of solar cell technology as the advancements in the liquid exfoliation technique and new deposition methods will enable the mass production of low cost transparent electrodes [123]. In other areas, graphene will have an astounding role in the next-generation lithium-ion batteries as will increase the conductivity in cathodes or its battery charge capacity [124].

Finally, graphene also could be interesting for biotechnological applications. Its chemical and mechanical characteristics would be applied in tissue engineering applications and regenerative medicine [125]. Moreover, graphene is lipophilic, meaning that can penetrate the membrane barrier of a given cell and with the correct functionalitzation aid in the drug delivery process [126]. In spite of that, real graphene biotechnology applications may require a better understanding of the toxiticy, biocompatibility and biodistribution of graphene material. This is a difficult problem, as graphene morphology and chemistry changes depending the synthesis process and is likely that the analysis have to be done for each of these different products individually. But in the other hand, this variability of types of graphene will arise variability in different toxicities, biocompatibilities and, in the end, different applications.

In conclusion, not only graphene properties will enable the desing of new types of devices, but also the tailoring of these properties will have an important role. Different types of graphene will rise different applications, from energy generation (solar cells) to biotechnology (tissue engineering). Still there is work to do in order to

implement graphene in these devices, but although the material is relatively new great effort have been invested in develop these new technologies and in the next few years the first graphene-based application would appear.

2.4. State of the art of gas sensing with carbon nanostructures

During the last years the necessity of obtain a sensor device capable of operate in a wide range of applications and situations have increased the interest for the nanomaterials as a sensing layer [127]. This kind of materials allows the fabrication of more simple sensing devices that at the same time are more sensitve and electronically stable than their expensive and complicated instrumental methods.

Among all the nanomaterials, carbon nanostructures have attracted a lot of attention, as its physical and chemical properties are very convenient to use it for chemical sensing applications [128]. In the first place, carbon nanostructures have almost all of its carbon atoms exposed to the environment, offering a high specific surface area and thus a high sensitivity. Moreover, carbon nanostructures like CNT and graphene have almost perfect crystal lattice in contrast with polycrystalline metal oxides. This feature permits to avoid grain boundary poisoning and increase the long-term stability of the sensors. Moreover, the perfect crystanillity of these carbon nanostructures are easier to understant than polycrystalline structures, and could be used as a base for running computational chemistry studies in order to understand the sensing mechanism of this material [129].

From the point of view of fabrication, carbon nanostructures can be synthesised with a wide range of methods, allowing the fabrication of gas sensor devices with different configurations and properties, including flexible gas sensors.

2.4.1. Carbon nanofibers based gas sensors

Usually in gas sensor applications two types of CNF are used: the vapour grown nanofibers [130] and the synthesised by electrospinning technique [131]. In the fist case, the CNF are mixed in a polymer matrix in order to create a sensitive composite [132]. The idea is improve the black carbon – polymer composites that suffers of a long-term instability as carbon black particles tends to aggregate when vapour is absorved by the composite. Then, adding CNF instead of carbon black this instability is eliminated as CNF, because its higher aspect ratio resists the movement through the polymer matrix when vapour is absorbed.

Another possibility is to synthesis the CNF by the use of electrospinning technique. It has attracted some attention as is possible to synthetise CNF with different funcionalitzations or metal nanoparticle decorations [133]. These surface treatments can be done during or after the synthesis, so this technique proved to be very versatile.

1.4.2. Carbon nanotubes based gas sensors

The first CNT based gas sensors were done in the year 2000 [134,135]. From the data extracted, was clear that the CNT were extremely sensitive to the local chemical environment. In one of the first experiments a single SWCNT was contacted and its change of resistance measured. In that case, the SWCNT was a hole-doped semiconductor. Two kinds of gases were tested: a reducing gas (ammonia, NH_3) and a oxydizing one (nitrogen dioxide, NO_2). After exposure to ammonia is observed a reduction of conductance. This phenomena occurs as the ammonia molecules when are adsorbed to the sidewall of the nanotube shifts its valence band away from the Fermi level forcing a hole depletion. In contrast, exposure to nitrogen dioxide induces an increase in conductance, as the valence band is shifted towards the Fermi level, increasing the hole carrier concentration of the CNT. Moreover, is found that the response to gases of CNT mats and single CNT is different, being the single CNT signal better than mats. Was found that this is because a double effect: in one hand in the mats the signal is the average between semiconductor and metallic CNT and in the other hand the inner CNT of the mat are not exposed to the gas, and thus there are no change in the resistance signal.

Another study performed in the same year showed that CNTs were very sensitive to oxygen molecules, as was possible to change its electrical resistance by the adsorption of a small amount of oxygen molecules. This means that there is the danger that measurements done in air atmosphere with CNT may be compromised by this affinity to oxygen molecules. Moreover, this behaviour may indicate the presence of defects in the CNT walls or that the ends of the CNT are open. This

was demonstrated later in a systematic study of the exposure of SWNT mats to different gases. It was shown that after a thermal treatment that purified the surface of the SWCNT the response to gases like oxygen, nitrogen or carbon monoxide was neutralized, meaning that that the sensivity towards these gases depends on the impurities of the surface of the nanotube [136]. In contrast, the SWCNT mats were still sensitive to ammonia, nitrogen dioxide and sulphur oxide. These results give the conclusion that is needed a control of the surface chemistry and defects of the CNT in order to reach consistent sensivity results.

These results suggest that the funcionalization of CNT walls it can be obtained a better chemical bonding to a specific target gas molecule, thus increasing the selectivity to the given gas [137,138]. For example, decorating SWCN with Pd nanoparticles is possible to detect hydrogen gas in a concetration around 400 ppm [139]. In this case, the role of the Pd nanoparticles is of a catalyst: the molecular hydrogen dissociates in atomic hydrogen on the surface of the Pd nanoparticle lowering the work function of Pd and, in consequence, promotes the electron transfer from the Pd to the nanotube lowering the hole-carriers of the nanotube and hence its conductance. A theorical study involving CNT-Al clusters confirmed these results [140], and concluded that the metal nanoparticles have to be as small as possible in order to take advantage of the effect of the adsorbates over the metal cluster, that at the same time after the donation of acceptation of a given charge will affect the electron transport in the CNT. So, the objective of the decoration is obtain the smaller metal clusters dispersed homogenously over the carbon nanotube surface. This poses a challenge, as metal clusters tends to move across the CNT surface and coalesce into bigger clusters, promoting the instability of the sensor [141]. One strategy

used to cope with this problem is the generation of nucleation sites by means of a cold reactive plasma treatment (oxygen plasma) [142–144].

By this way, the metal atoms will move across the untouched carbon surface until will find a nucleation entre, or in other words, an impurity. Another technique to decorate the CNT is the use of sputtering [145–147]. Different metals have been used with this technique (Au, Pt, Pd, Ru, Ag…). Is possible to decorate CVD-grown CNT forest directly over the gas sensor transducer, avoiding the transfer process. Moreover, seems that the plasma used for the

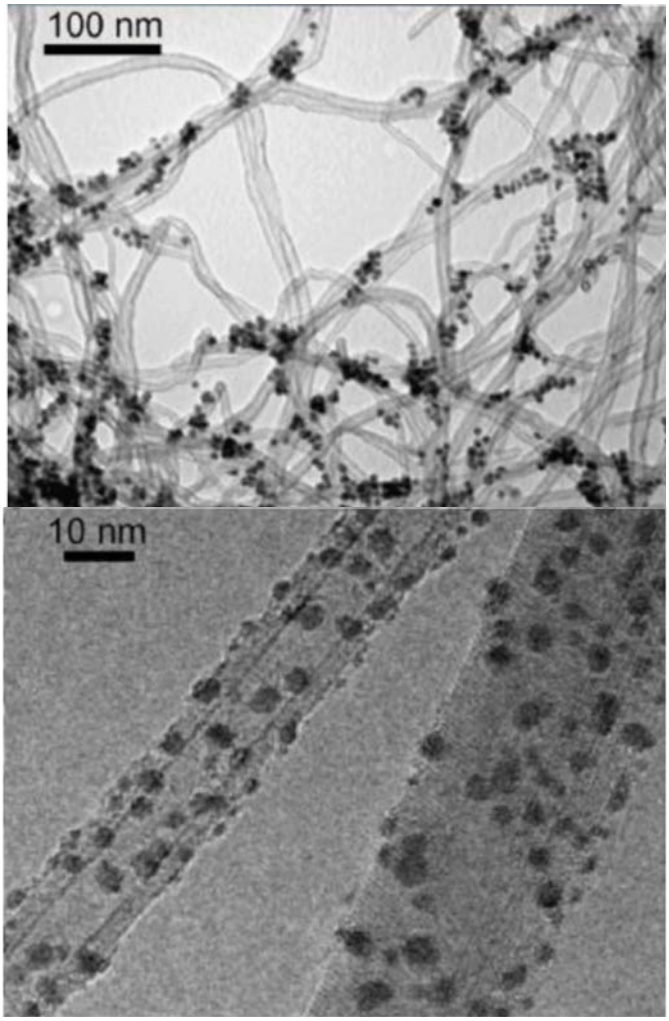

Figure 17. Different metal-nanoparticle decorations of CNT. From [142]

sputtering helps in the functionalization of the CNT sidewalls. It have been reported the response towards nitrogen dioxide and ammonia, hydrogen, hydrogen sulphide and carbon monoxide using this decoration technique.

Another possibility to enhance the selectivity of CNT is its functionialization with organic molecules. Have been demonstrated the functionalization with single-stranded DNA [148] that react with different gases (like explosives) that bare CNT do not detect. The interesting property of this type of sensor is that the selectivity could be tuned by selecting the base sequence of the strand of DNA.

In order to be able to fabricate low-cost and reliable gas sensors devices based in CNT several problems may be resolved. One of the main problems is the different humidity levels that will find the gas sensor when working in the real world [149], as the reaction of this humidity with the carbon nanotube (funcionalized or decorated) may difficult the detection of other molecules, specially for the volatile organic compounds (VOCs). Recently have been proposed a solution by coating the carbon nanotubes with different polycyclic aromatic hydrocarbons (PAH) [150] with the objective to self-assemble a electron rich molecular stacks that guarantees the good charge carrier transport along the stack. Moreover, PAH molecules also form sponge-like structures with a high surface area to volume ratio. With this strategy is possible discriminate polar and nonpolar VOCs in samples with variable humidity levels between 5% to 80 % RH. Similarly, have been coated carbon nanotubes with aminophenylamino cyclodextrin (PCD) [151] with the objective to detect persistent organic pollutants (POP). This strategy leaded to a variation of the electrical conductance

of the CNT-PCD hybrids when exposed to different POPs. Another problem to be addressed is the efficient use of individual carbon nanotubes instead of mats in order to enhance the sensitivity and selectivity [134]. The current transfer techniques are insufficient as the CNT ends up contaminated by the additional steps, changing its sensing properties. Recently have been reported a novel method for growing a single CNT between the gas sensor device contacts with only one extra step for evaporate Pd using a self-aligned on-chip shadow mask [152].

2.4.3. Graphene based gas sensors

The first graphene gas sensor was developed by Novoselov's group in 2007 [34]. Graphene was obtained by micromechanical exfoliation and then, using standard lithographic techniques, was patterned as a multiterminal Hall bar. They found that exposure to ppm of gases changes the resistivity of the graphene layer, and the changes were dependent of the concentration of the gases. Moreover, was possible to return to the signal baseline by simply heating the sensor at 150ºC under vacuum conditions. From the signal measured, was possible to know if the gas was an electron acceptor (like in the case of nitrogen dioxide) or electron donor (like ammonia). In addition, as the noise levels obtained were very low, they realised long-term measurements with very dilute nitrogen oxide samples, obtaining step like changes during adsorption and desorption. These changes were interpreted as the detection of adsorption or desorption of individual gas molecules.

In the same fashion that CNT sensors, it was demonstrated that nanolithographic techniques leaves impurities over the graphene layer,

changing its sensing characteristics [153]. After cleaning the graphene layer using H_2/Ar it was found that the real responses to different gases

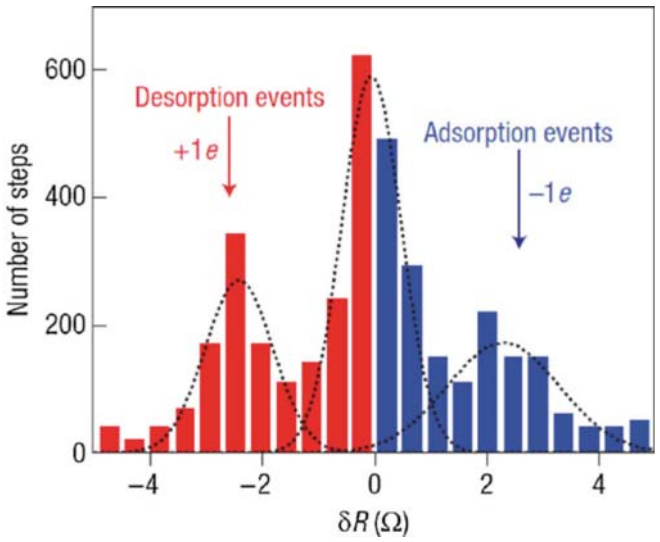

Figure 18. Statistical distribution of step changes in device resistance considered as a proof that there is adsorbtion and desorption of individual molecules. From [34].

were very low and in order to reach sub-ppm detection the surface of graphene have to be modified [154]. One option is the substitucional doping, as computational studies suggest that doping graphene with B or S would enhance the sensitivity towards nitric oxide and nitrogen dioxide [155].

The use of reduced graphene oxide also have been studied as a sensing layer for gas sensors [156]. As commented before, rGO is easier to produce and manipulate than pure graphene, opening the door for cheaper gas sensors. On the other hand, is needed to first reduce graphene oxide material in order to obtain rGO. This reduction can be controlled, obtaining a graphene flakes with oxygen functional groups attached in its basal planes. This "forced" funcionalitzation is useful for the detection, for example, of different kind of warfare agents simulants

[157]. In spite of that, the functional groups are related to the noise level of the signal, and higher oxidations giver higher noise levels. By this way, is needed to find a compromise between the optimal lower limit of detection and the gas species that we want to detect. Moreover, the functionalized surface is a perfect platform to generate metal clusters. For example, Pd-rGO was synthesised obtaining ppb detection level to nitric acid [158].

References

[1] D.D.L. Chung, Review Graphite, J. Mater. Sci. 7 (2002) 1475–1489.

[2] A.C. Ferrari, J. Robertson, Interpretation of Raman spectra of disordered and amorphous carbon, Phys. Rev. B. 61 (2000) 95–107.

[3] J.L. Tuinstra, F., Koenig, Raman spectrum of Graphite, J. Chem. Phys. 53 (1970) 1126 – 1130.

[4] A.C. Ferrari, Raman spectroscopy of graphene and graphite: Disorder, electron–phonon coupling, doping and nonadiabatic effects, Solid State Commun. 143 (2007) 47–57.

[5] a K. Geim, K.S. Novoselov, The rise of graphene., Nat. Mater. 6 (2007) 183–91.

[6] K.S. Novoselov, a K. Geim, S. V Morozov, D. Jiang, Y. Zhang, S. V Dubonos, et al., Electric field effect in atomically thin carbon films., Science. 306 (2004) 666–9.

[7] S. Ijima, Helical microtubules of graphitic carbon, Nature. 354 (1991) 56–58.

[8] G.G. Tibbets, Carbon fibers produced by pyrolysis of natural gas in stainless steel tubes, Appl. Phys. Lett. 42 (1983) 666–668.

[9] R.M. Taylor, R., Walton, The chemistry of fullereness, Nature. 363 (1993) 685–693.

[10] I.T. Ijima, S., Single-shell carbon nanotubes of 1-nm diameter, Nature. 363 (1993) 603–605.

[11] R. Andrews, D. Jaques, D. Quian, T. Rantell, Multiwall Carbon Nanotubes: Synthesis and Application, Acc. Chem. Res. 35 (2002) 1008–1017.

[12] R.H. Baughmann, A.A. Zakhidov, W.A. de Heer, Carbon nanotubes - the Route Toward Applications, Science (80-.). 297 (2002) 787–792.

[13] A.G. Rinzler, J. Liu, H. Dai, P. Nikolaev, C.B. Huffman, F.J. Rodríguez-Macías, et al., Large-scale purification of single-wall carbon nanotubes: process, product, and characterization, Appl. Phys. A. 67 (1998) 29–37.

[14] R. Andrews, D. Jaques, A.M. Rao, F. Derbyshire, D. Quian, X. Fan, et al., Continuous production of aligned carbon nanotubes: a step closer to commercial realization, Chem. Phys. Lett. 303 (1999) 467–474.

[15] S. Frank, P. Poncharal, Z.L. Wang, W.A. de Heer, Carbon nanotube quantum resistors, Science (80-.). 280 (1998) 1744–1746.

[16] J.P. Small, L. Shi, P. Kim, Mesoscopic thermal and thermoelectric measurements of individual carbon nanotubes, Solid State Commun. 127 (2003) 181–186.

[17] E.W. Wong, P.E. Sheehan, C.M. Lieber, Nanobeam Mechanics: Elasticity, Strength, and Toughness of Nanorods and Nanotubes, Science (80-.). 277 (1997) 1971–1975.

[18] M.H. Al-Saleh, U. Sundararaj, A review of vapor grown carbon nanofiber/polymer conductive composites, Carbon N. Y. 47 (2009) 2–22.

[19] J. Vera-Agullo, H. Varela-Rizo, J.A. Conesa, C. Almansa, C. Merino, I. Martin-Gullon, Evidence for growth mechanism and helix-spiral cone structure of stacked-cup carbon nanofibers, Carbon N. Y. 45 (2007) 2751–2758.

[20] I. Martingullon, J. Vera, J. Conesa, J. Gonzalez, C. Merino, Differences between carbon nanofibers produced using Fe and Ni catalysts in a floating catalyst reactor, Carbon N. Y. 44 (2006) 1572–1580.
[21] O.C. Carneiro, N.M. Rodriguez, R.T.K. Baker, Growth of carbon nanofibers from the iron–copper catalyzed decomposition of CO/C2H4/H2 mixtures, Carbon N. Y. 43 (2005) 2389–2396.
[22] K. Mukhopadhyay, D. Porwal, D. Lal, K. Ram, G. Narayan-Mathur, Synthesis of coiled/straight carbon nanofibers by catalytic chemical vapor deposition, Carbon N. Y. 42 (2004) 3254–3256.
[23] S. Helveg, C. López-Cartes, J. Sehested, P.L. Hansen, B.S. Clausen, J.R. Rostrup-Nielsen, et al., Atomic-scale imaging of carbon nanofibre growth, Nature. 427 (2004) 426–429.
[24] N.M. Rodriguez, A. Chambers, R.T.K. Baker, Catalytic Engineering of Carbon Nanostructures, Langmuir. 11 (1995) 3862–3866.
[25] Yoon, Seong-Ho, S. Lim, S. Hong, W. Qiao, D.D. Whitehurst, I. Mochida, et al., A conceptual model for the structure of catalytically grown carbon nanofibers, Carbon N. Y. 43 (2005) 1828–1838.
[26] M. Endo, Y.A. Kim, T. Hayashi, Y. Fukai, K. Oshida, Structural characterization of cup-stacked-type nanofibers with an entirely hollow core, Appl. Phys. Lett. 80 (2002) 1267 – 1269.
[27] N.M. Rodriguez, A review of catalytically grown carbon nanoflbers, J. Mater. Res. 8 (1993) 3233–3250.
[28] S.G. Prolongo, M. Burón, M.R. Gude, R. Chaos-Morán, M. Campo, A. Ureña, Effects of dispersion techniques of carbon nanofibers on the thermophysical properties of epoxy nanocomposites, Compos. Sci. Technol. 68 (2008) 2722–2730.
[29] N.D. Mermin, Crystalline order in two dimensions, Phys. Rev. 176 (1968) 250–254.
[30] J.C. Meyer, a K. Geim, M.I. Katsnelson, K.S. Novoselov, T.J. Booth, S. Roth, The structure of suspended graphene sheets., Nature. 446 (2007) 60–3.
[31] a. C. Ferrari, J.C. Meyer, V. Scardaci, C. Casiraghi, M. Lazzeri, F. Mauri, et al., Raman Spectrum of Graphene and Graphene Layers, Phys. Rev. Lett. 97 (2006) 1–4.
[32] D. Graf, F. Molitor, K. Ensslin, C. Stampfer, a. Jungen, C. Hierold, et al., Raman imaging of graphene, Solid State Commun. 143 (2007) 44–46.
[33] B. Partoens, F.M. Peeters, From graphene to graphite: Electronic structure around the K point, Phys. Rev. B. 74 (2006) 075404.
[34] F. Schedin, a K. Geim, S. V Morozov, E.W. Hill, P. Blake, M.I. Katsnelson, et al., Detection of individual gas molecules adsorbed on graphene., Nat. Mater. 6 (2007) 652–5.
[35] K.S. Novoselov, Z. Jiang, Y. Zhang, S. V. Morozov, H.L. Stormer, U. Zeitler, et al., Room-Temperature Quantum Hall Effect in Graphene, Science (80-.). 315 (2007) 1379.
[36] A.F. Young, P. Kim, Quantum interference and Klein tunnelling in graphene heterojunctions., Nat. Phys. 5 (2009) 222–226.
[37] N. Stander, B. Huard, D. Goldhaber-Gordon, Evidence for Klein Tunneling in Graphene p-n Junctions, Phys. Rev. Lett. 102 (2009) 026807.
[38] A. a Balandin, S. Ghosh, W. Bao, I. Calizo, D. Teweldebrhan, F. Miao, et al., Superior thermal conductivity of single-layer graphene., Nano Lett. 8 (2008) 902–7.

[39] C. Lee, X. Wei, J.W. Kysar, J. Hone, Measurement of the elastic properties and intrinsic strength of monolayer graphene., Science. 321 (2008) 385–8.
[40] R.R. Nair, P. Blake, A.N. Grigorenko, K.S. Novoselov, T.J. Booth, T. Stauber, et al., Fine Structure Constant Defines Visual Transparency of Graphene, Science (80-.). 320 (2008) 1308.
[41] D. Li, M.B. Müller, S. Gilje, R.B. Kaner, G.G. Wallace, Processable aqueous dispersions of graphene nanosheets., Nat. Nanotechnol. 3 (2008) 101–5.
[42] O.C. Compton, S.T. Nguyen, Graphene oxide, highly reduced graphene oxide, and graphene: versatile building blocks for carbon-based materials., Small. 6 (2010) 711–23.
[43] S.-S. Li, K.-H. Tu, C.-C. Lin, C.-W. Chen, M. Chhowalla, Solution-processable graphene oxide as an efficient hole transport layer in polymer solar cells., ACS Nano. 4 (2010) 3169–74.
[44] K.P. Loh, Q. Bao, G. Eda, M. Chhowalla, Graphene oxide as a chemically tunable platform for optical applications., Nat. Chem. 2 (2010) 1015–24.
[45] Y. Zhu, W. Cai, R.D. Piner, A. Velamakanni, R.S. Ruoff, Transparent self-assembled films of reduced graphene oxide platelets, Appl. Phys. Lett. 95 (2009) 103104.
[46] A. Bagri, C. Mattevi, M. Acik, Y.J. Chabal, M. Chhowalla, V.B. Shenoy, Structural evolution during the reduction of chemically derived graphene oxide., Nat. Chem. 2 (2010) 581–7.
[47] H. a Becerril, J. Mao, Z. Liu, R.M. Stoltenberg, Z. Bao, Y. Chen, Evaluation of solution-processed reduced graphene oxide films as transparent conductors., ACS Nano. 2 (2008) 463–70.
[48] T. Koyama, Formation of Carbon Fibers from Benzene, Carbon N. Y. 10 (1972) 757–758.
[49] A. Tanaka, S.H. Yoon, I. Mochida, Preparation of highly crystalline nanofibers on Fe and Fe-Ni catalysts with a variety of graphene plane alignments, Carbon N. Y. 42 (2004) 591–597.
[50] N. Krishnankutty, C. Park, N.M. Rodriguez, R.T.K. Baker, The effect of copper on the structural characteristics of carbon filaments produced from iron catalyzed decomposition of ethylene, Catal. Today. 37 (1997) 295–307.
[51] O.S. Carneiro, J.A. Covas, A. Bernardo, G. Caldeira, F.W.J. Van Hattum, J.M. Ting, et al., Production and assessment of polycarbonate composites reinforced with vapour-grown carbon fibres, Compos. Sci. Technol. 58 (1998) 401–407.
[52] A. Tanaka, S.H. Yoon, I. Mochida, Formation of fine Fe-Ni particles for the non-supported catalytic synthesis of uniform carbon nanofibers, Carbon N. Y. 42 (2004) 1291–1298.
[53] M. Ishioka, T. Okada, K. Matsubara, Preparation of vapor-grown carbon fibers in straight form by floating catalyst method in Linz-Donawitz converter gas., Carbon N. Y. 31 (1993) 123–127.
[54] T. Masuda, S.R. Mukai, K. Hashimoto, The liquid pulse injection technique: A new method to obtain long vapor grown carbon fibers at high growth ratesNo Title, Carbon N. Y. 31 (1993) 783–787.
[55] G.G. Tibbets, D.W. Gorkiewicz, R.L. Alig, A new reactor for growing carbon fibers from liquid- and vapor-phase hydrocarbons, Carbon N. Y. 31 (1993) 809–814.

[56] M. Endo, Y. a. Kim, Y. Fukai, T. Hayashi, M. Terrones, H. Terrones, et al., Comparison study of semi-crystalline and highly crystalline multiwalled carbon nanotubes, Appl. Phys. Lett. 79 (2001) 1531.
[57] Y.A. Kim, T. Hayashi, S. Naokawa, T. Yanagisawa, M. Endo, Comparative study of herringbone and stacked-cup carbon nanofibers, Carbon N. Y. (43AD) 3005–3008.
[58] K.S. Novoselov, V.I. Fal'ko, L. Colombo, P.R. Gellert, M.G. Schwab, K. Kim, A roadmap for graphene, Nature. 490 (2012) 192–200.
[59] Y. Hernandez, V. Nicolosi, M. Lotya, F.M. Blighe, Z. Sun, S. De, et al., High-yield production of graphene by liquid-phase exfoliation of graphite, Nat. Nanotechnol. 3 (2008) 563–568.
[60] P. Blake, P.D. Brimicombe, R.R. Nair, T.J. Booth, D. Jiang, F. Schedin, et al., Graphene-based liquid crystal device., Nano Lett. 8 (2008) 1704–8.
[61] D.R. Dreyer, R.S. Ruoff, C.W. Bielawski, From Conception to Realization: An Historial Account of Graphene and Some Perspectives for Its Future, Angew. Chemie Int. Ed. 49 (2010) 9336–9344.
[62] H. Varela-Rizo, I. Rodriguez-Pastor, C. Merino, I. Martin-Gullon, Highly crystalline graphene oxide nano-platelets produced from helical-ribbon carbon nanofibers, Carbon N. Y. 48 (2010) 3640–3643.
[63] B. Martín-Medina, M.M. Velázquez, F. Rossella, V. Bellani, E. Diez, J.L.G. Fierro, et al., Functionalization of Reduced Graphite Oxide Sheets with a Zwitterionic Surfactant, ChemPhysChem. 13 (2012) 3682–3690.
[64] H.C. Schniepp, J.L. Li, M.J. Mcallister, H. Sai, M. Herrera-Alonso, D.H. Adamson, et al., Functionalized single graphene sheets derived from splitting graphite oxide, J. Phys. Chem. B Lett. 110 (2006) 8535–8539.
[65] X. Li, W. Cai, J. An, S. Kim, J. Nah, D. Yang, et al., Large area synthesis of high quality and Uniform graphene films on copper foils, Science (80-.). 324 (2009) 1312–1314.
[66] M. Wang, S.K. Jang, W.J. Jang, M. Kim, S.Y. Park, S.W. Kim, et al., A Platform for Large-Scale Graphene Electronics – CVD Growth of Single-Layer Graphene on CVD-Grown Hexagonal Boron Nitride, Adv. Mater. 25 (2013) 2746–2752.
[67] Y. Lee, S. Bae, H. Jang, S. Jang, S.E. Zhu, S.H. Sim, et al., Wafer-Scale Synthesis and Transfer of Graphene Films, Nano Lett. 10 (2010) 490–493.
[68] J.D. Caldwell, T.J. Anderson, J.C. Culbertson, G.G. Jernigan, K.D. Hobart, F.J. Kub, et al., Technique for the dry transfer of epitaxial graphene onto arbitrary substrates, ACS Nano. 4 (2010) 1108–1114.
[69] S. Bae, H. Kim, Y. Lee, X. Xu, J.S. Park, Y. Zheng, et al., Roll-to-roll production of 30-inch graphene films for transparent electrodes, Nat. Nanotechnol. 5 (2010) 574–578.
[70] I. Forbeaux, J.M. Themlin, J.M. Debever, Heteroepitaxial graphite on 6H-SiC(0001): Interface formation through conduction-band electronic structure, Phys. Rev. B. 58 (1998) 16396–16406.
[71] G. Nanoelectronics, C. Berger, Z. Song, T. Li, X. Li, A.Y. Ogbazghi, et al., Ultrathin Epitaxial Graphite : 2D Electron Gas Properties and a Route toward, Society. (2004) 19912–19916.
[72] T. Ohta, A. Bostwick, T. Seyller, K. Horn, E. Rotenberg, Controlling the electronic structure of bilayer graphene, Science (80-.). 313 (2006) 951–954.

[73] C. Virojanadara, M. Syväjarvi, R. Yakimova, L.I. Johansson, A.A. Zakhidov, T. Balasubramanian, Homogeneous large-area graphene layer growth on 6H-SiC(0001), Phys. Rev. B. 78 (2008) 245403.
[74] Y. Lin, C. Dimitrakopoulos, K.A. Jenkins, D.B. Farmer, H. Chiu, A. Grill, et al., 100-GHz transistors from wafer-scale epitaxial graphene, Science (80-.). 327 (2010) 662.
[75] M.F.L. De Volder, S.H. Tawfick, R.H. Baughmann, A.J. Hart, Carbon Nanotubes: Present and Future Commercial Applications, Science (80-.). 339 (2013) 535–539.
[76] O. Breuer, U. Sundararaj, Big Returns From Small Fibers: A Review of Polymer/Carbon Nanotube Composites, Polym. Compos. 25 (2004) 630–645.
[77] W. Bauhofer, J.Z. Kovacs, A review and analysis of electrical percolation in carbon nanotube polymer composites, Compos. Sci. Technol. 69 (2009) 1486–1498.
[78] T.-W. Chou, L. Gao, E.T. Thotenson, Z. Zhang, J.-H. Byun, An assessment of the science and technology of carbon nanotube-based fibers and composites, Compos. Sci. Technol. 70 (2010) 1–19.
[79] F.H. Gojny, M.H.G. Wichmann, U. Köpke, B. Fiedler, K. Schulte, Carbon nanotube-reinforced epoxy-composites: enhanced stiffness and fracture toughness at low nanotube content, Compos. Sci. Technol. 64 (2004) 2363–2371.
[80] J. Suhr, N. Koratkar, P. Keblinski, P. Ajayan, Viscoelasticity in carbon nanotube composites, Nat. Mater. 4 (2005) 134–137.
[81] T. Kahiwagi, F. Du, J.F. Douglas, K.I. Winey, R.H. Harris, J.R. Shields, Nanoparticle networks reduce the flammability of polymer nanocomposites, Nat. Mater. 4 (2005) 928–933.
[82] A. Beigbeder, P. Degee, S.L. Conlan, R.J. Mutton, A.S. Clare, M.E. Pettitt, et al., Preparation and characterisation of silicone-based coatings filled with carbon nanotubes and natural sepiolite and their application as marine fouling-release coatings, Biofouling. 24 (2008) 291–302.
[83] Z. Wu, Z. Chen, X. Du, J.M. Logan, J. Sippel, M. Nikolou, et al., Transparent, Conductive Carbon Nanotube Films, Science (80-.). 305 (2004) 1273–1276.
[84] S. De, J.N. Coleman, The effects of percolation in nanostructured transparent conductors, MRS Bull. 36 (2011) 774–781.
[85] S.J. Tans, A.R.M. Verschueren, C. Dekker, Room-temperature transistor based on a single carbon nanotube, Nature. 393 (1998) 49–52.
[86] J. Appenzeller, Y.M. Lin, J. Knoch, P. Avouris, Band-to-Band Tunneling in Carbon Nanotube Field-Effect Transistors, Phys. Rev. Lett. 93 (2004) 196805.
[87] A.D. Franklin, M. Luisier, S.-J. Han, G. Tulevski, C.M. Breslin, L. Gignac, et al., Sub-10 nm Carbon Nanotube Transistor, Nano Lett. 12 (2012) 758–762.
[88] Q. Cao, A. Rogers, Ultrathin Films of Single-Walled Carbon Nanotubes for Electronics and Sensors: A Review of Fundamental and Applied Aspects, Adv. Mater. 21 (2009) 29–53.
[89] P. Chen, Y. Fu, R. Aminirad, C. Wang, J. Zhang, K. Wang, et al., Fully Printed Separated Carbon Nanotube Thin Film Transistor Circuits and Its Application in Organic Light Emitting Diode Control, Nano Lett. 11 (2011) 5301–5308.
[90] N. Chiodarelli, S. Masahito, Y. Kashiwagi, Y. Li, K. Arstila, O. Richard, et al., Measuring the electrical resistivity and contact resistance of vertical

carbon nanotube bundles for application as interconnects, Nanotechnology. 22 (2011) 085302.
[91] R. Xie, M.H. van der Veen, K. Arstila, T. Hantschel, B. Chen, G. Zhong, et al., Carbon nanotube growth for through silicon via application, Nanotechnology. 24 (2013) 125603.
[92] M.H. van der Veen, B. Vereecke, C. Huyghebaert, D.J. Cott, M. Sugiura, Y. Kashiwagi, et al., Electrical characterization of CNT contacts with Cu Damascene top contact, Microelectron. Eng. 106 (2013) 106–111.
[93] L. Dai, D.W. Chang, J.-B. Baek, W. Lu, Carbon Nanomaterials for Advanced Energy Conversion and Storage, Small. 8 (2012) 1130–1166.
[94] K. Evanoff, J. Khan, A. a Balandin, A. Magasinsky, W.J. Ready, T.F. Fuller, et al., Towards Ultrathick Battery Electrodes: Aligned Carbon Nanotube–Enabled Architecture, Adv. Mater. 24 (2012) 533–537.
[95] C. Merino, P. Soto, E. Vilaplana-Ortego, J.M. Gomez de Salazar, F. Pico, J.M. Rojo, Carbon nanofibres and activated carbon nanofibres as electrodes in supercapacitors, Carbon N. Y. 43 (2005) 551–557.
[96] T. Matsumoto, T. Komatsu, K. Arai, T. Yamazaki, M. Kijima, H. Shimizu, et al., Reduction of Pt usage in fuel cell electrocatalysts with carbon nanotube electrodes, Chem. Commun. (Camb). 2004 (2004) 840–841.
[97] J.M. Lee, J.S. Park, S.H. Lee, H. Kim, S. Yoo, S.O. Kim, Selective Electron- or Hole-Transport Enhancement in Bulk-Heterojunction Organic Solar Cells with N- or B-Doped Carbon Nanotubes, Adv. Mater. 23 (2011) 629–633.
[98] N.M. Gabor, Z. Zhong, K. Bosnick, J. Park, P.L. McEuen, Extremely Efficient Multiple Electron-Hole Pair Generation in Carbon Nanotube Photodiodes, Science (80-.). 325 (2009) 1367–1371.
[99] J. Wei, Y. Jia, Q. Shu, Z. Gu, K. Wang, D. Zhuang, et al., Double-Walled Carbon Nanotube Solar Cells, Nano Lett. 7 (2007) 2317–2321.
[100] T. Kurkina, A. Vlandas, A. Ahmad, K. Kern, K. Balasubramanian, Label-Free Detection of Few Copies of DNA with Carbon Nanotube Impedance Biosensors, Angew. Chem. Int. Ed. Engl. 50 (2011) 3710–3714.
[101] D.A. Heller, H. Jin, B.M. Martinez, D. Patel, B.M. Miller, T.-K. Yeung, et al., Multimodal optical sensing and analyte specificity using single-walled carbon nanotubes, Nat. Nanotechnol. 4 (2009) 114–120.
[102] X. Shi, A. von dem Bussche, R.H. Hurt, A.B. Kane, H. Gao, Cell entry of one-dimensional nanomaterials occurs by tip recognition and rotation, Nat. Nanotechnol. 6 (2011) 714–719.
[103] S.Y. Hong, G. Tobias, K.T. Al-Jamal, B. Ballesteros, H. Ali-Boucetta, S. Lozano-Perez, et al., Filled and glycosylated carbon nanotubes for in vivo radioemitter localization and imaging, Nat. Mater. 9 (2010) 485–490.
[104] C.A. Poland, R. Duffin, I. Kinloch, A. Maynard, W.A.H. Wallace, A. Seaton, et al., Carbon nanotubes introduced into the abdominal cavity of mice show asbestos-like pathogenicity in a pilot study, Nat. Nanotechnol. 3 (2008) 423–428.
[105] G.M. Mutlu, G.R.S. Budinger, A.A. Green, D. Urich, S. Soberanes, S.E. Chiarella, et al., Biocompatible Nanoscale Dispersion of Single-Walled Carbon Nanotubes Minimizes in vivo Pulmonary Toxicity, Nano Lett. 10 (2010) 1664–1670.
[106] J.B. Oostinga, H.B. Heersche, X. Liu, A.F. Morpurgo, L.M.K. Vandersypen, Gate-induced insulating state in bilayer graphene devices, Nat. Mater. 7 (2008) 151–157.

[107] D.C. Elias, R.R. Nair, T.M.G. Mohiuddin, S. V. Morozov, P. Blake, M.P. Halsall, et al., Control of Graphene's Properties by Reversible Hydrogenation: Evidence for Graphane, Science (80-.). 323 (2009) 610–613.
[108] K.P. Loh, Q. Bao, P.K. Ang, J. Yang, The chemistry of graphene, J. Mater. Chem. 20 (2010) 2277–2289.
[109] K. Kim, J.-Y. Choi, T. Kim, S.-H. Choi, H.-J. Chung, A role for graphene in silicon-based semiconductor devices, Nature. 479 (2011) 338–344.
[110] L. Britnell, R.V. Gorvachev, R. Jalil, B.D. Belle, F. Schedin, A. Mishchenko, et al., Field-Effect Tunneling Transistor Based on Vertical Graphene Heterostructures, Science (80-.). 335 (2012) 947–950.
[111] X. Li, X. Wang, L. Zhang, S. Lee, H. Dai, Chemically derived ultrasmooth graphene nanoribbon semiconductors, Science (80-.). 319 (2008) 1229–1232.
[112] F. Schwierz, Graphene transistors, Nat. Nanotechnol. 5 (2010) 487–496.
[113] L. Liao, J. Bai, R. Cheng, Y.-C. Lin, S. Jiang, Y. Qu, et al., Sub-100 nm Channel Length Graphene Transistors, Nano Lett. 10 (2010) 3952–3956.
[114] S.-J. Han, K.A. Jenkins, A. Valdes Garcia, A.D. Franklin, A.A. Bol, W. Haensch, High-Frequency Graphene Voltage Amplifier, Nano Lett. 11 (2011) 3690–3693.
[115] Z.Q. Li, E.A. Henrisken, Z. Jiang, Z. Hao, M.C. Martin, P. Kim, et al., Dirac charge dynamics in graphene by infrared spectroscopy, Nat. Phys. 4 (2008) 532–535.
[116] F. Xia, T. Mueller, Y.-M. Lin, A. Valdes-Garcia, P. Avouris, Ultrafast graphene photodetector, Nat. Nanotechnol. 4 (2009) 839–843.
[117] T. Mueller, F. Xia, P. Avouris, Graphene photodetectors for high-speed optical communications, Nat. Photonics. 4 (2010) 297–301.
[118] T.J. Echtermeyer, L. Britnell, P.K. Jasnos, a Lombardo, R. V Gorbachev, a N. Grigorenko, et al., Strong plasmonic enhancement of photovoltage in graphene., Nat. Commun. 2 (2011) 458.
[119] M. Liu, X. Yin, E. Ulin-Avila, B. Geng, T. Zentgraf, L. Ju, et al., A graphene-based broadband optical modulator, Nature. 474 (2011) 64–67.
[120] Z. Sun, T. Hasan, F. Torrisi, D. Popa, G. Privitera, F. Wang, et al., Graphene Mode-Locked Ultrafast Laser, ACS Nano. 2 (2010) 803–810.
[121] Q. Bao, H. Zhang, B. Wang, Z. Ni, C.H.Y.X. Lim, Y. Wang, et al., Broadband graphene polarizer, Nat. Photonics. 5 (2011) 411–415.
[122] S. Chen, L. Brown, M. Levendorf, S.W. Cai, S.-Y. Ju, J. Edgeworth, et al., Oxidation Resistance of Graphene-Coated Cu and Cu/Ni Alloy, ACS Nano. 5 (2011) 1321–1327.
[123] X. Wang, L. Zhi, K. Müllen, Transparent, conductive graphene electrodes for dye-sensitized solar cells., Nano Lett. 8 (2008) 323–7.
[124] E. Yoo, J. Kim, E. Hosono, H.-S. Zhou, T. Kudo, I. Honma, Large Reversible Li Storage of Graphene Nanosheet Families for Use in Rechargeable Lithium Ion Batteries, Nano Lett. 8 (2008) 2277–2282.
[125] T.R. Nayak, H. Andersen, V.S. Makam, C. Khaw, S. Bae, X. Xu, et al., Graphene for Controlled and Accelerated Osteogenic Differentiation of Human Mesenchymal Stem Cells, ACS Nano. 5 (2011) 4670–4678.
[126] V.C. Sanchez, A. Jachak, R.H. Hurt, A.B. Kane, Biological Interactions of Graphene-Family Nanomaterials: An Interdisciplinary Review, Chem. Reseach Toxicol. 25 (2012) 15–34.
[127] G. Jiménez-Cadena, J. Riu, F.X. Rius, Gas sensors based on nanostructured materials, Analyst. 132 (2007) 1083–1099.

[128] M.E. Roberts, M.C. LeMieux, Z. Bao, Sorted and Aligned Single-Walled Carbon Nanotube Networks for Transistor-Based Aqueous Chemical Sensors, ACS Nano. 3 (2009) 3287–3293.
[129] N. Peng, Q. Zhang, C.La. Chow, O.K. Tan, N. Marzari, Sensing Mechanisms for Carbon Nanotube Based NH3 Gas Detection, Nano Lett. 9 (2009) 1626–1630.
[130] A. Oberlin, M. Endo, T. Koyama, Filamentous growth of carbon through benzene decomposition, J. Cryst. Growth. 32 (1976) 335–349.
[131] C. Kim, Y. Il Jeong, B.T.N. Ngoc, K.S. Yang, M. Kojima, Y.A. Kim, et al., Synthesis and Characterization of Porous Carbon Nanofibers with Hollow Cores Through the Thermal Treatment of Electrospun Copolymeric Nanofiber Webs, Small. 3 (2007) 91–95.
[132] B. Zhang, R. Fu, M. Zhang, X. Dong, L. Wang, C.U. Pittman, Gas sensitive vapor grown carbon nanofiber/polystyrene sensors, Mater. Res. Bull. 41 (2006) 553–562.
[133] J.S. Im, S.C. Kang, S.-H. Lee, Y.-S. Lee, Improved gas sensing of electrospun carbon fibers based on pore structure, conductivity and surface modification, Carbon N. Y. 48 (2010) 2573–2581.
[134] J. Kong, N.R. Franklin, C. Zhou, M.G. Chapline, S. Peng, K. Cho, et al., Nanotube molecular wires as chemical sensors, Science (80-.). 287 (2000) 622–625.
[135] P.G. Collins, K. Bradley, M. Ishigami, A. Zetti, Extreme Oxygen Sensitivity of Electronic Properties of Carbon Nanotubes, Science (80-.). 287 (2000) 1801–1804.
[136] A. Goldoni, R. Larciprete, L. Petaccia, S. Lizzit, Single-Wall Carbon Nanotube Interaction with Gases: Sample Contaminants and Environmental Monitoring, J. Am. Chem. Soc. 125 (2003) 11329–11333.
[137] P. Bondavalli, P. Legagneux, D. Pribat, Carbon nanotubes based transistors as gas sensors: State of the art and critical review, Sensors Actuators B Chem. 140 (2009) 304–318.
[138] D.R. Kauffman, A. Star, Carbon nanotube gas and vapor sensors., Angew. Chem. Int. Ed. Engl. 47 (2008) 6550–70.
[139] J. Kong, M.G. Chapline, H. Dai, Functionalized Carbon Nanotubes for Molecular Hydrogen Sensors, Adv. Mater. 13 (2001) 1384–1386.
[140] Q. Zhao, M.B. Nardelli, W. Lu, J. Bernholc, Carbon Nanotube–Metal Cluster Composites: A New Road to Chemical Sensors?, Nano Lett. 5 (2005) 847–851.
[141] A. Star, V. Joshi, S. Skarupo, D. Thomas, J.-C.P. Gabriel, Gas sensor array based on metal-decorated carbon nanotubes., J. Phys. Chem. B. 110 (2006) 21014–20.
[142] R. Ionescu, E.H. Espinosa, E. Sotter, E. Llobet, X. Vilanova, X. Correig, et al., Oxygen functionalisation of MWNT and their use as gas sensitive thick-film layers, Sensors Actuators B Chem. 113 (2006) 36–46.
[143] E.H. Espinosa, R. Ionescu, C. Bittencourt, a. Felten, R. Erni, G. Van Tendeloo, et al., Metal-decorated multi-wall carbon nanotubes for low temperature gas sensing, Thin Solid Films. 515 (2007) 8322–8327.
[144] R. Leghrib, E. Llobet, Quantitative trace analysis of benzene using an array of plasma-treated metal-decorated carbon nanotubes and fuzzy adaptive resonant theory techniques, Anal. Chim. Acta. 708 (2011) 19–27.

[145] M. Penza, R. Rossi, M. Alvisi, G. Cassano, M. a. Signore, E. Serra, et al., Pt- and Pd-nanoclusters functionalized carbon nanotubes networked films for sub-ppm gas sensors, Sensors Actuators B Chem. 135 (2008) 289–297.
[146] M. Penza, R. Rossi, M. Alvisi, G. Cassano, E. Serra, Functional characterization of carbon nanotube networked films functionalized with tuned loading of Au nanoclusters for gas sensing applications, Sensors Actuators B Chem. 140 (2009) 176–184.
[147] M. Penza, R. Rossi, M. Alvisi, E. Serra, Metal-modified and vertically aligned carbon nanotube sensors array for landfill gas monitoring applications., Nanotechnology. 21 (2010) 105501.
[148] C. Staii, A.T. Johnson, DNA-Decorated Carbon Nanotubes for Chemical Sensing, Nano Lett. 5 (2005) 1774–1778.
[149] N. Barsan, D. Koziej, U. Weimar, Metal oxide-based gas sensor research: How to?, Sensors Actuators B Chem. 121 (2007) 18–35.
[150] Y. Zilberman, R. Ionescu, X. Feng, K. Müllen, H. Haick, Nanoarray of Polycyclic Aromatic Hydrocarbons and Carbon Nanotubes for Accurate and Predictive Detection in Real-World Environmental Humidity, ACS Nano. 5 (2011) 6743–6753.
[151] L. Kong, J. Wang, F. Meng, X. Chen, Z. Jin, M. Li, et al., Novel hybridized SWCNT–PCD: synthesis and host–guest inclusion for electrical sensing recognition of persistent organic pollutants, J. Mater. Chem. 21 (2011) 11109–11115.
[152] M. Muoth, T. Helbling, L. Durrer, S.W. Lee, C. Roman, C. Hierold, Hysteresis-free operation of suspended carbon nanotube transistors, Nat. Nanotechnol. 5 (2010) 589–592.
[153] I. Childres, L.A. Jauregui, M. Foxe, J. Tian, R. Jalilian, I. Jovanovic, et al., Effect of electron-beam irradiation on graphene field effect devices, Appl. Phys. Lett. 97 (2010) 173109.
[154] Y. Dan, Y. Lu, N.J. Kybert, Z. Luo, A.T.C. Johnson, Intrinsic Response of Graphene Vapor Sensors, Nano Lett. 9 (2009) 1472–1475.
[155] J. Dai, J. Yuan, P. Giannozzi, Gas adsorption on graphene doped with B, N, Al, and S: A theoretical study, Appl. Phys. Lett. 95 (2009) 232105.
[156] J.T. Robinson, F.K. Perkins, E.S. Snow, Z. Wei, P.E. Sheehan, Reduced Graphene Oxide Molecular Sensors, Nano Lett. 8 (2008) 3137–3140.
[157] J.D. Fowler, M.J. Allen, V.C. Tung, R.B. Kaner, B.H. Weiller, Practical Chemical Sensors from Chemically Derived Graphene, ACS Nano. 3 (2009) 301–306.
[158] W. Li, X. Geng, Y. Guo, J. Rong, Y. Gong, L. Wu, et al., Reduced Graphene Oxide Electrically Contacted Graphene Sensor for Highly Sensitive Nitric Oxide Detection, ACS Nano. 5 (2011) 6955–6961.

3. Experimental section

3.1. Synthesis and treatment processes

3.1.1. Carbon nanofibers

Carbon nanofibers were synthesised in Grupo Antolín Ingenieria using the floating catalysit method [1]. A scheme of the synthesis procedure is presented in Figure 1 [2]. In this synthesis technique, the precursors are introduced in the top end of a vertical furnace. These precursors are composed by the metal precursor, this case nickel, and natural gas that will act as the carbon source. A small quantity of sulphur is added in order to stabilize the reaction. All the process is done in hydrogen reducing atmosphere.

Then, when the precursor are introduced, the high temperatures dissociate the nickel precursor forming nickel nanoparticles that will act as catalytic seeds for its reaction with the carbon atoms obtained from the decomposition of the natural gas. By this way, the carbon nanofiber is formed. During the synthesis, the newly formed nanofibers falls through the vertical furnace to the bottom region, where can be collected.

The obtained carbon nanofibers are of the type helical-ribbon (or stacked-up). Its external diameter can range from 50 to 100 nm, meanwhile its interior diameter falls between 20 and 50 nm. FESEM images (Fig. 2) show highly tangled carbon nanofiber material but the images suggest that the nanofibers have a very high aspect ratio. This is confirmed by TEM imaging (Fig. 3). Moreover it can be seen that the carbon nanofibers posses an high crystanillity as the carbon planes can

be seen perfectly in spite of the disruptive presence of the nickel catalyst nanoparticles.

In order to increase the crystalline quality the carbon nanofibers are treated following a process called graphitication. In this process, the nanofibres are annealed at high temperatures around 2800ºC in a reducing atmosphere, usually argon. This process eliminates the impurities left by the synthesis process like the nickel catalyst and enhances the crystal structure of the carbon nanofibers. This can be seen in the Raman spectrum of the nanofibers, as the graphitication process increases the G/D ratio of the nanofibers.

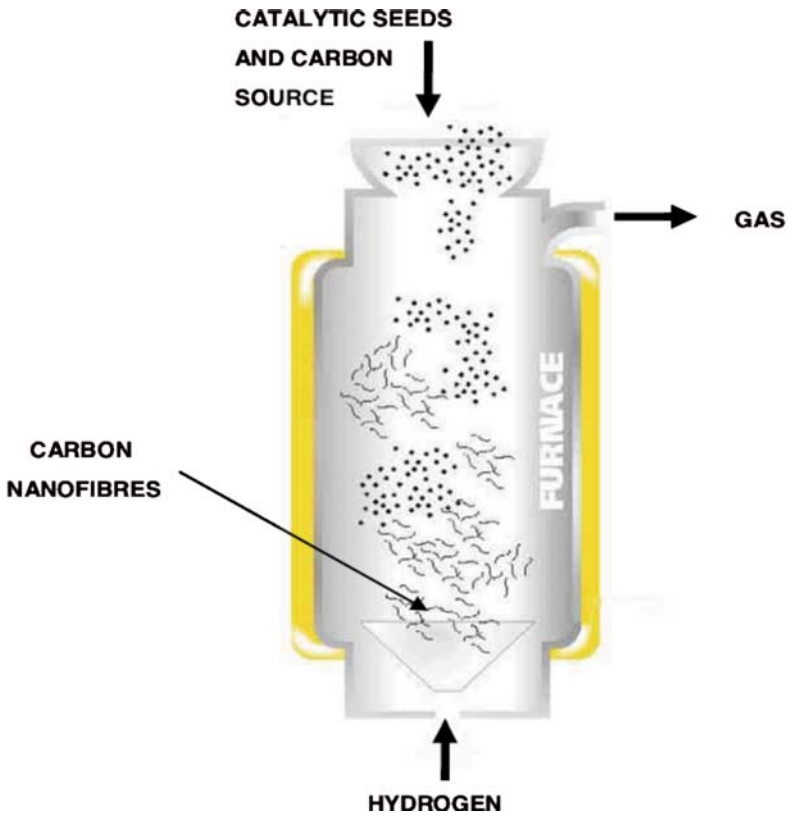

Figure1. Schematic illustration of the synthesis of carbon nanofibers by the floating catalyst method. Adapted from [2]

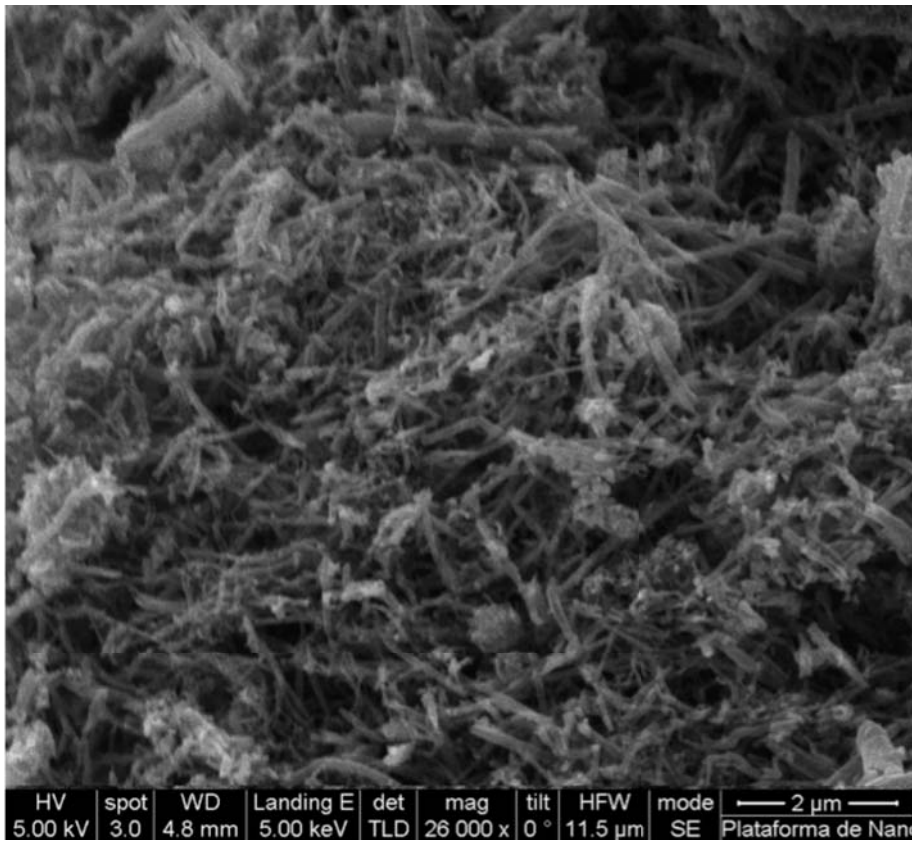

Figure 2. FESEM image of the as synthesised carbon nanofibers.

3.1.2. Graphene oxide and reduced graphene oxide

Graphene oxide was synthesised using a modified Hummers method [3–5]. The idea is to strongly oxidize the carbon nanofibers in order to separate the graphitic layers. In order to achieve this, the nanofibers are first mixed in sulphuric acid and potassium permanganate. Then, the mix is heated up to around 55ºC for finish the reaction. Afterwards the temperature is increased again to 70ºC and is let to stabilize. Then the solution is left to cool down to room temperature to later being poured over 400 ml of ice of oxygenated

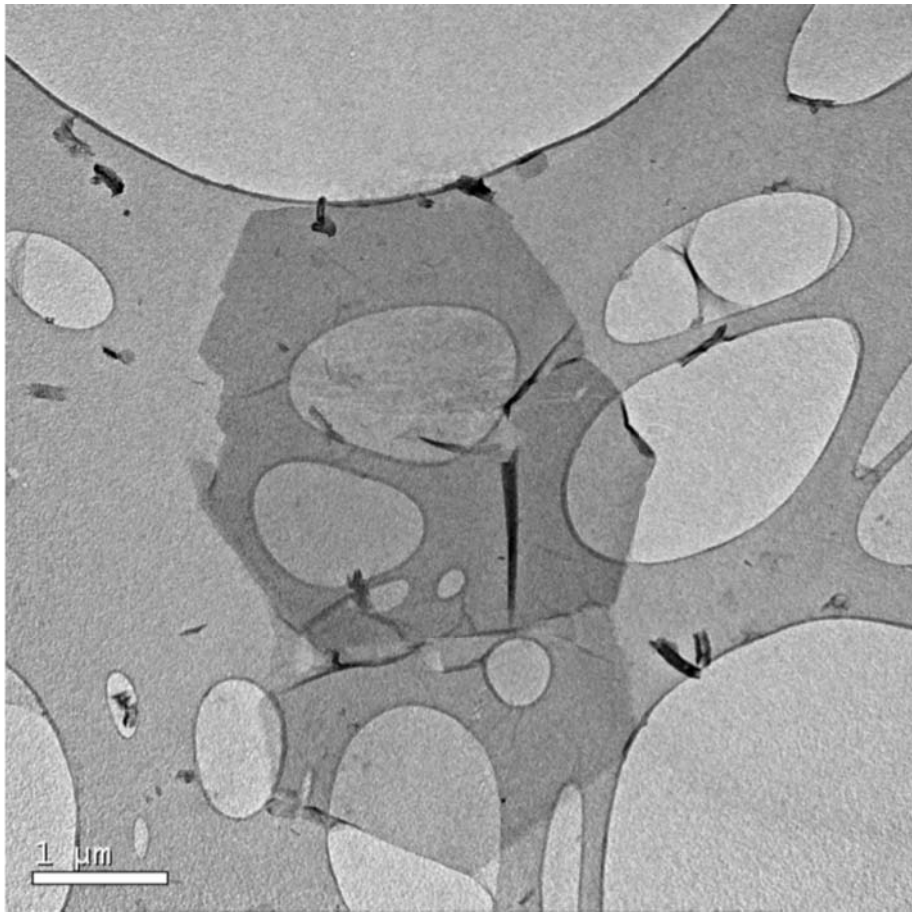

Figure 3. TEM image of a graphene oxide platelet obtained by the modified Hummers method using the carbon nanofibers as a starting material.

water. The oxygenated water consumes the residues of $KMnO_4$ and prevents the precipitation of MnO_2 [4]. The filtered solid is cleaned with distilled water and is flocculated with a dissolution of 20% HCl before filter again. The recovered material is cleaned with ethanol and is filtered again.

This material still is not graphene oxide, as is needed to exfoliate it. In order to do it, the material is dissolved in isopropanol, acetone or water and is sonicated with an ultrasonic tip with a power of 30W during 2 hours, with ON-OFF intervals of 1 minute each. The graphene oxide obtained (Fig. 4) is fully stable in polar solvents.

Because the type of reaction used to synthesise the graphene oxide the material ends up totally oxidized. This material is totally insulator and although may be useful for some applications [6–8] is interesting to try to reduce this material in order to recover the graphene characteristics [9–11]. In this work have been studied three kinds of reduction techniques:

- Thermal reduction

In this case, the graphene oxide is treated at temperatures around 2800ºC in vacuum during a short period of time with the objective to eliminate the functional groups by burning them out [12]. The major drawback is that is a explosive reaction, as the functional groups are burned out at almost the same time and surely the structure will be damaged. The process has been done at Grupo Antolín Ingenieria installations.

- Chemical reduction

As the name indicates, with this method the graphene oxide is mixed with a reducing chemical that will react with the oxygen functional groups, eliminating them. In spite that a chemical reaction could be more controllable, depending of what reducing chemical is used is possible to damage the graphene structure. In our studies were used two reducing agents:

- Hydrazine: in this case was followed the Stankovich method [13], were the GO aqueous dispersion is mixed with hydrazine hydrate and heated at 100ºC over 24ºC. The obtained product is filtered and washed with water and methanol.
- Vitamin C: first the pH of the GO dispersion was adjusted to 9-10 using an ammonia solution of 25%. After that Vitamine C (2mM) was added, and the solution is heated at 95ºC during 15 min [14]. The obtained product is filtered with a PVDF membrane.

The chemical reduction was performed by Dr. David López Díaz and Prof. Mecedes Velazquez at Universidad de Salamanca.

- Plasma etching

In this strategy the graphene oxide surface is bombarded by reducing ions like Ar or N generated from a cold plasma. It was used a Plasma Cleaner PDC-002, a model that have three different energies: low (7.16 W), medium (10.15 W) and high (29.6 W). The processes have been preformed with argon gas at times of 30min, 1h, 1h 30 min and 2h. This process was done at the Clean Room of the Physics Faculty at the University of Barcelona.

3.1.3. Decoration of carbon nanofibers

In order to enhance the selectivity and sensitivity of the future gas sensors that use carbon nanofibers as a sensing layer, a metal decoration have been performed over the nanostructures. First the CNFG are annealed at 400ºC during 3 hours in a oxygen atmosphere in order make them stable in polar solvents. After that, a 1mg/ml solution of CNFG in acetone is done and is sonicated during 30 min. When the solution is stable, the metal precursor is added. Could be $AuCl_3$ or $PdCl_2$, in the concentration desired respect the CNFG (in our case, 2%, 20% or 50%). The resulting solution is again sonicated during 30 min in order to homogenize the mixture. The next step is proceeding to a ball milling process. The solution is poured in two cylindrical zirconia containers with three 4-mm zirconia balls inside. After closing the containers these are introduced into the ball miller to make the process. The containers will have an orbital movement: one movement circular around the centre the machine in addition a rotation around its own axis. The rotation velocity is 2500 rpm. With this treatment the wetting of the surface of the nanofiber with the metal precursor will be maximized. Next the solvent of the solution obtained is evaporated, obtaining the dry nanofibers with the metal precursor that will be annealed again at 400ºC during 3h in an oxygen atmosphere. This will result with the carbon nanofibers decorated with nanoparticles of the metal desired (Au or Pd).

3.2. Analysis techniques

The study of the different carbon nanostructures needs a wide range of analysis techniques. These include morphological, structural and chemical analysis techniques in order to fully characterize the nanostructures.

3.2.1. Field-Emission Scanning Electron Microscopy (SEM)

With a SEM microscope is possible to obtain high resolution images of a surface. This instrument emits electrons from a cathode source that are accelerated towards an anode. The electrons can be emitted either thermally or by field-emission, being the later one the technique with the better resolution. The electron beam energy can go from hundred of eV to 50 eV. The electrons scan the sample and a detector counts the quantity of electrons coming form the sample. Depending on the signal measured is possible also to distinguish differences between elements (backscattering) or qualitatively obtain the amount of the elements present in the surface (EDX).

The FESEM images of this work were acquired in a Nova NanoSEM 230-FEI microscope located at the Parc Cientific de Barcelona (PCB), using the high-resolution detector in high-vacuum (HV) mode, usually applying an accelerating voltage of 10kV.

3.2.2. Transmission Electron Microscopy (TEM)

In this technique, similar to SEM, the sample is bombarded with electrons. But instead of analyse the secondary electrons emitted by the sample are the electrons that cross the sample that are detected. Because this, the samples have to be very thin. In our case, both carbon nanofibers and graphene are ideal for TEM analysis. The TEM microscope used in this study is a JEOL 2100 TEM located at Centres Cíentifics I Tecnològics de la Universitat de Barcelona (CCiTUB)

3.2.3. Atomic Force Microscopy (AFM)

This microscope is a mechanical-optical instrument with the capacity to detect forces in the range of pN. Basically consist of a small tip coupled at the end of a very flexible lever usually made of silicon. Using a laser is possible to control the flexion of this lever that is caused by an interaction between the atoms of the tip with the atoms of the sample. There are different modes of operation of the AFM but usually the tapping mode is used. In this mode, the cantilever is oscillating near its resonance frequency very close to the surface. When there is change in the height of the sample, the oscillating frequency of the cantilever changes that is detected by a sensor. The signal generated is introduced into a feedback system that controls a piezoelectric actuator that controls the height of the tip over the surface, moving it away (or closer) of the sample until the original oscillating frequency is

recovered. By this way, is possible to obtain the topography map of the sample by scanning the plane of its surface (Fig. 4).

The equipment used in this thesis is a Dimension AFM microscopy located at the CCiTUB.

3.2.4. Elemental analysis CHNS-O

The Elemental Analysis technique measures the mass percentage of C, H, N and S of the sample. The quantity of oxygen is

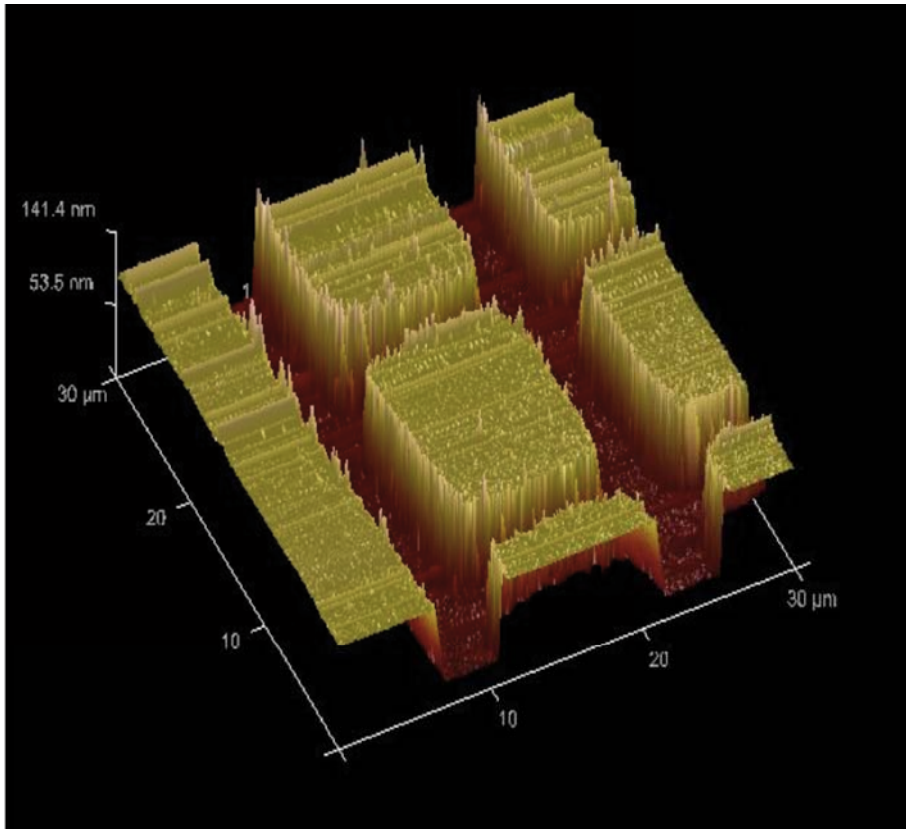

Figure 4. Example of a topographic measurement with tapping-mode AFM of an etched silicon substrate

estimated by difference up to 100 of the sum of the percentages of C, H, N, and S and the quantity of ashes obtained by calcination in a high temperature oven.

The technique consists in the flash combustion of the samples in an oxygen atmosphere at high temperature. The generated gases, usually CO_2, H_2O, SO_2 and N_2 cross a gas chromatograph with a detector of thermal conductivity (TCD). The signal obtained is compared with a pattern, permitting the quantification of these complexes.

The equipment used to do the measurements was a Thermo EA 1108 CHNS-O Carlo Erba Instruments located at the CCTiUB.

3.2.5. Thermogravimetric analysis (TGA)

This analysis technique is based in the measurement of the variation of the mass of the sample when is put through to a programmed temperature variation in a controlled atmosphere. The variation of mass could be positive or negative. Is possible to couple the thermogravimetry with other techniques, like DTA or DSC.

The equipment used is a Thermobalance TGA-SDTA 851e/SF/1100 of Mettler Toledo located at the CCTiUB.

3.2.6. X-ray photoelectron spectroscopy (XPS)

XPS is technique capable to measure the stoichiometry, chemical state and the electronic structure of the elements present in a material. For this, a sample is irradiated with X-rays and the energy and number of the electrons that escapes from the surface of the sample. Is important to note that the technique only analyses the surface of the sample, as only probes 2-5 nm deep into the sample.

The equipment used is a photoelectron spectroscope PHI ESCA-5500 located at the CCiTUB installations. Two kind of analysis were performed: a survey analysis that is a low resolution XPS spectra in all of the energy range in order to detect the main peaks and a multiplex measurement, where a more high resolution XPS spectra centred in the peaks of interest are performed.

The analysis of the peaks is done with the commercial program MultiPak V6.0A from Physical Electronics (Fig 5). With this programme are obtained the atomic percentages of the elements from the survey analysis meanwhile is possible to perform a detailed study of the high resolution peaks obtained with the multiplex, among other applications. The adjustment of the peaks is done using a Shirley baseline and the peaks are a combination of Gauss and Lorentz shapes. Instead of using fixed values these are permitted to vary in a given range that has been previously defined for obtaining a better fit (see Chapter 4 for more details).

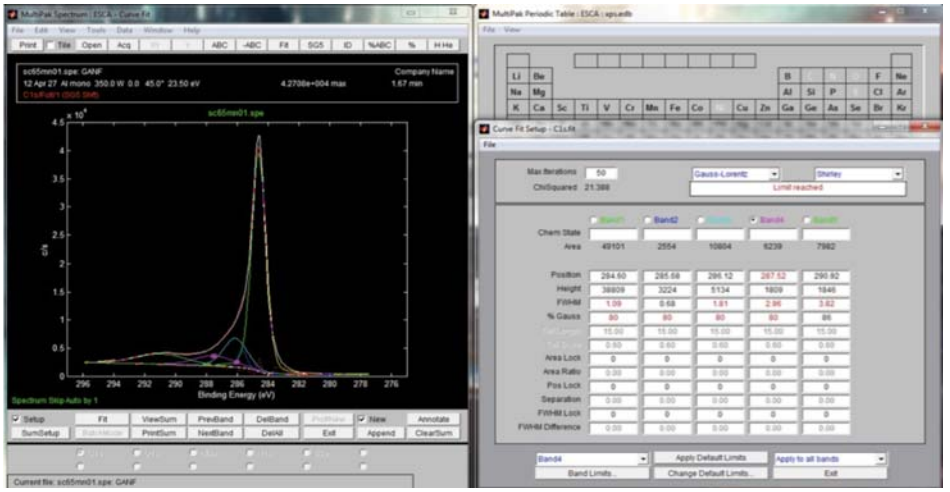

Figure 5. Image of the Mulltipak interface that allows the deconvolution of a main peak, in this case the C1s peak of a carbon nanofibers sample.

3.2.7. X-Ray powder diffraction (XRD)

In XRD analysis a monochromatic X-ray is irradiated towards a sample with a incident angle θ respect a family of crystallographic planes (hkl) and then is diffracted forming an angle 2θ. This reflection only can occur if the Bragg law is satisfied:

$$\eta \cdot \lambda = 2 \cdot d_{hkl} \cdot \sin(\theta)$$

Where λ in the wavelength of the incident radiation, d_{hkl} is the distance between the planes (hkl) and η is the refraction index of the family of planes.

Moreover, is possible to compute the grain size in the sample using the Scherrer formula:

$$D = \frac{\lambda}{\beta \cdot \cos\theta}$$

Where D is the mean grain size, λ is the wavelength of the incident beam, θ is the angle of the reflections and β is the ratio between the area and the intensity of the analysed reflection.

The equipment used was a PANalytical X'Pert PRO MRD located at the CCiTUB, using Cu Kα radiation (λ=1.540598 Å) with a operating voltage of 45 kV and current of 40 mA. Data were collected in steps of 0.025 degrees from 5 to 100 degrees (2θ) during 195 seconds per step.

3.2.8. Raman spectroscopy

This technique is based in the inelastic scattering of light first observed by Sir Chandrasekhara Venkata Raman in 1928 (Fig. 6). When light (usually a monochromatic laser) is focused over a material its interaction with phonons or other excitations in the system makes that the photons energy becomes shifted up or down. This shift can be measured and information about the system obtained as each element has its own active vibrational modes, permitting us make chemical or structural analysis. Raman spectroscopy is a very versatile technique as is not destructive and is possible to use excitation lasers from IR to UV, permitting us to activate o deactivate certain vibrational modes in some cases.

The equipment used is a Raman microscope Horiba Jobin-Yibon HR800 LabRam located at the CCiTUB. The excitation laser have a wavelength of 532 nm, the objective used 50x and the incident power was regulated at 0.5 mW using the filters of the microscope in order to avoid burning the sample. As a reference the Raman spectra of the Si was acquired, checking the main band at 520.7 cm^{-1}. Usually the carbon spectrum was acquired with an average of 3 spectrums of 15 seconds each. In order to obtain a statistically confident measurement, 6 spectrums have been done for each sample measured.

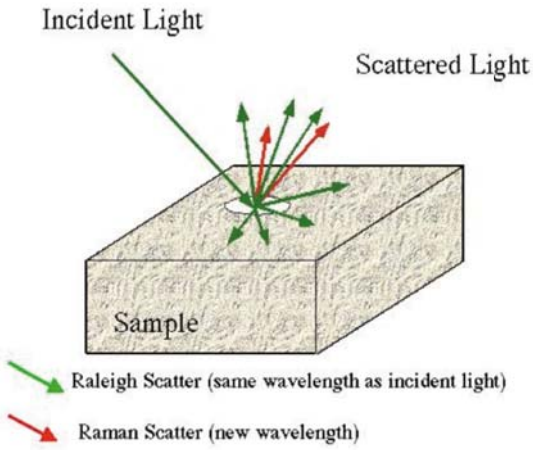

Figure 6. Schematic explanation of principle of Raman scattering.

3.3 Deposition techniques

3.3.1. Drop coating and spin coating

Carbon nanofibers and graphene like materials have been deposited on SiO_2/Si substrates in order to be characterized in different techniques like FESEM or Raman spectroscopy.

Drop coating method was the standard deposition technique for its ease and quick application. After the sample is dispersed in isopropanol, around 20μl are drop casted over a 1cmx1cm SiO_2/Si substrate using a micropipette. The substrate has the native oxide layer (around 2nm) that facilitates the observation in FESEM avoiding any charging effects. The drop is dried in an oven at 70ºC. This temperature is selected as is near the boiling point of isopropanol (82 ºC), promoting the rapid evaporation of the solvent and minimizing the coffee-ring effect. When the solvent is evaporated, the temperature is increased to 100ºC and later the substrate is placed inside a vacuum chamber in order to eliminate the possible isopropanol residues.

In order to totally avoid the coffee-ring effect another method have to be used. Because the planar geometry of the graphene oxide layers spin-coating is one of the ideal methods of deposition for fabrication of layers. First, a 1cmx1cm SiO_2xSi substrate is placed over the rotor and secured using a vacuum line. Then, a 10 μl drop of solution is casted at the centre of the substrate. After closing the spinner, this is activated. The substrate is spinned up from 0 rpm to

2000 rpm with an acceleration time of 600s. After reaching the final 2000 rpm velocity the process is maintained 1000 s more. After the process a homogenous layer of graphene oxide platelets is obtained (Fig. 7). The superficial concentration can be adjusted by repeating the process several times. Usually 6 processes results in a continuous layer of graphene oxide.

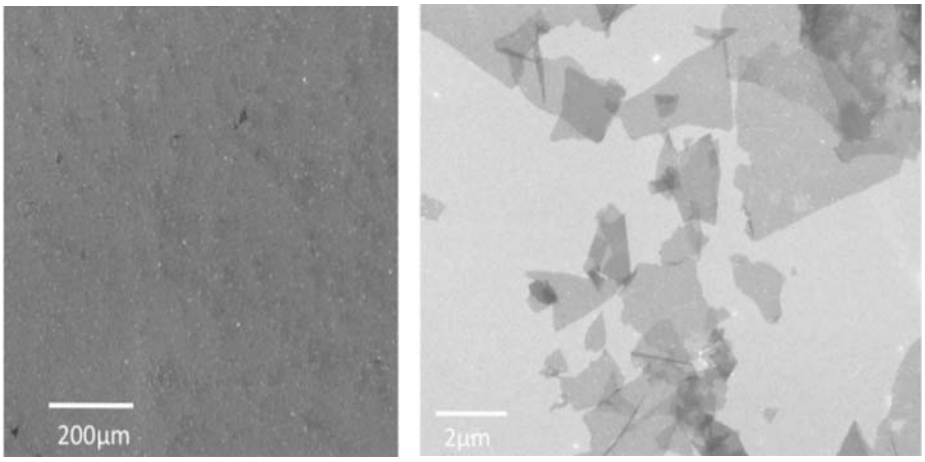

Figure 7. Example of graphene oxide platelets deposited by the spin-coating method after one process.

3.3.2. Langmuir–Blodgett method

With this technique is possible to create homogenous films over a suitable substrate [15]. All the process is done in a special pool filled with a liquid, usually water. Over this liquid a subphase of material by drop casting a solution which solvent is insoluble with the liquid of the pool. When the layer subphase is formed, a substrate is dipped and the subphase layer carefully compressed in order to increase the superficial density of molecules of the material until obtain a continuous layer. Finally, the substrate is pulled out gently in order to achieve the

transference of the subphase layer to the substrate (Fig. 8). Is possible to create multilayer coatings by repeating the process.

Dr. David López and Prof. Mercedes did the Langmiur-Blodgett deposits of GO and rGO at the installations of Universidad de Salmanca. The Lagmuir-Blodgett system used was a KSV2000 System 2 from KSV meanwhile the pressure-area isotherms of the material were recorded on a Langmuir Minitrough (KSV). Both systems were placed on an antivibration table. The GO sheets were transferred from the air/water interface onto silicon by symmetric barrier compression (50 mmmin^{-1}) of the substrate into the through by vertically dipping it up at 5mmmin^{-1}. The spreading solution (0.1 mg mL^{-1}) was deposited onto the water subphase with a micrometer Hamilton syringe with a precision of 1 μL. The surface pressure was measured with a Pt Wilhelmy plate connected to an electrobalance. The subphase temperature was maintained at 20.0±0.1 ºC by flowing thermostated water through jackets at the bottom og the trough. The temperature close to the surface was measured with a calibrated sensor from KSV,

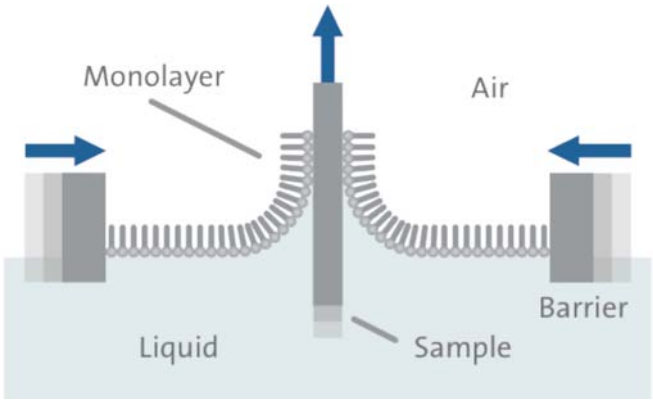

Figure 8. Schematic illustration of the Langmuir-Blodgett technique.

while the water temperature was controlled by means of a Lauda Ecoline RE-106 thermostat/cryostat.

3.4. Flexible gas sensor fabrication

The objective is to fabricate a flexible gas sensor using the carbon nanofibers supplied by Grupo Antolín Ingenieria. The fabrication is divided in 2 parts: for one hand the fabrication of the metal contacts, and on the other hand the deposition of the carbon nanofibers over these. For this reason two types of techniques have been combined: ink-jet printing for the metal contacts and electrospray deposition for the carbon nanofibers deposition.

3.4.1. Ink-jet printing

This technology has emerged as a serious alternative for the on-demand electronic fabrication as wide range of materials can be ink-jet printed using the suitable ink. This technique could fill the gap between microelectronic fabrication and the more classical Printed Circuit Board (PCB) fabrication techniques. In this case, the ink-jet printer used Xenjet 4000 from Xennia Technology Ltd (UK) with a cartridge Omnidot 760 (Xaar, Ltd., UK) based on piezoresistive technology to eject the ink (Fig. 9)

Figure 9 Picture of the Xenjet 4000 printer from Xeni Ltd.

Kapton film (poly(4,4'-oxydiphenylene-pyromellitimide)), purchased from DuPont, with thickness of 50 μm was chosen as a flexible substrate. This kind of material is suitable for electronic circuitry, as it has a typical dielectric strength of 240kV/mm [16]. Moreover, this polyimide can be heated up to 350 ºC, as a second order thermal glass transition occurs between 360 ºC and 410 ºC [16]. This is one of the main advantages compared to other polymers, as it allows us to do moderate thermal treatments of the materials deposited over the kapton substrate. This kind of material also displays good flexibility and mechanical resistance. Like most of the polymers, kapton films have a low mass, which makes it more resistant to vibration and sudden mechanical energy transfers. This makes it suitable for future devices of enhanced reliability to be used in environments where mechanical

resistance is a special concern, such as automotive applications. All these points justify the election of kapton.

The metal contacts were fabricated by inkjet printing using commercial silver ink U5603 (Suntronic Inc., USA) with 20% wt. of silver. Once the ink was deposited, the circuits were cured at a temperature of 150 ºC, sufficient for evaporating the ink solvent. In Figure 1 we can see the circuit design used in this work. Both sides of the kapton substrate were printed (Fig. 10). In the topside, there is an array of 4 interdigitated sensor electrodes with their connection pads. In the bottom side, there is a heater that covers all four interdigitated electrodes. All the connection pads were designed to fit in a clamp-like connector.

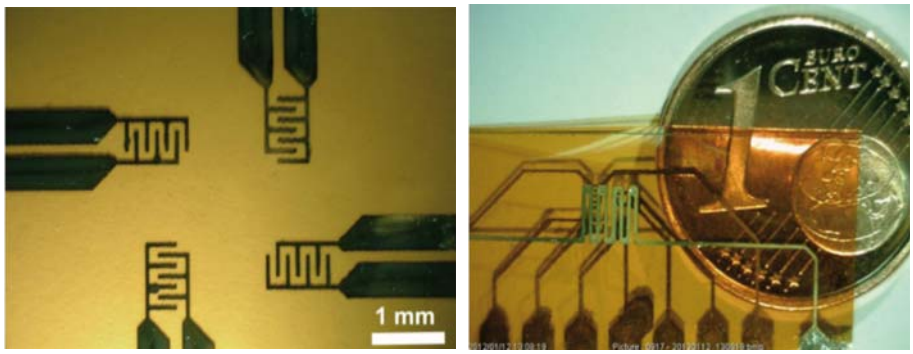

Figure10. Optical image of the four interdigitate sensor configuration (left) and the heater printed in the other side of the kapton substrate (right).

The heater was calibrated applying pulses power from 0 to 450 mW of power and using a thermographic camera (NEC Thermoshot F30) to monitor its temperature. Figure 11 shows an infrared image of the heater. We can see that only the heater increase its temperature, which seems to be fairly constant in all the structure.

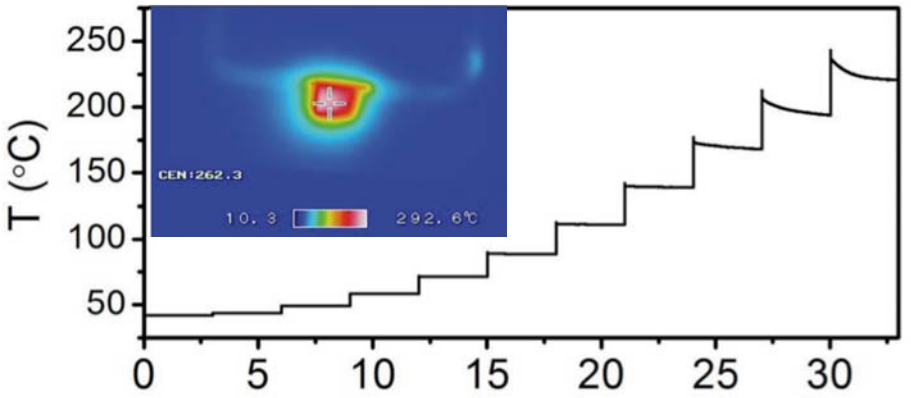

Figure 11. Infrared image of the heater during its operation (inset) and variation of the temperature respect time. It can be seen clearly a change in the heater response around 150 ºC.

In order to stabilize the heater thermal response, its temperature was steadily increased. This process revealed a change in the slope of the temperature vs. power plot (Fig. 12). Below the curing temperature (150 ºC), the heater response is stable and repeatable. Above the curing temperature, further annealing of the metal seems to occur, possible related to the elimination of the remaining the organic residues of the ink. This results suggest that 1) the metal depositions produced by these method must be thermally stabilized at temperatures above their expected operation temperature and 2) that the annealing process can be, at least partially, carried out using only the self- heating effect in the heater.

3.4.2. Electrospray depostion

The electrospray technique is based in the atomization of a liquid using strong electric fields. The first observation of the phenomena was in the 16th century by William Gilbert, and later

described mathematically by Lord Raighley and Sir. Geoffrey Ingram Taylor. Under the influence of a strong electric field a droplet will deform because the displacement of the internal charges. At one point the surface tension will not be enough for maintain the integrity of the droplet and a jet of liquid will be ejected and later will disintegrate into droplets. Electrospray have been already used to form thin films of different materials [17,18] and will be interesting for the case of carbon nanofibers for generate the sensing layers of the gas sensors.

The electrospray equipment is a commercial Yflow Electrospinner 2XX (Fig. 12). This equipment has two high voltage sources, one for the emitter (metallic needle) and other for the collector. Moreover, have two pumps as is possible to work in coaxial configuration. Also is equipped with a video camera for controlling the

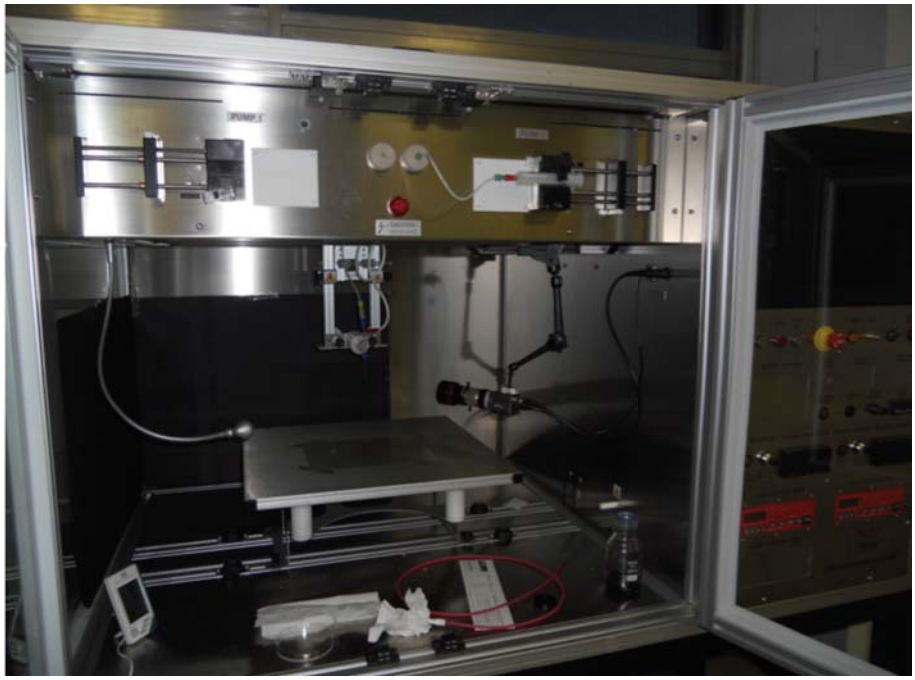

Figure12. Picture of the electrospinner system used.

Taylor cone and make easier control the deposition.

For achieve a good deposition the electrospinner was modified slightly. First of all, the interdigitated sensor was connected directly to the negative voltage source (Fig. 13). This was done for try to focus directly the jet of droplets into the sensor electrode in order to increase the rate of deposition and decrease the time of contact. It was found necessary to cover the pads of the sensor with alumina to avoid the deposition there. The alumina protection has two roles: physical, as

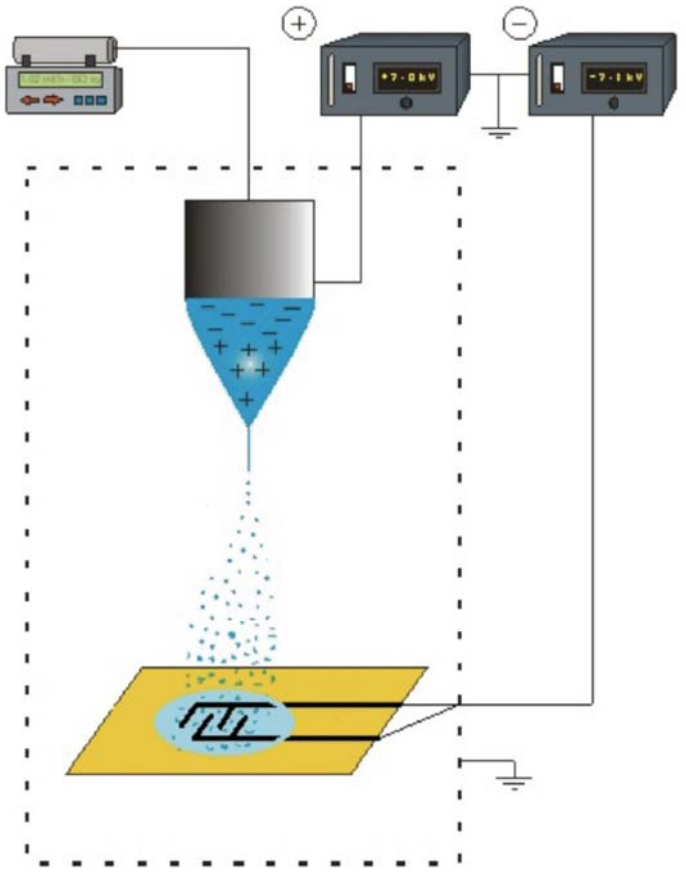

Figure13. Schematic illustration of the electrospray deposition used.

avoids that the droplets fall between undesired pads, and electrostatic, as deflects the electrical field in order to further focalize the electric field over the metal contacts of the sensor. Usually isopropanol was used as a carrier solvent, as shows the best jet stability. As have a relatively high boiling point (82ºC), when the deposition is done at room temperature there is a risk to fully wet the deposition surface, as there is no time to dry the isopropanol, thus loosing the deposited layer. In order to avoid this, a heater carpet is placed under the sensor.

Because the high voltages managed by the electropinner (up to 15kV) is necessary to electrically isolate the charged sensor of the heater in order to avoid hazardous sparks. In our case a thick piece of glass was enough. With this configuration is possible to heat up the substrate until 60 ºC, obtaining a faster dry of the isopropanol droplets and a better depostion.

The precursor solution is treated CNFG (see Chapter 4 for details) mixed in isopropanol in a concentration around 0.5 mg/ml. After 30 min of sonication (in order to obtain a good CNFG dispersion) the solution is transferred into a srynge and pumped in the electrospinner at a rate of 0.5 ml/h. The negative voltage is set at -12 kV meanwhile the positive voltage is set at around 3 kV. The voltages may vary slightly between depositions by variations of external temperature and humidity, but the stability of the jet can be controlled using the video camera.

With this configuration and deposition conditions is possible to deposit material only over a relatively big interdigitate electrode (0.5x0.5 mm) without the use of any masks (Fig 14a). The minimum time of deposition until there is electrical contact between pads is

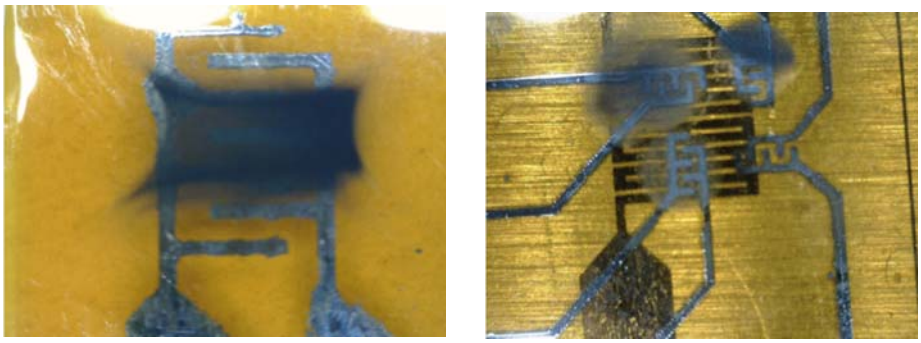

Figure 14 Deposition over a 0.5x0.5 mm electrode (left) and deposition over the 4-interdigitate electrode used in the measurements (right).

around 15-20 min for this kind of electrode. Also is possible to deposit to smaller electrodes (Fig 14b), like the four-interdigitated electrodes presented in the ink-jet printing section. In this case, is necessary to charge only the objective electrode and use a kapton mask in order to avoid the fall of material on the other electrodes. In this case, the time of contact is reduced to 5 min approx.

3.4.3. Gas sensor measurement

Sensing characterization was carried out in a gas test system conceived to characterize micro and nanodevices, wich included a MPG-2 gas mixer (Gometrics S.L., Spain) and a Keithley 4200-SCS Semiconductor Characterization System equipped with 3 sourcemeter units. A LabVIEW program controlled all these components. The experiments were exclusively performed in a customized chamber of 15 ml in volume, using a gas flow of 200 ml/min. The gases used were NH3 with a concentration of 500 ppm in synthetic air (SA, which contains 21% of O2 diluted in 79% of N2) and NO2 (5 ppm in SA).

References

[1] I. Martin-Gullon, J. Vera-Agullo, J.A. Conesa, J.L. González, C. Merino, Differences between carbon nanofibers produced using Fe and Ni catalysts in a floating catalyst reactor, Carbon N. Y. 44 (2006) 1572–1580.

[2] G. Antolín, GANF Hoja Técnica, n.d.

[3] W.S. Hummers, E.E. Offeman, Preparation of Graphitic Oxide, J. Am. Chem. Soc. 80 (1958) 1339–1339.

[4] D. V. Kosynkin, A.L. Higginbotham, A. Sinitskii, J.R. Lomeda, A. Dimiev, B.K. Price, et al., Longitudinal unzipping of carbon nanotubes to form graphene nanoribbons, Nature. 458 (2009) 972–876.

[5] H. Varela-Rizo, I. Rodriguez-Pastor, C. Merino, I. Martin-Gullon, Highly crystalline graphene oxide nano-platelets produced from helical-ribbon carbon nanofibers, Carbon N. Y. 48 (2010) 3640–3643.

[6] Y. Zhu, S. Murali, M.D. Stoller, A. Velamakanni, R.D. Piner, R.S. Ruoff, Microwave assisted exfoliation and reduction of graphite oxide for ultracapacitors, Carbon N. Y. 48 (2010) 2118–2122.

[7] H.Y. Jeong, J.Y. Kim, J.W. Kim, J.O. Hwang, J.-E. Kim, J.Y. Lee, et al., Graphene oxide thin films for flexible nonvolatile memory applications., Nano Lett. 10 (2010) 4381–6.

[8] S.-S. Li, K.-H. Tu, C.-C. Lin, C.-W. Chen, M. Chhowalla, Solution-processable graphene oxide as an efficient hole transport layer in polymer solar cells., ACS Nano. 4 (2010) 3169–74.

[9] J.T. Robinson, F.K. Perkins, E.S. Snow, Z. Wei, P.E. Sheehan, Reduced Graphene Oxide Molecular Sensors, Nano Lett. 8 (2008) 3137–3140.

[10] H. a Becerril, J. Mao, Z. Liu, R.M. Stoltenberg, Z. Bao, Y. Chen, Evaluation of solution-processed reduced graphene oxide films as transparent conductors., ACS Nano. 2 (2008) 463–70.

[11] P.H. Wöbkenberg, G. Eda, D.-S. Leem, J.C. de Mello, D.D.C. Bradley, M. Chhowalla, et al., Reduced graphene oxide electrodes for large area organic electronics., Adv. Mater. 23 (2011) 1558–62.

[12] S.H. Huh, Thermal Reduction of Graphene Oxide, Eng. Technol. (2010).
[13] S. Stankovich, D. a. Dikin, R.D. Piner, K. a. Kohlhaas, A. Kleinhammes, Y. Jia, et al., Synthesis of graphene-based nanosheets via chemical reduction of exfoliated graphite oxide, Carbon N. Y. 45 (2007) 1558–1565.
[14] M.J. Fernández-Merino, L. Guardia, J.I. Paredes, S. Villar-Rodil, P. Solís-Fernández, A. Martínez-Alonso, et al., Vitamin C Is an Ideal Substitute for Hydrazine in the Reduction of Graphene Oxide Suspensions, J. Phys. Chem. C. 114 (2010) 6426–6432.
[15] R.W. Corkery, Langmuir−Blodgett (L−B) Multilayer Films, Langmuir. 13 (1997) 3591.
[16] DuPont Kapton HN polymide film [online], (n.d.).
[17] a. Jaworek, Electrospray droplet sources for thin film deposition, J. Mater. Sci. 42 (2006) 266–297.
[18] a. Jaworek, a. T. Sobczyk, Electrospraying route to nanotechnology: An overview, J. Electrostat. 66 (2008) 197–219.

4. Carbon nanofibers

4.1 Graphitication effects over the CNF surface

As grown carbon nanofibers collected directly from the end of the reactor tube have different contaminants as a result of the precursors and gases used for the synthesis [1]. Chemical analysis of the surface of the nanofibers using XPS confirms the presence of nickel, sulphur and oxygen a part of pure carbon. This corresponds with the chemical compounds used for the synthesis of the CNF, being nickel the catalyst, sulphur the residue from the stabilizing agent and oxygen as an undesired product of the natural gas used as a carbon source. From the point of view of gas sensors, these undesired elements present in the nanofiber surface may adsorb or desorbs gas species that may interfere with the real measurement generating noise in the sensor signal [2]. Moreover, these different chemicals may change the nanofiber physical properties respect to pure carbon nanofiber. For this reason is necessary a process to eliminate these undesired products. An

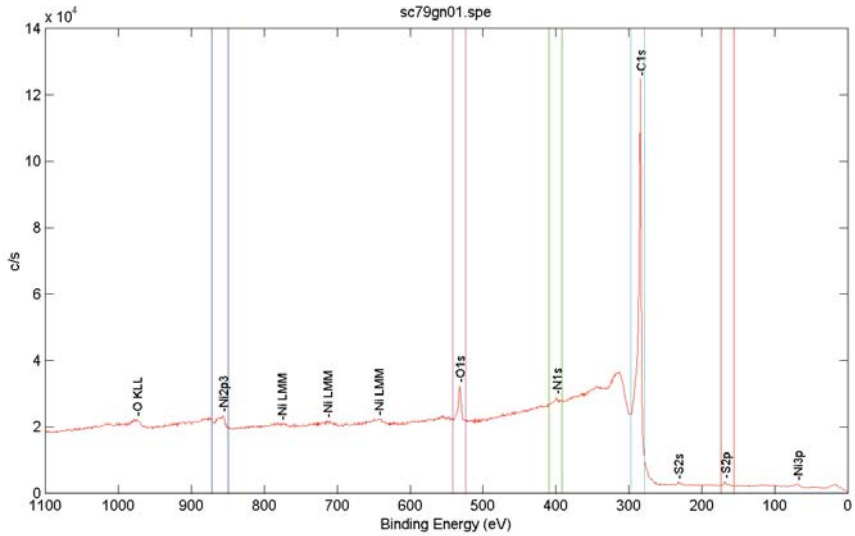

Figure 1. General XPS spectra of bare carbon nanofibers.

effective way is the graphitication process, where the nanofibers are treated at very high temperature (around 2800ºC) in a reducing atmosphere [3], for example argon. Thanks to that high temperature, the contaminants are burned out meanwhile the carbon structure is maintained and even is reorganized for obtaining a better crystal lattice.

4.1.1. Discussion about XPS analysis of CNF surface

X-ray photoelectron microscopy is the natural technique to study the chemical composition of the surface of the nanofibers as only probe 2-5 nm depth of the sample. As is explained in the Experimental Section (see Chapter 3), with this technique we will be allow to detect the atoms of each element and it's bond types. Usually, in order to discriminate the latter ones is necessary make a deconvolution of the peak of the element studied, a methodology that may lead us to several mathematical conclusions inconsistent with the physical or chemical properties of the material. Because that, extensive bibliographic research has been undergone in order to decide which configuration of peaks would have more sense.

For this calibration, bare carbon nanofibers were used. In the first survey analysis, carbon, oxygen, nickel, nitrogen and sulphur were found in different concentrations (Fig 1). This is not surprising as all those elements are involved in the reaction of the synthesis of the nanofibers [1]. The next step was to perform a more detailed measurement of the most prominent peaks of each element (namely C1s, N1s, O1s, S2p and Ni2p). We will analyse each peak individually:

- S2p

The high resolution spectra of the S2p peak shows two differentiate subpeaks, one around 164.2 eV and the other in 169.2 eV. According to the literature, the first one corresponds to pure suphur meanwhile the second is assigned to SO_2 [4,5]. No other subpeaks are detected, so we have only these two compounds. Calculating the area of the subpeaks, the 79% of the S2p corresponds to SO_2 in opposite to only 21% of S, so is plausible to assume that during the synthesis process the majority of the sulphur adsorbed over the surface ends up oxidized.

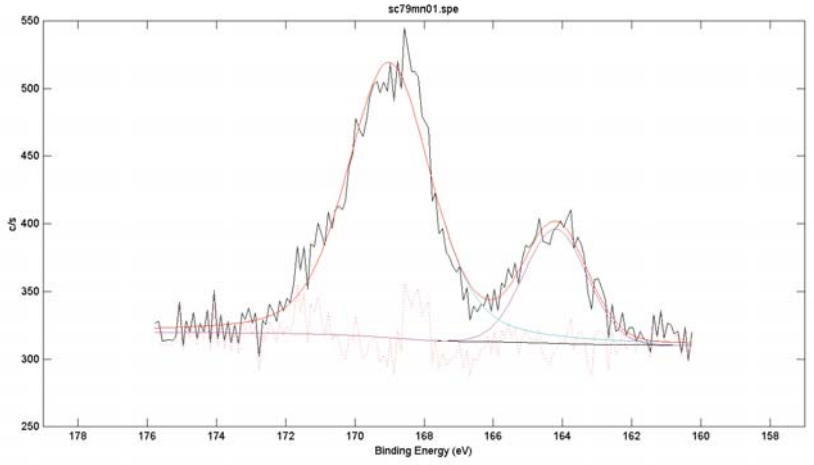

Figure 2. High resolution spectra of S2p peak of bare carbon nanofibers.

- N1s

Although the obtained signal of this peak is just above the resolution limit of the experimental apparatus we can distinguish clearly one peak around 399 eV that corresponds with the presence of Nitrogen over the surface of the carbon nanofibers without any kind of extra bond [6]. This means that during the process some nitrogen from the natural gas used as a precursor of carbon is adsorbed on the surface of the nanofiber.

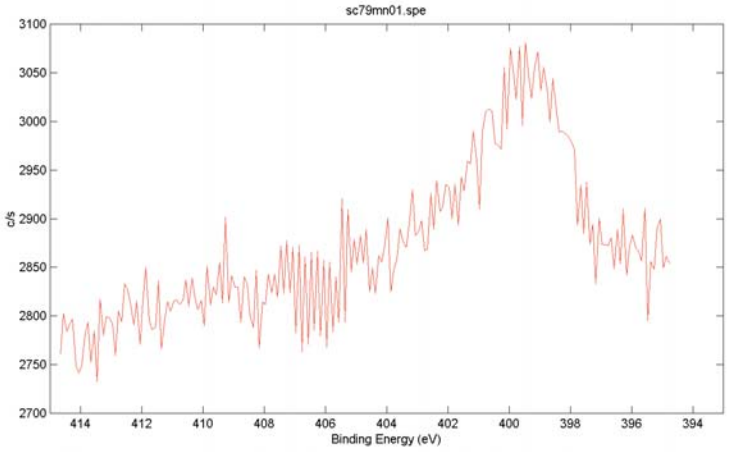

Figure 3. High resolution XPS spectra of N1s of bare carbon nanofibers

- Ni2p

This spectrum is somewhat more complicated than the previous ones as is composed by different subpeaks [7,8]. Comparing our spectra with different models and measurements present in the literature it is clear that this spectra corresponds to the NiO instead of

pure Ni, meaning that during the synthesis process the obtained nanoparticles that act as seeds are oxidized. It was decided not to study the oxidation state of the nanoparticles, as the signal is relatively weak and in subsequent processes this material will be eliminated of the nanofibers.

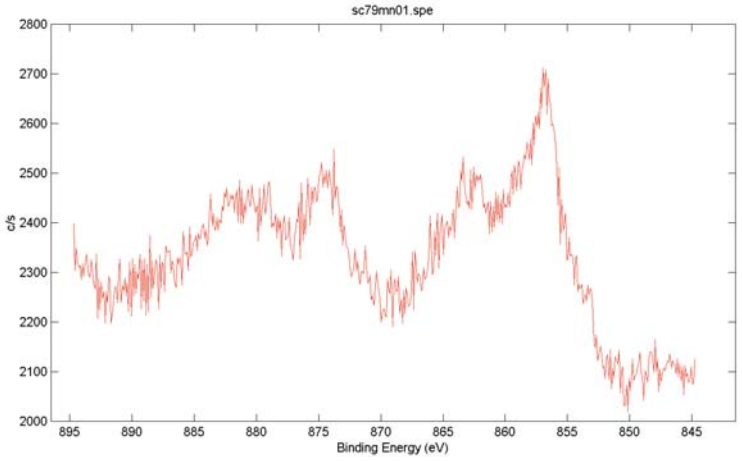

Figure 4. High resolution XPS spectra of Ni2p peak of bare carbon nanofibers.

- C1s

This peak, along with the O1s, is the one from which we can extract more information. It will inform us about the functional groups present in the surface of the nanofiber and its concentrations. As C1s appears as a one wide solid peak, this information can be extracted only after performing a deconvolution of the peak, obtaining the theoretical signals for each functional group.

First of all, it is needed to have an idea of the possible functional groups present in the surface of the nanofiber. As said before, the

general XPS suggest that the elements present in the sample are the same (or come from) the elements used during the synthesis process. Almost all the sample is carbon with some oxygen, and then residual quantities of other elements like the nickel of the seeds or the nitrogen from the natural gas that have been adsorbed in the nanofibre surface. So, is plausible to make the approximation that the sample is composed by carbon nanofibers with oxygen on its surface, or in other words, activated carbon. We can underestimate the other elements as the signals detected are around the detection limit of the XPS detector. This is important as we can avoid the addition of extra peaks a part of the O-related ones simplifying the analysis of the C1s peak.

With this simplification, we can search in the literature for information about XPS analysis of activated carbons. In the different studies it is clear that after treated (for example, using different kind of acids), the surface of the carbon material is covered by oxygen containing functional groups [9–13]. The bonds of these functional groups are usually of the type C-O (eters, hydroxyls), C=O (carbonyl) or C=-O (carboxylic). Although that there is a general consensus about what types of functional groups may be in the surface of activated carbons, there is a certain controversy about its peak positions and configurations in order to adjust the C1s peak. These results depend on the author criteria, and for similar materials, different numbers of peaks can be used or the positions of equivalent peaks are slightly different. Moreover, in addition to the functional group peaks there are the peaks from the pure carbon bonds. Usually there are three reported [14,15]: the one from the sp^2 type bonds (284.6 eV), other that originates because the sp^3 and one wide peak located at higher energies related to plasmons over the carbon surface. There are some cases, especially if

the energy resolution of the XPS detector is not high enough, the peaks sp^2 and sp^3 forms one sole peak, and is named simply C-C peak [9]. As will be seen later, our experimental resolution is sufficient for distinguish between sp^2 and sp^3 peaks. This is important, because comparing these two peaks we can have an idea of the quality of the crystal structure of the surface of the carbon nanofiber. So, taking into account that only oxygen will be chemically bonded with the carbon atoms, we will have six types of peaks that will adjust the C1s peak:

Peak	Type	Binding Energy (eV)
1	sp^2 (C-C, graphitic carbon)	284.5-284.7
2	sp^3 (amorphous carbon)	284.9-285.3
A	C-O (hydroxils and eters)	286.0-287.0
B	C=O (carbonyl groups in quinones and ketones)	287.3-288.1
C	C=-O (carboxylic groups)	288.7-290.0
3	Plasmon	291.2-291.6

Table 2. Peaks proposed for the adjustment of C1s peak.

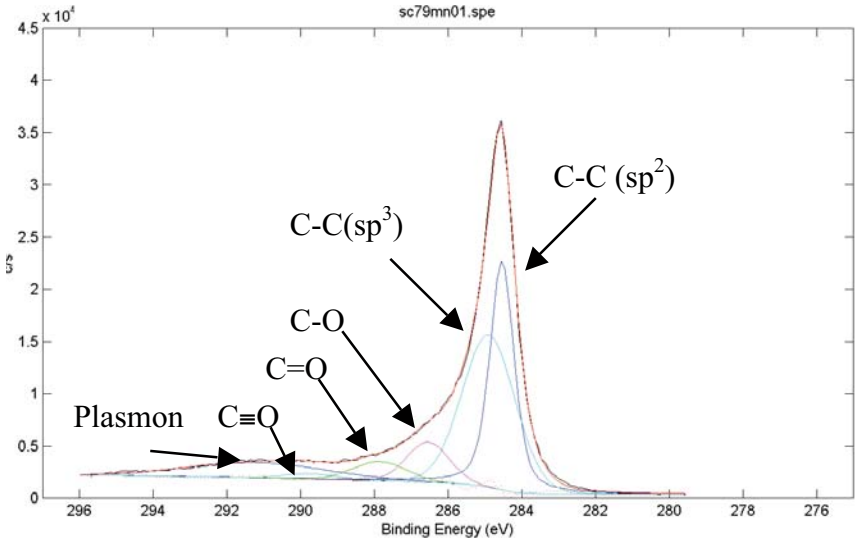

Figure 5. Adjustment of the C1s using the peaks proposed in Table 1.

Instead of using one energy central position for the peaks, it has been found most suitable to use a range were the energy values of the peaks could fall. These ranges were obtained after collect all the binding energies reported from different sources [11,12,14], as seems plausible that our peak energy positions will fall between these regions. Moreover, our adjustment software has the possibility to restrain the movement of the peak on a certain range that will be useful for the future deconvolution using this strategy.

Another point to take into account is the origin of the binding energies. In XPS we can obtain the type of binding between atoms, so depending of the type of bond we can obtain different binding energies for the same elements. In the case of carbon and specially bonds

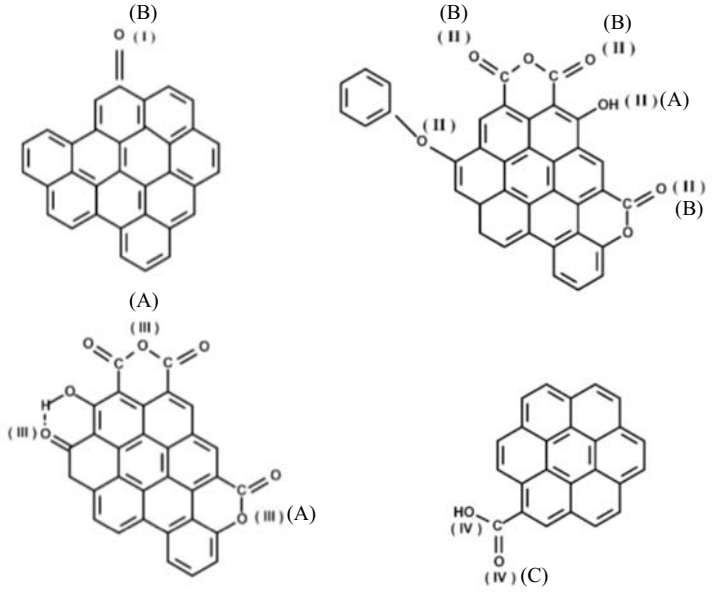

Figure 6. Different oxygen functional groups present in the carbon nanofibre surface and its realted peaks.

between carbon and oxygen atoms the binding energies also depends of the type of functional group that carbon is attached to (Fig. 6). For example, the peak that falls in the range 286.0-287.0 eV corresponds to carbon atoms that belong to hydroxyls or esters type of functional group. In this kind of functional groups the carbon atom is single bonded to an oxygen atom and is because this reason that usually this peak is defined as C-O. The peak ranged between 287.3-288.1 is originated from bonds type C=O. The peak signal includes the signal of quinoid carbonyls (C=O bonded directly to the carbon lattice) and carbonyls oxygen atoms bonded in esters. Finally, the carboxylic groups can be detected in the range of 288.7-290.0. This information is important for future analysis, where it will be studied the variation of these functional groups after different treatments and have more sense talk about variation of functional groups than bonds.

- O1s

As the functional groups are only composed by C and O also is interesting to analyse the signal from the O atoms. In the same way that the C1s case, the signal of the oxygen atoms will be deconvoluted using different peaks, depending on the type of binding or the type of functional group where the O atom is attached.

Following the same classification than in the C1s, the O peak can be divided in four subpeaks:

Peak	***Type***	***Binding Energy (eV)***
I	C=O	531.0-531.9
II	C-O y C=O	532.3-532.8
III	C-O	533.1-533.8
IV	C≡O	534.4-535.4

Table 3. Peaks proposed for the adjustment of the O1s.

In the O1s, the Peak I corresponds to quinoid carbonyls oxygen atoms meanwhile Peak II corresponds to carbonyls oxygen bonded to esters and oxygen atoms in hydroxyl groups (bond type C-O). Peak III corresponds to oxygen atoms with a single bond in esters. Finally, Peak IV corresponds to the signal originated from carboxylic groups. So, it can be seen that instead of having all the signals of each bond (C-O,

C=O, C≡O) separated like in the case of the C1s peak, we have a mixing of signals in Peak II.

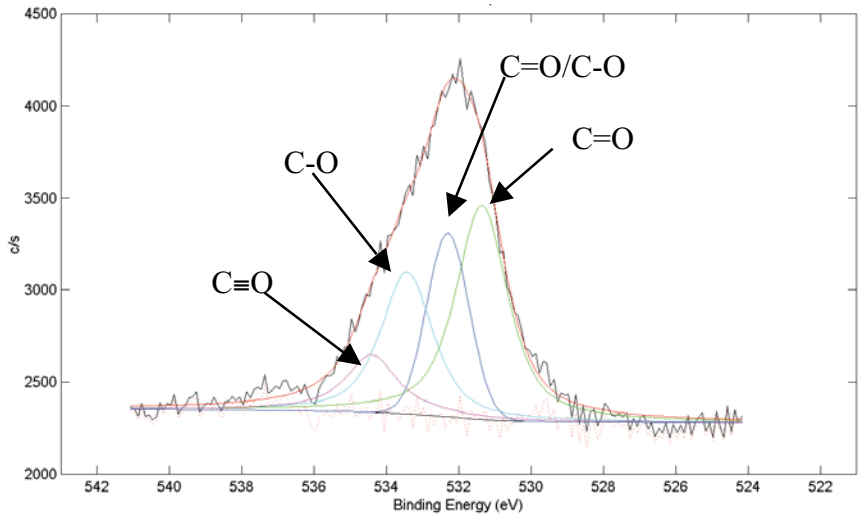

Figure 7. Adjustment of the O1s peak using the peaks proposed in Table 2.

4.1.2 Detailed analysis of graphitication process

Taking into account this peak classification we are in condition to analyse the graphitication process using XPS. We know that the bare carbon nanofibers have some impurities as a result of the chemicals used during the synthesis process, and is need an additional step in order to eliminate these impurities. The process used is the graphitication that is the treatment of the carbon nanofibers at temperatures around 2800ºC in a reducing atmosphere, usually argon.

The objective of this study is to analyse in detail the changes in the surface chemistry and the implications that would have. In order to do that the following XPS measurement routine was planned:

1) General spectra
2) Multiplex of C1s, O1s, S2p, N1s and Ni2p
3) Cleaning with argon of 30s
4) General spectra
5) Multiplex of C1s, O1s, S2p, N1s and Ni2p

This routine is divided in two parts: first is analysed the surface of the nanofibers without any modification. Because there is the possibility that the surface may be covered by an amorphous layer of carbon due the natural exposition to the atmosphere, a process of cleaning was applied over the analysis area using argon sputtering. With this process is expected eliminate the these possible impurities, but also force a certain reduction and elimination of the functional groups thanks to the reduction properties of argon and hopefully obtaining more information about the evolution of the oxygen content during the graphitication process.

- General spectrum

In Table 3 it is shown the atomic percentages of each peak identified from the general spectrum for every sample. The two major peaks are the C1s and O1s, meanwhile the signals form the other peaks,

corresponding to the impurities from the reaction, are around or below the detection limit of the experimental apparatus. The results confirm that the nanofibers obtained of the graphitication process (CNFG) have all the impurities removed from the surface, assuring the suitability of the process in order to purify the carbon nanofibers. Another interesting result is the oxygen content of the all samples. The CNF samples have a C/O ratio around 26, meanwhile the CNFG the C/O ratio is around 99, meaning that there is an important reduction process during the graphitication treatment. In spite of that, still 1% of oxygen remains in the CNFG samples, so some functional groups remains in the surface of the carbon nanofibres even after being treated in a reducing atmosphere at 2800ºC. Also is interesting the effect of the argon sputtering over the surface of the nanofiber. Again, there is a reduction of the surface, as the C/O ratio is increased from 26 to 80. For the case of GANFG, the Ar treatment seems that have a lower effect on the oxygen content. This may demonstrate that the remaining functional groups of the graphitication process are far more difficult to eliminate than the case of the bare CNF.

	C1s (%)	N1s (%)	O1s (%)	S2p (%)	Ni2p (%)
CNF1	94.2	0.9	3.6	0.7	0.6
CNF1+Ar	96.6	0.5	1.2	0.6	1.1
CNFG1	98.9	0.0	1.0	0.0	0.1
CNF+Ar	98.9	0.0	1.0	0.1	0.0

Table 4. Atomic percentages of the different samples obtained from the corresponding general spectrum.

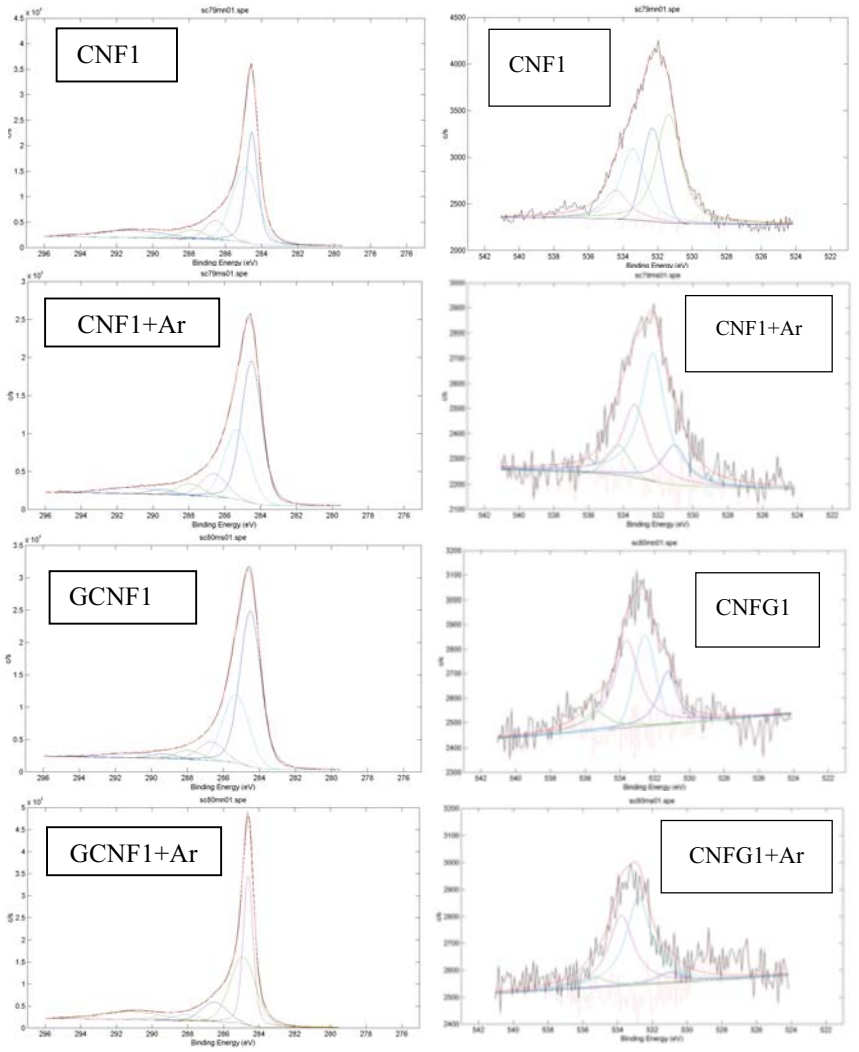

Figure 8. Adjustments performed in all the samples for the C1s and O1s peak.

- High resolution spectrum

The multiplex measurements of each peak will offer us the evolution of the different functional groups (or binding types) during the processes. Figure 8 shows the peaks obtained of the deconvolution of the C1s and O1s main peaks, meanwhile in Table 4 there are the positions and percentage of area occupied for each

CNF					
C1s			O1s		
Peak	Position	%Area	Peak	Position	%Area
1	284.54	36.91	I	531.36	40.58
2	284.90	38.62	II	532.30	21.13
A	286.55	8.55	III	533.43	26.23
B	287.85	5.03	IV	534.41	12.06
C	289.73	1.48			
3	291.20	10.41			
CNF+Ar					
C1s			O1s		
Peak	Position	%Area	Peak	Position	%Area
1	284.50	50.31	I	531.06	15.22
2	285.30	28.25	II	532.30	49.84
A	286.60	9.35	III	533.35	28.25
B	287.95	4.78	IV	534.30	6.69
C	289.50	2.11			
3	291.15	5.20			
CNFG					
C1s			O1s		
Peak	Position	%Area	Peak	Position	%Area
1	284.62	36.28	I	531.25	19.92
2	284.90	38.32	II	532.58	26.31
A	286.52	10.59	III	533.63	44.26
B	288.10	3.31	IV	535.40	9.51
C	290.00	1.18			
3	291.19	10.33			
CNFG+Ar					
C1s			O1s		
Peak	Position	%Area	Peak	Position	%Area
1	284.50	55.98	I	531.00	5.89
2	285.30	27.64	II	532.80	48.77
A	286.67	7.43	III	533.80	39.46
B	287.93	3.62	IV	535.40	5.87
C	289.32	1.91			
3	291.20	3.43			

Table 5. Values obtained alfter the adjustments of the C1s and O1s peaks.

subpeak. At first glance, the C1s main peaks are very similar between the different treatments. First will focus in the peaks corresponding to sp^2 and sp^3 that will give us information about the crystallinity of the **surface** of the carbon nanofiber. This may not be confused with the bulk crystallinity of all the nanofiber obtained, for example, by Raman spectroscopy or XRD. In Table 5 it is shown the ratios sp^2/sp^3 obtained. As can be seen, after the graphitication process the ratio between sp^2 and sp^3 bonds do not change substantially. On the other hand, the attack with argon increases notably this ratio for both bare CNF and CNFG. Argon sputtering is generally used for cleaning the surface of the target of possible organic compounds that have been adsorbed due the contact with the environment.

Sample	sp^2/sp^3	C-C/C-O	C-C/C=O	C-C/C≡O
CNF	0.86	4.40	7.46	23.66
CNF+Ar	2.08	5.43	10.76	23.19
CNFG	0.88	3.26	10.49	25.87
CNFG+Ar	2.51	5.56	12.70	26.34

Table 6. Ratios calculated from the areas of the different subpeaks of C1s.

Carbon nanofibers are not any exception, and surely there is layer of organic impurities (amorphous carbon) over its surface. The attack with argon eliminates this layer exposing the clean surface of the nanofiber. This surface, without the interference of the adsorbed layer, is more crystalline. Moreover, sp^2/sp^3 ratio analysis suggests that the surface of

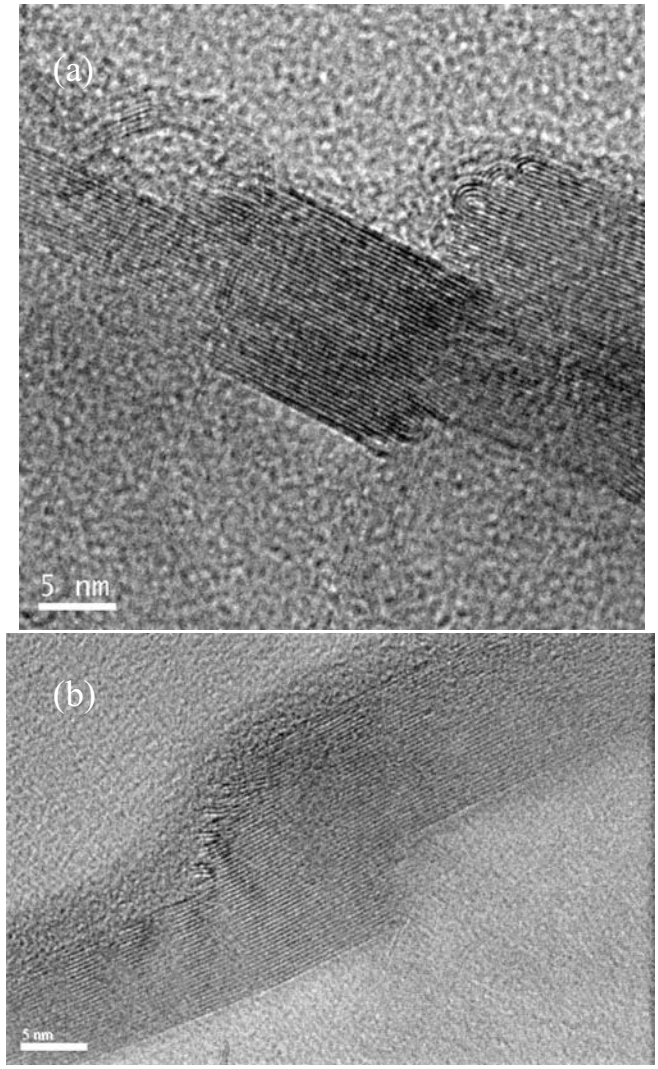

Figure 9. Examples of (a) closed ends in CNFG and (b) open ends in bare CNF.

the CNFG seems that is more ordered than the CNF. TEM analysis also hints this tendency, as the images of the CNFG show that the surface edges are closed (Fig. 9), as it the graphene layers edges that forms the carbon nanofiber reorient itself in order to expose only its surface. At contrary, in the case of bare CNF the edges are open, showing a higher disorder in the XPS measurements.

The evolution of the oxygen functional groups also is monitored in the C1s peak. In this case, the ratio between the graphitic carbon bound and the functional group is studied (Table 5). After the attacks with argon ions (CNF+Ar and CNFG+Ar) there is a general increase in the case of C-C/C-O and C-C/C=O ratios, meanwhile the C-C/C≡O seems to be fairly stable. Taking into account the decrease of oxygen detected, this change in the ratios suggests that there is a major destruction of bonds of the type C=O (quinoid carbonyl or carbonyl oxygen atoms in esters), meanwhile the destruction of C-O type bonds (carbons bonded in hydroxyl groups or ether oxygens) is lower. On the other hand, the carboxylic atoms seem to be fairly resistant to the reduction process. The graphitication process affect slightly different the surface functional groups. In this case, the C-O bonds seems to tend to increase, meanwhile both C=O and C≡O bonds are reduced in different extent. In spite of that, the chemical analysis have to be interpreted form the point of view that a layer of carbon impurities is adsorbed over the surface of the nanofiber and may change the oxygen proportions measured.

In order to confirm these tendencies, the O1s peak evolution is also studied during the two types of treatment (Fig. 8). Is important to note that in this case the signal of the O1s peak decrease importantly after the reduction treatment (either with the graphitication process or the attack with argon), being its intensity close to the experimental resolution of the XPS apparatus. This means that the peak obtained will be more noisy, specially in the case of the analysis of the CNFG attacked with argon that have the lowest amount of oxygen, being the data obtained of the adjustment less confident, but still will show us some insight in the evolution of the oxygen atoms attached to the

functional groups of the surface. First of all, we have to decide how the ratios are calculated. As in the C1s analysis we found that the remaining carboxylic groups are very resistant to the reduction processes (either graphitication and argon sputtering), is plausible to use the C≡O peak (named IV) as reference for the ratios. In the following table (Table 6) these ratios are presented:

	I/IV	**II/IV**	**III/IV**
CNF	3.4	1.7	2.2
CNF+Ar	2.3	7.4	4.2
CNFG	2.1	2.8	4.7
CNFG+Ar	1.0	8.3	6.7

Table 7. Ratios of the different peaks using the carboxyl peak as a reference.

Respect the oxygen atoms, the chemical composition of the bare CNF and CNFG is different. Meanwhile for bare CNF the carbonyls bonds were dominant, in the CNFG there is a dominance of II peak (C-O and C-O) and III peak (C-O). In order to obtain more information, it can be compared with the evolution of the A peak of the C1s, that increase respect the graphitic carbon. Taking into account that there is a decrease of the C=O bonds respect the C-C, we can say that during the graphitication process there is a elimination of mostly carbonyl groups, meanwhile the hydroxyl and oxygen bonded to ester groups tend to survive.

This can be confirmed by studying the samples cleaned by argon sputtering. In the case of CNF, a similar tendency is detected but with a higher effect, as the peak II increases 4 times respect the C≡O bonds, confirming the survival of hydroxyl groups. On the other hand, also is detected an increase of C-O bonds in esters. Finally, the sample of CNFG cleaned with argon also shows the same tendencies but a higher extent.

4.2. Metal-nanoparticle decoration of carbon nanofibers for gas sensing applications.

Carbon nanofibers presents unique properties that makes an ideal candidate for being applied as a sensing layer for the next low cost gas sensors [16]. First of all, CNF surface is more reactive than pure carbon nanotubes as sp^3 reactive sites are exposed in its entire surface meanwhile usually in CNT this sites are in the ends, in the case that are open. This makes necessary to create defects in the CNT surface by different means, for example, using plasma etching [13]. In this case, the defects present in the carbon nanofibres surface permits its use as gas sensing layer directly without any use of a pre-treatment of the surface [17,18]. Moreover, these defects also will help in the decoration of the carbon nanofibers with metal nanoparticles, as there are naturally centres where the metal atoms can concentrate, at contrary to the smooth surface of carbon nanotubes.

In this section it will be described the decoration process of the carbon nanofibers for its integration in a gas sensor. It will be discussed the effect of these nanoparticles over the signal obtained after exposing the carbon nanofibers to different gases, like NH_3 or NO_2.

4.2.1. Preparation of the carbon nanofibres

As explained in section 4.1, the bare CNF obtained from Grupo Antolín have some impurities over its surface and a thermal treatment is needed to eliminate these contaminants. The resulting material (CNFG) offers a clean surface, with some oxygen functional groups. Its atomic concentration is very low (1 % respect the carbon material) and is not expected that will affect the sensing characteristics of the carbon nanofibres.

Another effect of the graphitication process is the rearrangement of the carbon lattice. In the surface, TEM measurements showed that the graphitic planes are closed, exposing only the sp^2 bonds of the carbon structure. This is confirmed with the XPS measurement of the graphitic signals, as the sp^2/sp^3 ratio increase after the treatment. This rearrangement of the carbon lattice is expected to reduce the reactivity of the carbon nanofiber. This can bee seen, for example, in its stability in solution. CNF have proved to be fairly stable in polar solvents like acetone or isopropanol, but CNFG aggregates and precipitates almost instantly. This phenomenon is undesired, as we need the CNF to be well dispersed in order to achieve good wetting process of the nanoparticle precursor.

Originally, the objective was increasing the oxygen functional groups in order to improve the stability of the CNFG in polar solvents. In order to do that, an annealing in oxygen atmosphere was performed. The temperature was selected in order to maximize the effect but avoiding burning the nanofiber. TGA analysis show that, in an oxygen atmosphere, the carbon nanofibers begin to burn at 400ºC, so this temperature was selected. After the treatment, the CNG showed a high stability in polar solvents as is possible to obtain solutions with concentrations as high as 1mg/ml. Surprisingly, the amount of oxygen (and type of functional group) after the annealing process do not change significantly to associate the improvement of the dispersion of the nanofibers to a chemical change in its surface. TEM analysis of the surface showed that the graphitic planes of the nanofibers were open again after the annealing process. So this means that is possible to increase the stability of the carbon nanofibers without changing the chemical composition of its surface, only exposing the rich sp^3 bond edges of its graphitic layers. This is important, as in the case of carbon nanotubes is necessary the use of surfactants or processes that vary the chemical composition of the surface that later will affect the gas sensor signal if not are removed. In our case, the return to the open edges configuration may increase the reactivity of the nanofiber to the surrounding environment and thus improving the sensor response.

4.2.2. Decoration of the carbon nanofibers

After the annealing of the CNFG, the material is ready for its decoration. The process is resumed in the following steps:

- Mix of CNFG and metal precursor in acetone using magnetic stirring.
- Ball milling process.
- Evaporation of the solvent.
- Annealing of the product at 400ºC during 3h in oxygen atmosphere.

The objective is to decorate the carbon nanofibers using noble metal nanoparticle, in particular Au and Pd. These metals have proved to be useful for the improvement on the detection of different gases [19–21] as acts a catalyst increasing the reactivity of the metal-CNFG composite compared by the bare CNFG. The precursors used were basically chlorides ($AuCl_3$, $PdCl_2$) as have a low sintering temperature and are very easy to decompose. In spite of that, is expected to be difficult to "wet" the surface of the nanofibers with these chlorides, as there is no chemical affinity between them and the carbon nanofibre surface. In order to maximize the wetting, a ball milling process is used. With this energetic process it will be possible to increase the concentration of precursor that can adhere to the surface of the nanofiber by mechanical interaction.

After the evaporation of the solvent, the resulting product was annealed at 400ºC during 3h in an oxygen atmosphere. Again, the temperature was chosen as is the maximum temperature at the CNFG are not burned. Moreover, working at these temperatures assures the correct dissociation and sintering of the metal nanoparticle precursor, obtaining a totally metal cluster.

Two kinds of samples were prepared. One with the 20% of metal precursor respect the CNFG (Au20%, Pd20%) and other with the 50% of metal precursor (Au50%, Pd50%). The resulting products were analysed with TEM, as can be seen in Figure 11. For one hand, we have a curious effect in the case of Au. At 20% concentration big metal clusters are obtained, meanwhile when the concentration is increased the Au nanoclusters become smaller. On the other hand, the Pd decoration has a somewhat contrary behaviour. With the 20% concentration we obtain a homogenous decoration of relatively big

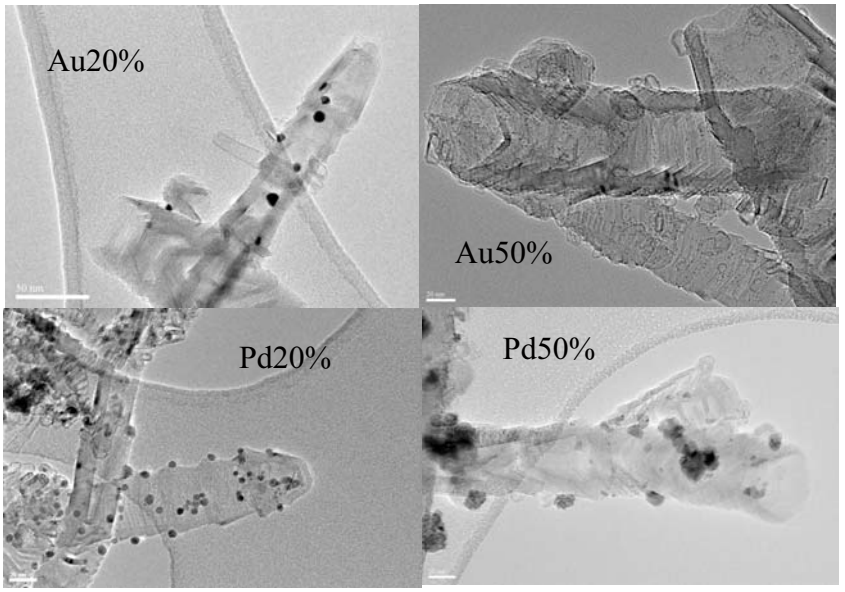

Figure11. TEM images of the resulting products after the metal-nanoparticle decoration.

clusters. With increasing concetration (50%) the cluster become large and loose its spherical shape, indicating an uncontrollable aggregation of the Pd atoms.

In this case, it is know that Pd atoms have very high mobility. So, there is two possibilities: there are no cluster observables, as the Pd atoms are dispersed over all the nanostructure surface without coalescence, or, as happens in our case, tends to concentrate into defects that act as “traps” for these atoms, generating big clusters. In the case of increase the concentration of Pd atoms, these clusters continue to get bigger, as we can see in the case of Pd50%.

For the case of gold was expected a similar behaviour, but instead an inverse result is obtained. Although is not clear the exact process that could permit this kind of behaviour, one of the key points may be that the mobility of the Au atoms over the carbon nanofibre surface is lower than the Pd one. Taking this into account, in the case of Au20% the lower superficial concentration of Au atoms will make harder to generate clusters. So, when one cluster is formed it becomes a trap for the rest of free Au atoms. Moreover, the smaller mobility of the Au atoms (compared with the Pd atoms) will favour the growing of more isolated clusters, as do not have options to disperse in a larger surface. When the precursor concentration is increased to 50 %, the superficial concentration of Au atoms will be higher and then will be easier to generate clusters. Of course, as more clusters are generated less Au atoms will be available that could feed the existing clusters, and then will be smaller. Moreover, these clusters will be anchored to the nanofiber structure, making harder the coalescence between them.

In order to verify this phenomenon, a new decoration with Au and Pd at 2% concentration of precursor was performed. Interestingly, the Au-decorated nanofibers shows clusters with sizes similar to the Au20% ones but more disperse. This means that is confirmed that for lower precursor concentrations less clusters are generated, that acts as a trap for the Au atoms of the vicinity of the cluster. For the Pd2% samples the proposed tendency is followed, as no clusters are visible by TEM, meaning that the superficial concentration of Pd atoms (that are homogenously distributed through the nanofiber surface) is not enough for initiate the growing of the clusters (Fig. 12).

4.2.3. Gas sensing characteristics of the CNFG and metal-decorated CNFG

In accordance with Ionescu *et.al.* [22] the catalytic particles have to be the smallest possible in order to achieve a good catalytic reaction that could affect the overall response of the sensor. For this

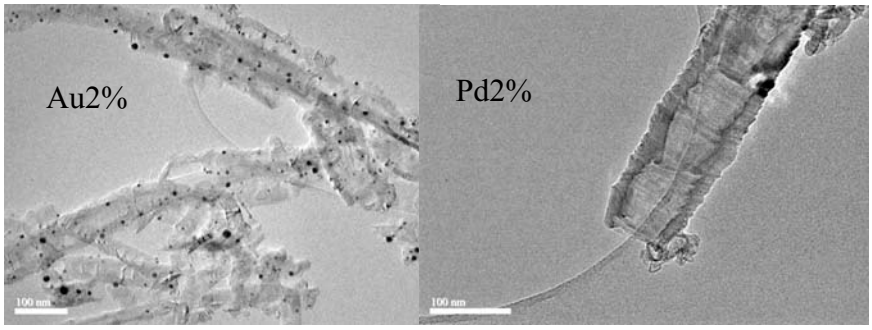

Figure12. Decoration of carbon nanofibers at 2% with Au and Pd.

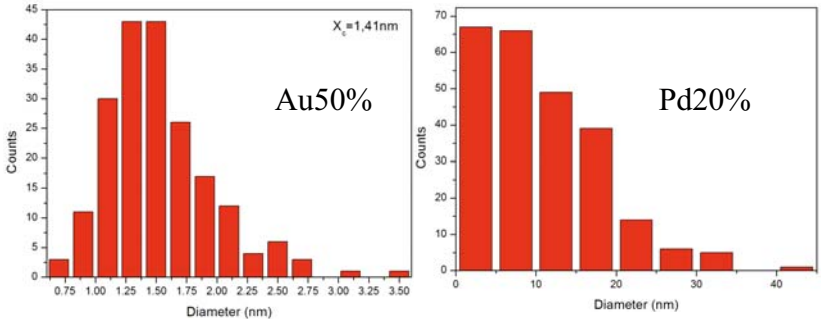

Figure 13. Distribution of diameters for the samples Au50% and Pd20%.

reason, it was selected as a sensing layer the samples Au50% and Pd20%. Meanwhile the Au50% samples have a nanoparticle diameter of around 1.4 nm (Fig 13), the sample Pd20% was more difficult to select, as the dispersion was wider and the diameters greater (Fig 13), but is expected that the smallest nanoparticles will offer the desired reactivity.

The sensor was fabricated using the same procedure described in the Experimental Section. The 4-interdigitated electrodes and the heater were fabricated using the inkjet printing technique using silver

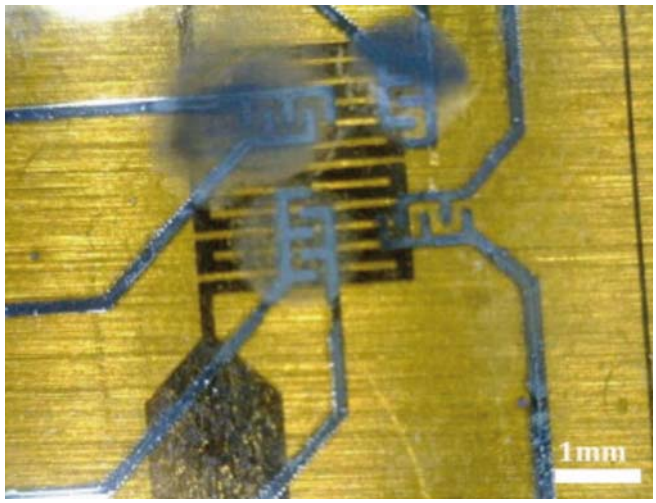

Figure 14. Gas sensor device with the CNFG layer deposited by electrospray technique.

as a metal. The three kind of CNFG (bare CNFG, Au-CNFG and Pd-CNFG) were deposited over three different interdigitate electrodes by means of electrospray technique (Fig. 14). The layers formed have a thickness around 200-300 nm.

The first measurements were performed over the bare CNFG using NH_3 as a target gas. It was found that the sensor was sensitive to this gas at room-temperature (22ºC) but a poisoning effect appeared. The detection at room-temperature is not surprising, as compared to other materials used in conductometric gas sensors, such as metal oxides [23], carbon-based nanostructures are expected to display gas sensing response even at room temperature [24,25] which is an advantage from the point of view of power consumption. For NH_3 the sensor response was linear with the gas concentration (Fig.15a). However, consecutive pulses of 1000 ppm NH_3 resulted in a decrease in the response, which is indicative of a persistent adsorption on the surface of the GANFG. This suggests that a process to clean and reset the nanofibre surface will be necessary.

The influence of humidity, still at room temperature, was also studied, as this is the most common interfering gas in real working conditions. We compare the response of the sensor against NH_3 with and without a reference relative humidity (RH) of 50%. We found that with humidity a shift in the baseline appears. Remarkably, the response to the different pulses of NH_3 can still be clearly detected in presence of humidity, and no significant variation in the relative sensor response was observed (Fig. 15b). For this reason, it was chosen to undergo all the following measurements at 50% RH.

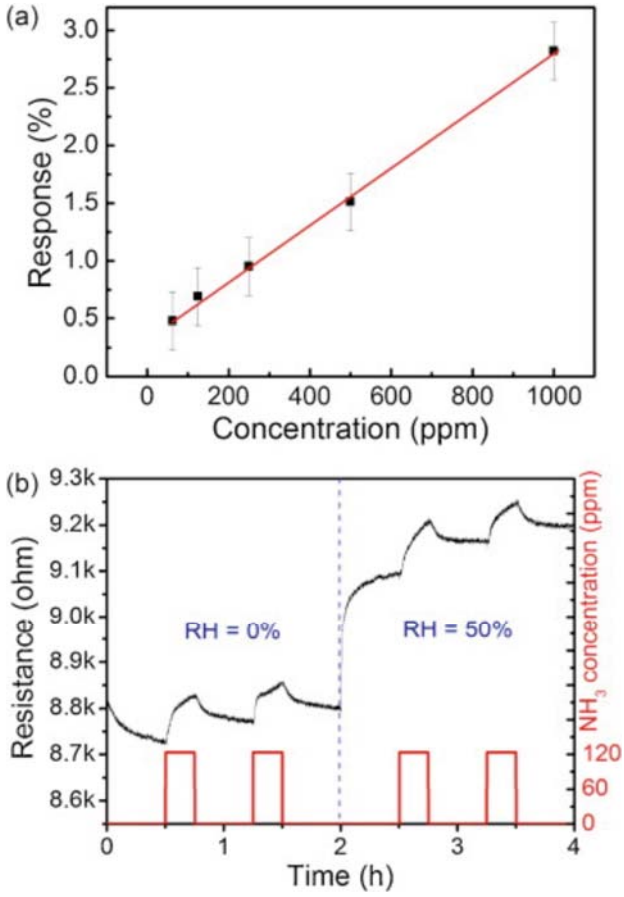

Figure 15. (a) Variation of the response of the raw CNFG with the NH_3 concentration. (b) Effect of the precense of the humidy with the raw CNFG and NH_3. All the measurements were done at 22ºC.

Metal decorated CNFG show different responses to different gases (Fig. 16). To 500 ppm of NH3 in 50% RH we found that the response of Au-GANFG was lower than the one obtained with the reference GANFG sample, while the Pd-GANFG sample displayed larger responses. Using 5 ppm of NO2 at 50% RH, the response is lower for the two types of metal. The decoration of the nanofiber with metal nanoparticles affects the total electronic density of states (DOS) of valence bands and increases its work function. The effective electronic interaction between metal nanoparticles and the CNF facilitates the detection of gases through the change in the electrical

conductivity of mats formed by these hybrid nanomaterials. Two possible gas molecule sensing mechanisms can be expected for the hybrid nanomaterials: (1) the gas molecule directly adsorbs onto defects located at the CNF sidewall, inducing electron transfer and changing the electrical conductivity of the hybrid nanomaterial; or (2) the gas molecule adsorbs onto a metal nanoparticle and this results in a significant charge transfer between the nanoparticle and the CNF, which eventually changes the electrical conductivity of the hybrid nanomaterial. This second mechanism corresponds to what is theoretically described in [26]. These results demonstrate that the here-proposed decoration method effectively modifies the response of CNFG to gases and open the door to further strategies to modulate the sensor selectivity, even at room temperature. The next step was the study of the sensor response activating the heater printed in the bottom side of the substrate. It was expected that the increase of temperature would clean and reset the surface of the nanofibers, forcing the desorption of the chemical species that change the sensor response. Using an automated routine, the temperature was increased by steps. For every step, two consecutive pulses of NH3 (500 ppm in SA) were applied. This strategy was chosen to obtain information about the response time and the response magnitude for each temperature, as well as detecting repeatability issues and any poisoning effect at each of the temperatures studied. Fig. 17A–C shows the results of this routine. We can see that the response time decreases dramatically with the temperature, from around 25 min at 42 °C to less of 5 min at 220 °C. Moreover, similar responses were obtained for each pair of equivalent pulses, which guarantee the repeatability of the measurements. Concerning the magnitude of the response, data shown in Fig. 8B

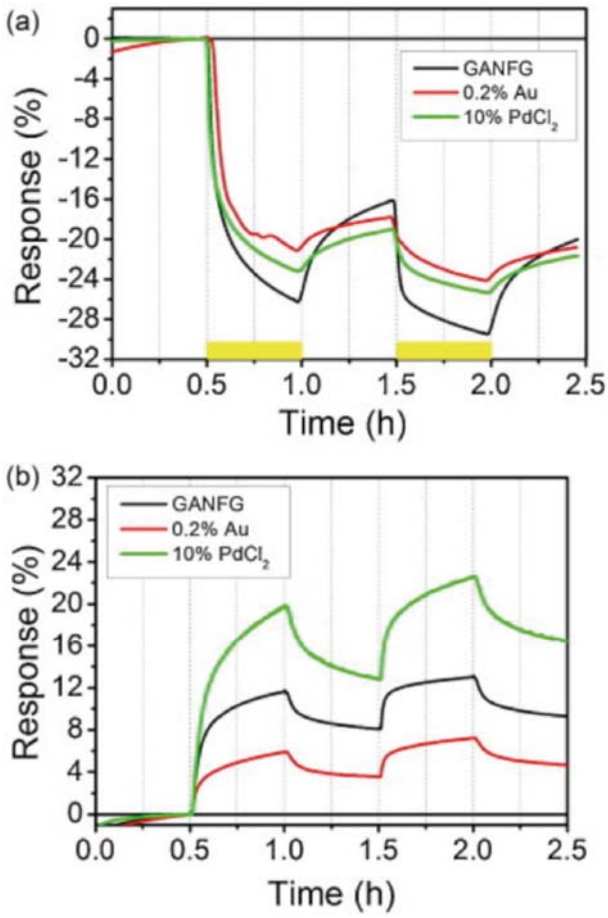

Figure 16. Response of the sensors in the presence of (a) NO_2 (5 ppm) and (b) NH_3 (500 ppm). All mesaurement were done at 22ºC.

indicate that the response increases until a maximum at around 70 °C, and then decreases again at higher temperatures. This maximum corresponds to a temperature where adsorption and desorption of molecules are almost balanced. At higher temperatures, desorption is higher than adsorption, leading to a decrease in the overall signal [ref 28 article]. This also implies that saturation will be reached faster, or in other words, the response time will be faster. These results suggest that a compromise between the response magnitude and the response time must, and can, be found. Specifically, found 110–120 °C was the optimum operation temperature of these sensors to 500 ppm of NH3 in

50% RH, in wich the response time is around 5 min and the response reaches 3%.

4.3. Conclusions

In this chapter a detailed analysis of the chemical composition of the carbon nanofibers was performed using XPS. It has been confirmed that because the products used during the synthesis process the surface of the nanofiber presents some residual elements, like nitrogen, nickel or sulfur. Moreover, the surface also is slightly oxidized as some functional groups become attached to the surface. A graphitication process is applied over these nanofibers in order to eliminate all these impurities. XPS measurements confirm that the surface is cleaned of all these residues, but still 1% of oxygen remains. This oxygen signal has been found that basically are hydroxyl (C-O type bound) and carboxyl functional groups (C≡O). Moreover, is demonstrated that a layer of amorphous carbon is covering the carbon nanofibers, as the sp^2/sp^3 ratio increases after an argon cleaning. This layer is formed due the contact of the nanofibers with the atmosphere, as the CNFG also presents this feature. After the elimination of this layer by argon sputtering, it is shown that the surface of the CNFG is more crystalline than the bare CNF. TEM analysis showed that the surface suffers a rearrangement of the planes, closing with it self and exposing the sp^2 bonds and thus increasing the sp^2/sp^3 ratio. This reordenation of the borders of the nanofibres make it less reative to the environement, as can be seen in the loose of solubility in polar solvents that have the bare

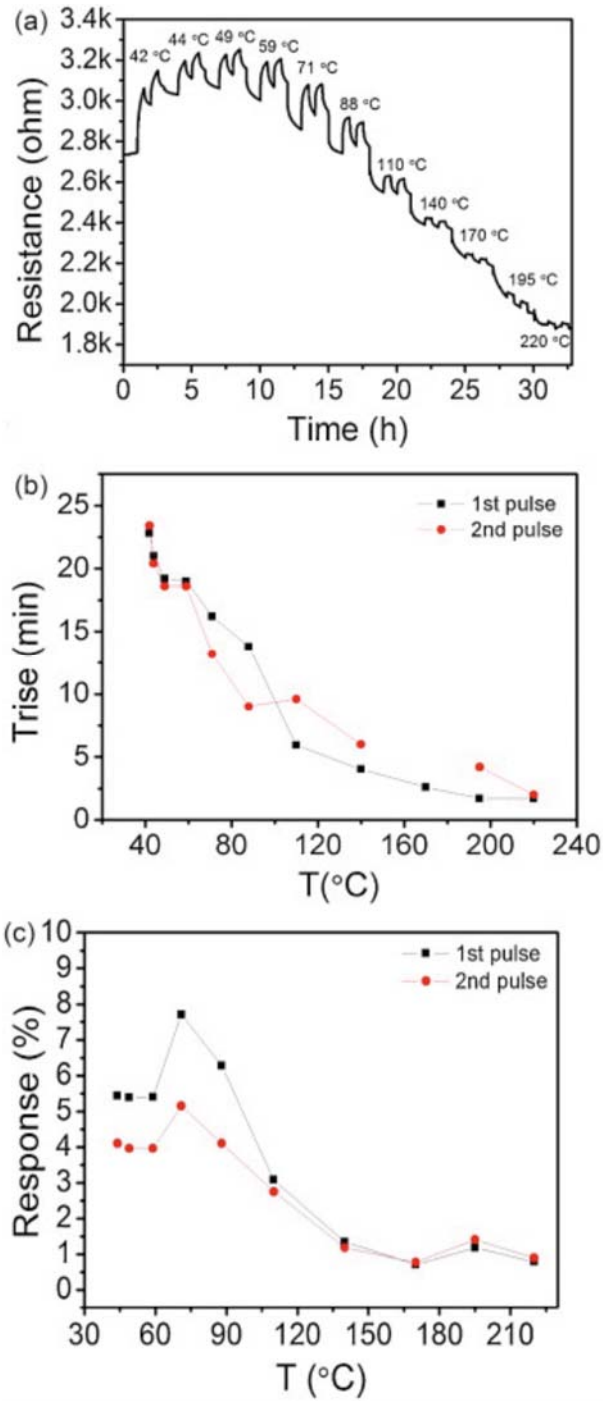

Figure 17. (a) Routine performed for calibrating the sensor using the heather. (b) Plot corresponding to the Response time versus Temperature. (c) Plot corresponding to the Response versus Temperature.

CNF. In order to recover this property the CNFG have been annealed at 400ºC in an oxygen atmosphere. This treatment proved useful to reopen the border and exposing the most reactive sp^3 sites. Moreover, this treatment do not increase the oxygen content, meaning that the recovery of the solubility of the CNFG can be explained only with the reopening of the border of the nanofibers.

The now stabilized CNFG can be used in the decoration process. A simple mix with chlorides precursors in acetones were done. Then, in order to maximize the wetting of the carbon nanofibre surface with the precursors, the solution is treated with a ball-milling process. Finally, after evaporate the solvent, the product is annealed at 400ºC during 3h. For Au-decorated CNFG it has been found that higher concentrations leaves smaller clusters with homogeneous superficial dispersion, meanwhile lower precursor concentrations promotes the growth of larger clusters but more disperse. This phenomenon is associated to the mobility of the Au atoms/clusters over the surface of the nanofibers. On the other hand, for the Pd nanoparticles, its higher mobilities difficults the formation of clusters and is needed more concentration for initiate the growth, following the more intuitive rule that more precursor concentration lead to larger Pd clusters over the carbon nanofibre surface.

A gas sensor using the three types of CNFG also was presented. It is shown that CNFG are sensitive to NH_3 even at room temperature and in presence of humidity. Moreover, the addition of metal clusters over the surface changes its response, opening a door for the increase of the selectivity and sensitivity of the CNFG sensor. Finally, it has been

demonstrated that the use of heat for reset the surface increase the response and decrease its response time.

References

[1] I. Martin-Gullon, J. Vera-Agullo, J.A. Conesa, J.L. González, C. Merino, Differences between carbon nanofibers produced using Fe and Ni catalysts in a floating catalyst reactor, Carbon. 44 (2006) 1572–1580.

[2] J.T. Robinson, F.K. Perkins, E.S. Snow, Z. Wei, P.E. Sheehan, Reduced Graphene Oxide Molecular Sensors, Nano Letters. 8 (2008) 3137–3140.

[3] M. Weisenberger, I. Martin-Gullon, J. Vera-Agullo, H. Varela-Rizo, C. Merino, R. Andrews, et al., The effect of graphitization temperature on the structure of helical-ribbon carbon nanofibers, Carbon. 47 (2009) 2211–2218.

[4] C. Polenius, X. Vanden Eynde, E. Grivel, H. Smet, N. Probst, P. Bertrand, ToF-SIMS and XPS study of sulphur on carbon black surface, Surface and Interface Analysis. 30 (2000) 420–424.

[5] Y.M. Sul'ga, V.I. Rubtsov, V.N. Vasilets, A.S. Lobach, N.G. Spitsyna, E.B. Yagubskii, EELS, XPS and IR study of C60·2S8 compound, Synthetic Metals. 70 (1995) 1381–1382.

[6] R.J.J. Jansen, H. van Bekkum, XPS of nitrogen-containing functional groups on activated carbon, Carbon. 33 (1995) 1021–1027.

[7] A.C. Miller, Simmons G.W., Nickel by XPS.pdf, Surface Science Spectra. 1 (1992) 312–317.

[8] A.N. Mansour, Characterization of NiO by XPS, Surface Science. 3 (1996) 231–238.

[9] S. Biniak, The characterization of activated carbons with oxygen and nitrogen surface groups, Carbon. 35 (1997) 1799–1810.

[10] M. Polovina, B. Babic, B. Kaluderovic, A. Dakanski, Surface characterization of oxidized activated carbon cloth, Carbon. 35 (1997) 1047–1052.

[11] C. Moreno-Castilla, Changes in surface chemistry of activated carbons by wet oxidation, Carbon. 38 (2000) 1995–2001.

[12] P. V. Lakshminarayanan, H. Toghiani, C.U. Pittman, Nitric acid oxidation of vapor grown carbon nanofibers, Carbon. 42 (2004) 2433–2442.

[13] R. Ionescu, E.H. Espinosa, E. Sotter, E. Llobet, X. Vilanova, X. Correig, et al., Oxygen functionalisation of MWNT and their use

as gas sensitive thick-film layers, Sensors and Actuators B: Chemical. 113 (2006) 36–46.
[14] S. Kaciulis, Spectroscopy of carbon: from diamond to nitride films, Surface and Interface Analysis. 44 (2012) 1155–1161.
[15] J. Díaz, G. Paolicelli, S. Ferrer, F. Comin, Separation of the sp3 and sp2 components in the C1s photoemission spectra of amorphous carbon films, Physical Review Letters. 54 (1996) 8064–8069.
[16] E. Llobet, Gas sensors using carbon nanomaterials: A review, Sensors and Actuators B: Chemical. 179 (2013) 32–45.
[17] O. Monereo, S. Claramunt, M. Martínez de Marigorta, M. Boix, R. Leghrib, J.D. Prades, et al., Flexible sensor based on carbon nanofiber with multifunctional sensing features, Talanta. 107 (2013) 239–247.
[18] S. Claramunt, O. Monereo, M. Boix, R. Leghrib, J.D. Prades, A. Cornet, et al., Flexible gas sensor array with an embedded heater based on metal decorated carbon nanofibres, Sensors and Actuators B: Chemical. 187 (2013) 401–406.
[19] M. Penza, R. Rossi, M. Alvisi, G. Cassano, M. a. Signore, E. Serra, et al., Pt- and Pd-nanoclusters functionalized carbon nanotubes networked films for sub-ppm gas sensors, Sensors and Actuators B: Chemical. 135 (2008) 289–297.
[20] M. Endo, Y.A. Kim, M. Ezaka, K. Osada, T. Yanagisawa, T. Hayashi, et al., Selective and Efficient Impregnation of Metal Nanoparticles on Cup-Stacked-Type Carbon Nanofibers, Nano Letters. 3 (2003) 723–726.
[21] H. Jiang, L. Zhu, K. Moon, C.P. Wong, The preparation of stable metal nanoparticles on carbon nanotubes whose surfaces were modified during production, Carbon. 45 (2007) 655–661.
[22] R. Ionescu, E.H. Espinosa, R. Leghrib, a. Felten, J.J. Pireaux, R. Erni, et al., Novel hybrid materials for gas sensing applications made of metal-decorated MWCNTs dispersed on nano-particle metal oxides, Sensors and Actuators B: Chemical. 131 (2008) 174–182.
[23] G. Korotcenkov, Metal oxides for solid-state gas sensors: What determines our choice?, Materials Science and Engineering B. 139 (2007) 1–23.
[24] A. Yang, X. Tao, R. Wang, S. Lee, C. Surya, Room temperature gas sensing properties of SnO[sub 2]/multiwall-carbon-nanotube composite nanofibers, Applied Physics Letters. 91 (2007) 133110.

[25] R.K. Roy, M.P. Chowdhury, A.K. Pal, Room temperature sensor based on carbon nanotubes and nanofibres for methane detection, Vacuum. 77 (2005) 223–229.
[26] R. Leghrib, A. Felten, F. Demoisson, F. Reniers, J.-J. Pireaux, E. Llobet, Room-temperature, selective detection of benzene at trace levels using plasma-treated metal-decorated multiwalled carbon nanotubes, Carbon. 48 (2010) 3477–3484.

5. Analysis of graphene oxide and its reduction process

5.1. About the Raman analysis of graphene oxide

Since its discovery by A.Geim and K.Novoselov [1] graphene has been widely studied as a potential alternative for different applications, from supercapacitors [2] to solar cells [3]. In order to transfer these ideas to the society, an industrial fabrication method has to be envisioned. Chemical oxidation and subsequent exfoliation [4] is one of the more promising approaches for obtain graphene in industrial quantities. In spite of that, this method has several disadvantages being the most important the oxidation of the surface of the graphene platelets, obtaining graphene oxide (GO), an insulator material [5]. In top of that, with a reduction process we will obtain reduced graphene oxide (rGO), a material not fully understood with properties only similar to the ones of graphene [6].

The use of Raman microscopy for the analysis of the reduction process of GO is a logical choice. First of all, is a non destructive analysis technique and easily scalable to an industrial level, making it a potential candidate for quality control of the as synthesised graphene. Moreover, the Raman spectra of carbon is well known and widely studied [7,8]. The most usual feature detected is a peak centred around 1582 cm^{-1}, called the G band, produced by the stretching between pairs of sp^2 C atoms corresponding to the E_{2g} symmetry. Is interesting to note that this is the only mode to be expected Raman active, but another band is detected around 1350 cm^{-1}, the D band. First assigned to a breathing mode of A_{1g} [7,9], is forbidden in a perfect graphite crystal, but appears when defects are present in the lattice. The origin of the D

band has been widely discussed, as the different models proposed failed to explain some phenomena associated to this band, like its dispersion in the position in function of the photon energy [9,10]. Finally, it was found that the D band is originated from inter-valley double resonance elastic phonon scattering with a defect close to the K point of the Brillouin zone [11,12]. Because that, the ratio between the intensity of the G and D bands is related to the sp^2 and sp^3 domains, and to the quality of the carbon materials [7]. In the other hand, the second-order peak 2D is essentially important for the study of graphene because its shape is related with the number of layers [13,14], being possible to identify its thickness only with Raman spectroscopy.

Meanwhile the different carbon nanostructures (nanotubes, nanofibers, graphene…) have similar Raman spectra than pure graphite [15–17]; GO and its reduction products have somewhat different spectra [18,19] (Fig. 1b), with apparently wider D and G bands, and a splitting of the second order peak in three sub-bands. Ferrari et. al. observed this kind of spectra in disordered and amorphous carbon [9,10,20], so is plausible to associate the structure of GO to a very defective carbon. In fact, has been already pointed out that in either GO and rGO the number of defects is very high due the attachment of functional groups over the sp^2 surface during the oxidation process for the synthesis of this material [4,5]. Despite these obvious differences in the structure and subsequent Raman spectra, it is established to keep using the ratio between the D and G bands in order to obtain the quality of GO and rGO [18,19,21,22].

We consider that this approximation may not be the most accurate one due to this defective nature of GO. Thus, when one compares the Raman spectra of graphene and GO side by side (Fig. 1), it can clearly see that is impossible to fit the GO Raman spectra with only two peaks. But if we add a third band centred around 1500 cm^{-1} we obtain a more accurate fit, meaning that may be more than two bands that can explain the GO Raman spectra. In fact, in the literature we can find examples of bands studied in carbon that can be applied in the study of GO. It has been reported a peak at 1620 cm^{-1} called D' for defective graphite [23,24]. This peak appears always when the sample contains certain level of defects, and its intensity increases when the defects increase [21]. So, it is plausible to suppose that this D' peak also could contribute in the overall of the Raman spectra of GO. On the other

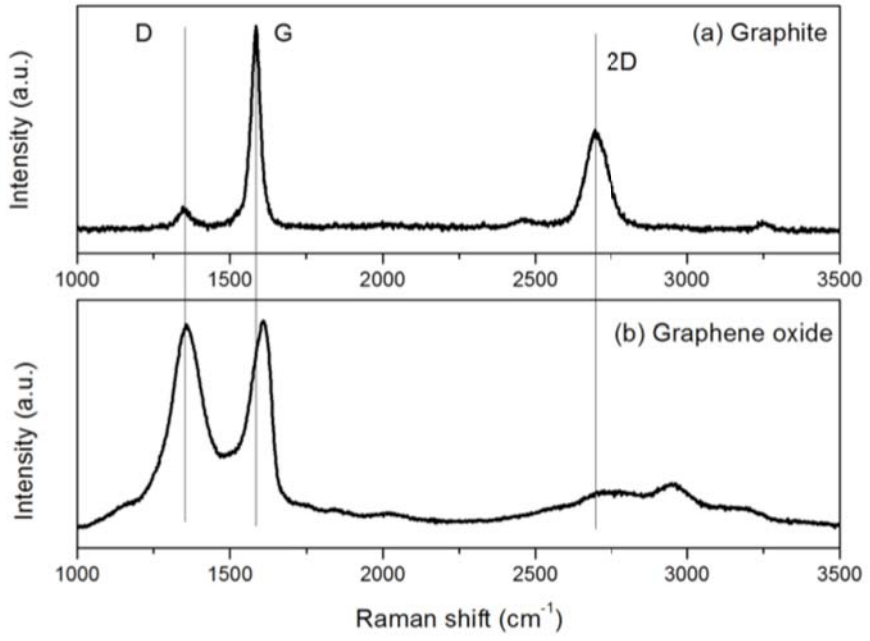

Figure 1. . Comparison between the Raman spectra of (a) graphite and (b) graphene oxide.

hand, the band around 1500-1550 cm^{-1} that we found after fitting the GO spectra has been previously proposed for materials chemically similar to GO as carbon black or soot, and is named D'' [24–29] (Fig. 2). This D'' band was associated to amorphous carbon [24] and particularly to interstitial defects caused by functional groups attached to the carbon layers structure [26–30]. Taking into account that the Raman spectra of the GO and these materials is very similar and that is already reported that the crystalline lattice of GO is distorted by the functional groups attached over its structure after the oxidation process, is plausible to think that the D'' band also is present in the deconvolution of Raman spectra of GO and its reduction products, and is needed to explain its chemical and structural properties instead of using only the G and D bands alone [27–29].

In the next sections we will show for the first time the use of the D'' band for the study of the Raman spectra of GO and rGO and its importance to achieve relevant information about its oxidative degree. To prove this assumption we have analysed the structural, chemical and morphological properties of GO and its reduction products by means of X-Ray Diffraction (XRD), Elemental Analysis, Raman spectroscopy and Field-Emission Scanning Electron Microscopy (FESEM). All results allowed using, for the first time, the D'' band to monitor the reduction process of GO prepared by the oxidation of GANF® nanofibers. Moreover, the new proposed deconvolution using the D'' band results in different ratio relations between the D and G bands that fits better with previously proposed models like the Tuinstra-Koening relation or the ones proposed by Cuesta et al. in contrast with the two peak deconvolution procedure.

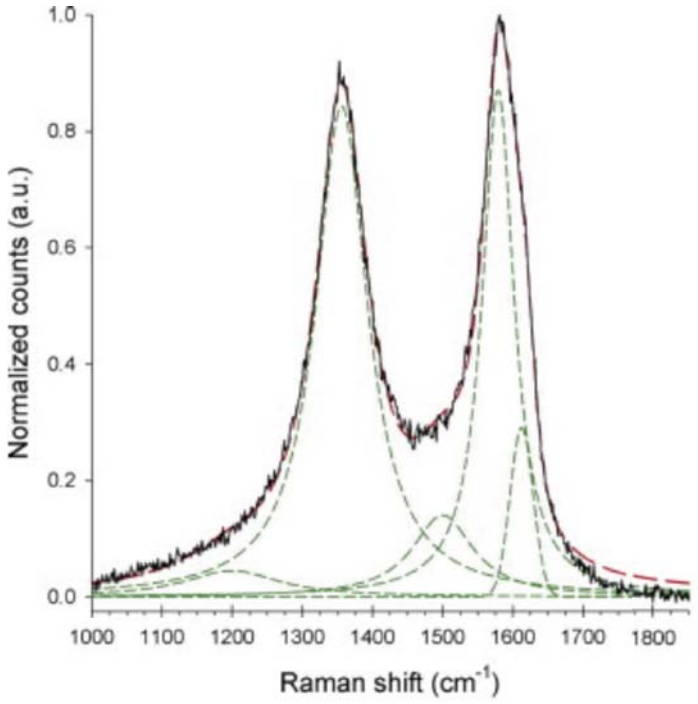

Figure 2. Example of a peak adjustment using the D'' peak. Adapted from [26].

5.2. Raman characterization of the reduction of graphene oxide by thermal treatment

The graphene oxide (GO) and reduced graphene oxide (rGO) samples were synthesised at Grupo Antolín Ingenieria following the synthesis technique described in Chapter 3. In summary, carbon nanofibers are oxydized in order to introduce oxygen functional groups between the graphitic layers that will increase the distance between them. Then is possible to separate the graphene flakes by appling energy, for example, sonic vibrations. Alternatively, the material can be annealed in a vacuum atmosphere in order to eliminate the functional

groups and reduce the sample, obtaining rGO. For this study, a same batch of GO is annealed in vacuum from 400ºC to 800ºC (see Table 1).

Samples	***Annealing temperature (ºC)***
GO	--
rGO1	400
rGO2	500
rGO3	600
rGO4	700
rGO5	800

Table 1. Samples of GO and rGO prepared in this study.

In Figure 3 are presented the FESEM image of the GO and one of the reduced products (500ºC). As we can see, it is clear that the reduction process conducts to an increase of the volume of the microstructure, forming a flower-like shape. In Figure 2c we can see a rGO single-layer, confirming that the structure is formed by GO layers and not by oxidized graphite.

Changes in the oxidation degree of graphene oxide induce changes in the interlaying structure. Therefore, we used the X-ray diffraction measurements (XRD) as an effective method of characterize the oxidative degree of our samples. In order to obtain the correct interlayer distance, the XRD measurements has been performed without any exfoliation of the samples (as shown in Fig. 2).

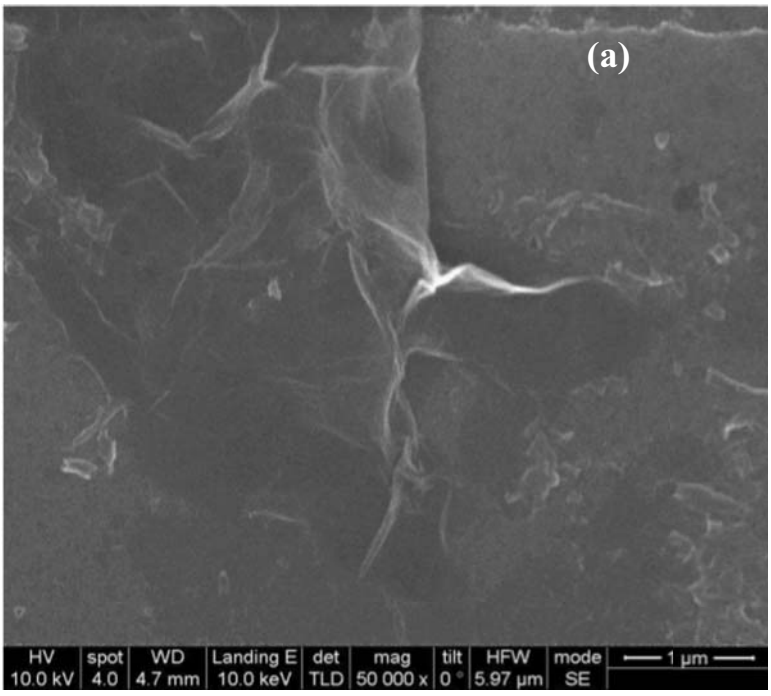
(a)
HV 10.0 kV
spot 4.0
WD 4.7 mm
Landing E 10.0 keV
det TLD
mag 50 000 x
tilt 0 °
HFW 5.97 µm
mode SE
1 µm

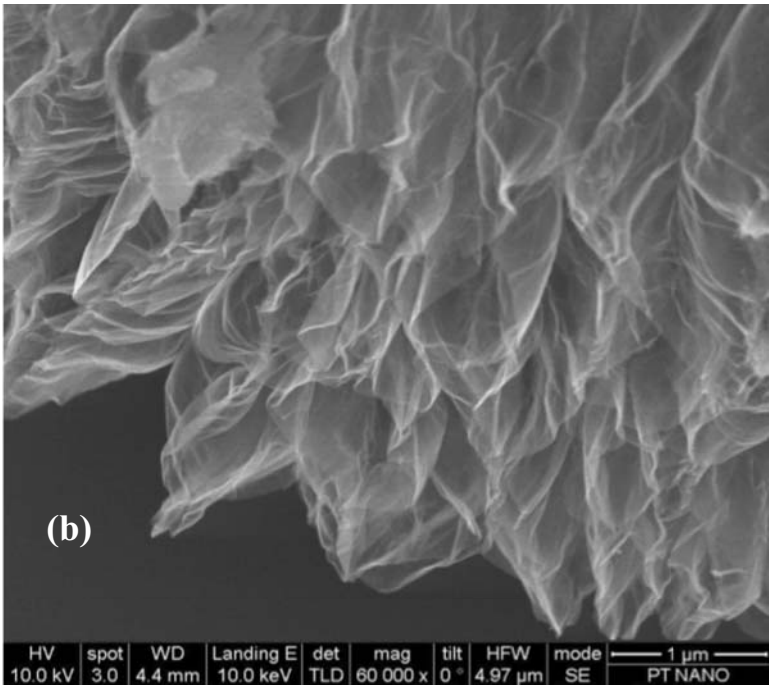
(b)
HV 10.0 kV
spot 3.0
WD 4.4 mm
Landing E 10.0 keV
det TLD
mag 60 000 x
tilt 0 °
HFW 4.97 µm
mode SE
1 µm
PT NANO

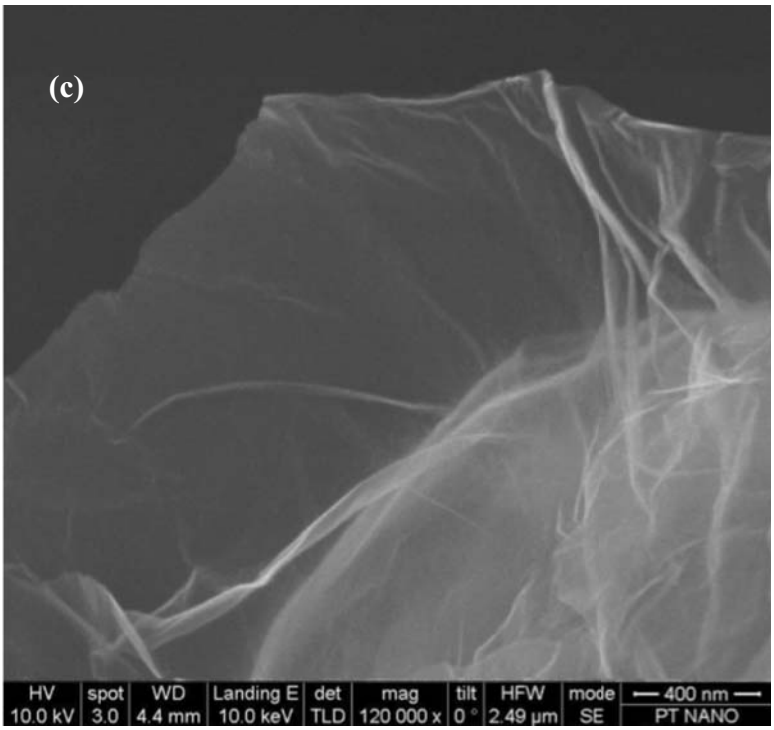

Figure 3. FESEM images of (a) GO, (b) rGO at 500ºC and (c) a single-layer rGO.

Figure 4 collects the XRD difractogram of the different samples. As it is well established, the graphite diffractogram presents a peak around 26º assigned to the (002) plane diffraction [31]. From this value and using the Bragg's law, the interlayer distance between sp^2 carbon layers for graphite can be calculated and the value found was 3.35 Å. This peak is shifted to smaller angles after oxidation. This behavior demonstrates an increase in the interlayer distance attributed to the formation of O-groups [32] and water molecules [35]. From our XRD results it can be concluded that the major feature corresponds to the 002 peak. The peak position for GO is around 10º and agrees very well with the position corresponding to oxide graphite [33]. As expected after the reduction process carried

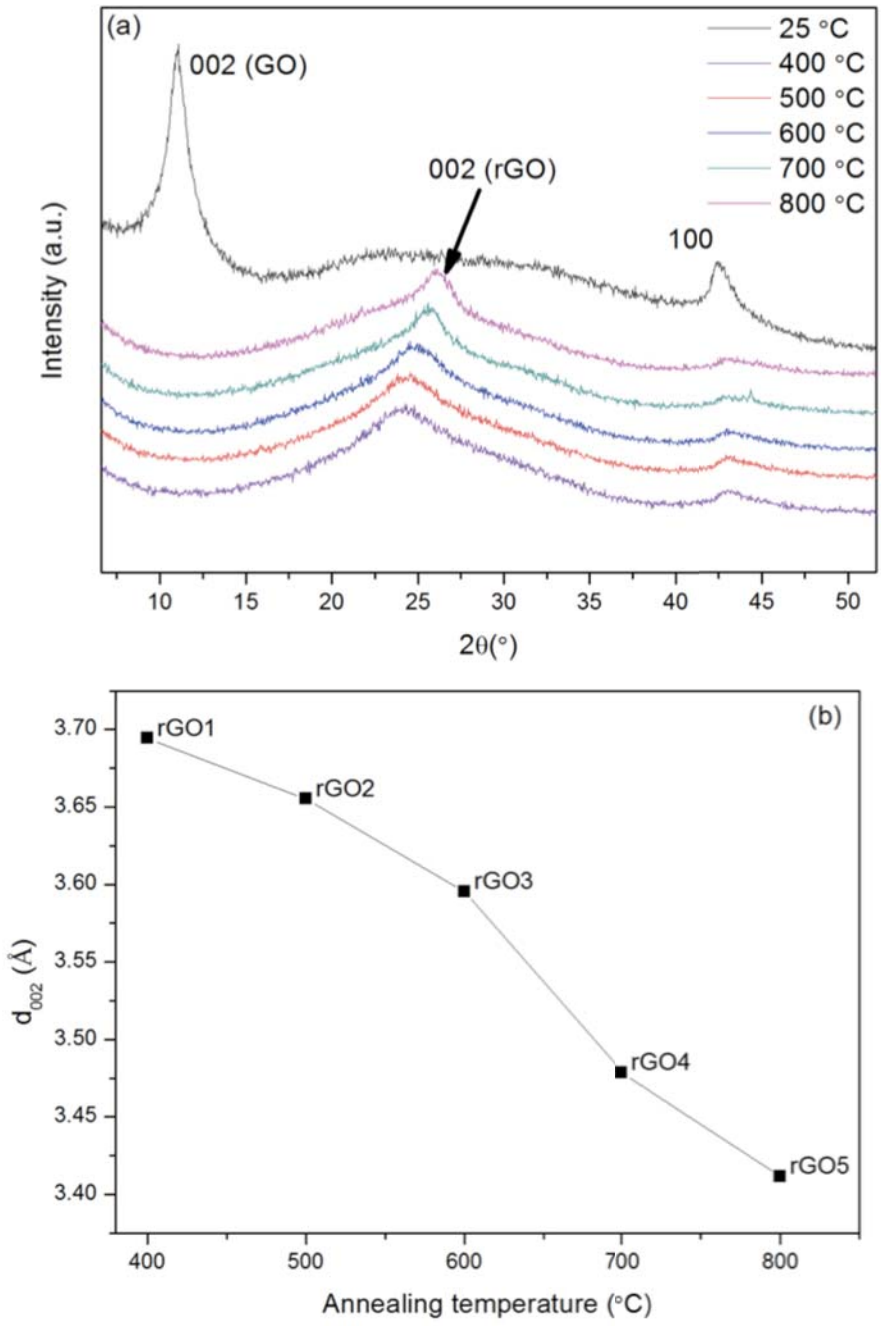

Figure 4. (a) XRD spectra for the different samples. (b) Evolution of the interlayer distance with the annealing temperature.

out by annealing, the 002 peak is shifted to higher values and because some functional groups are removed, the interlayer distance decreases again. Moreover, the XRD diffractograms demonstrate that the highest annealing temperature leads to the most shrunk structure; however, it does not reach the interlayer distance of graphite. This means that the reduction process is not complete, and some functional groups still remain intercalated after the annealing at 800ºC. In order to confirm this issue, Elemental Analysis of the samples was performed. The evolution of the oxygen content with the annealing temperature is shown in Fig. 5. As can be seen, a significant decrease of the oxygen content was observed after the annealing at 400ºC. Above this temperature, the oxygen content presents an almost lineal decrease with temperature. This behaviour is consistent with the linear trend observed for the interlayer distance (Fig. 4b). Also, its mutual relation also is almost linear (Fig. 5b), confirming the direct relation between the oxygen content, or quantity oxygen functional groups, and the interlayer distance between sp^2 layer. Finally, is also important to note that the Elemental Analysis results showed that the annealing at 800ºC does not completely eliminate the oxygen functional groups, as it was suggested from the XRD measurements. Figure 6 shows a representative Raman spectra of the 6 samples. As previously commented, each spectrum presents three major features: the D band centered at 1350 cm^{-1}, the G band at 1600 cm^{-1} and the broad band centred around 3000 cm^{-1}. Results allow concluding that the Raman spectra of reduced samples are quite similar to the GO one.

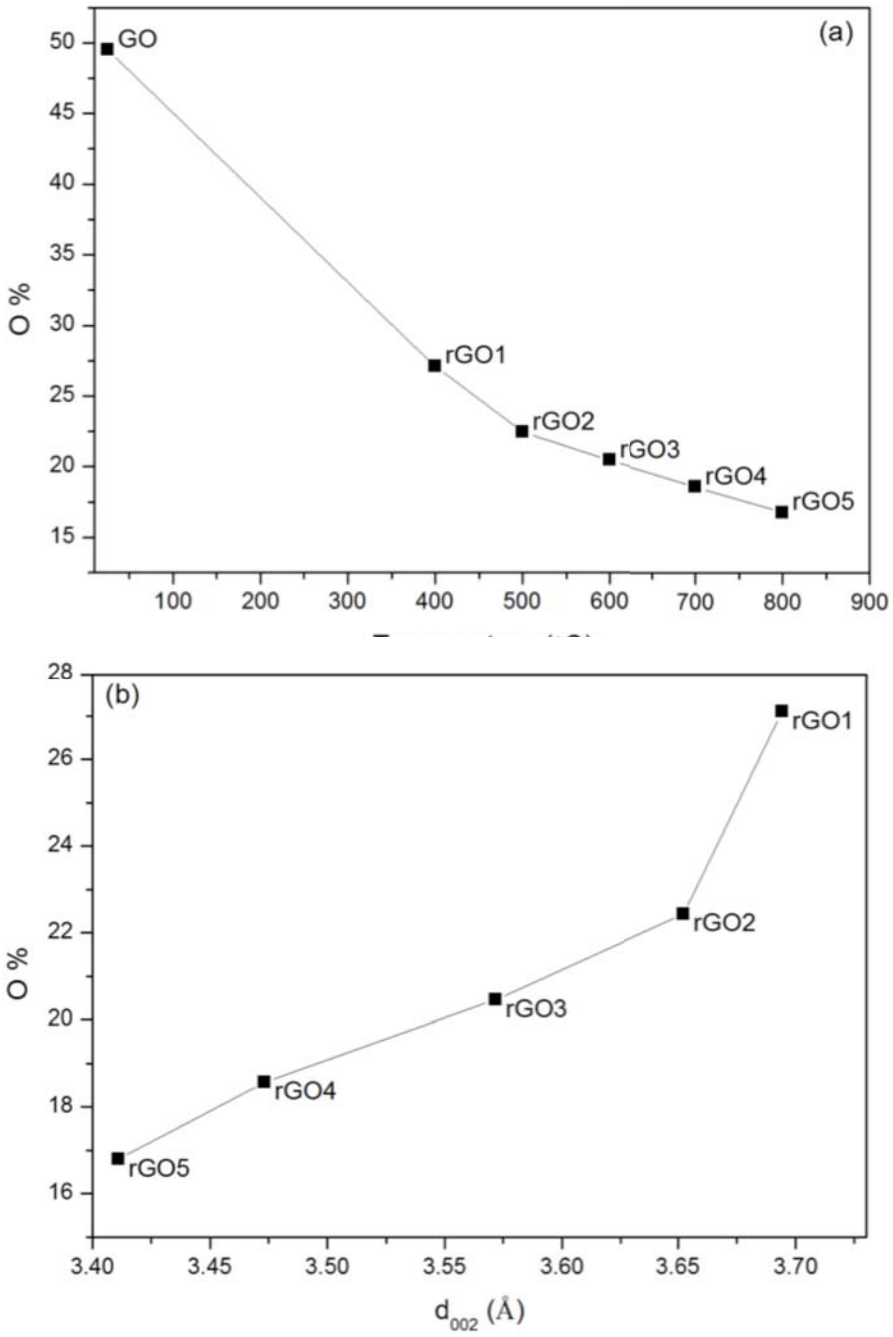

Figure 5. Evolution of the oxygen content (obtained by Elemental Analysis) of the different samples (a) with the annealing temperature and (b) the interlayer distance of the samples.

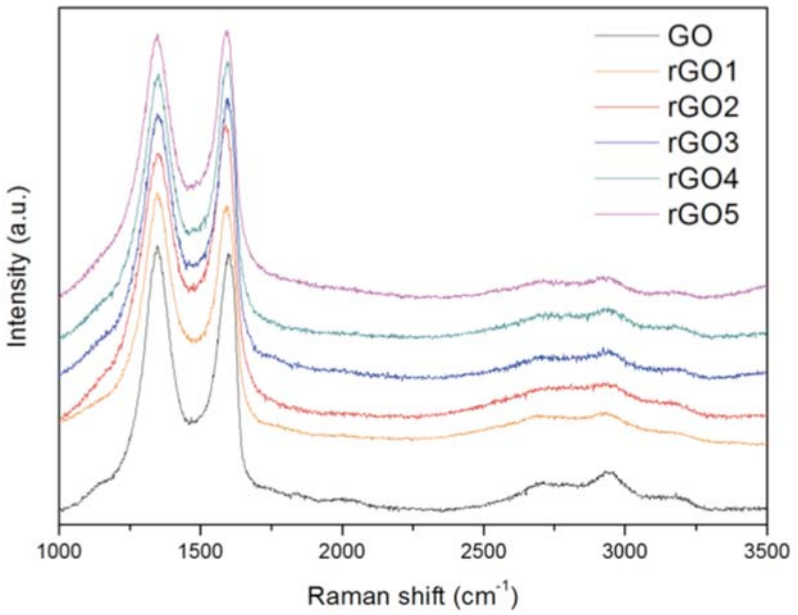

Figure 6. Raman spectra of GO (25ºC) and it reduction products at different temperatures.

This is an expected result if one takes into account that the XRD and Elemental Analysis results showed the existence of some O-groups after the annealing process, accordingly, Raman bands ascribed to basal defects produced by O-containing groups must be observed in our samples. We could estimate the degree of defect repair after the annealing by calculating the I_D/I_G ratio. As the I_D/I_G ratio is a measure of the defects in the sp^2 bonding character [7] the high values indicates the presence of unreduced groups or disorder introduced by functionalization of the graphene [34].

During analysis of the Raman spectra of GO and rGO we found some drawbacks. First of all, it is clear that the G band is an asymmetric peak that unlike the graphene case can be decomposed in several peaks. According to it we have decomposed the G band in three peaks ascribed to D' and D'' bands. These bands, as mentioned in the introduction section are associated to chemical defects caused by

covalent bounds between the carbon network and oxygen produced in the oxidation process (D' band) and to interstitial defects between two superimposed aromatic layers due to the oxygen functional groups [30]. So, we think that the use only the two-peak approximation (D and G bands) to study the reduction process by means of the Raman spectroscopy may lead to the incorrect interpretation of the data obtained.

In Figure 7 we present an example of the deconvolution of the Raman spectra the GO sample using a 4-peak fitting. Now, the G peak is less intense than in the 2-peak approximation and the D' peak helps to the shape of the total "sp^2" peak. In the other hand, the shape of the D peak does not change, and represents almost the totality of the "sp^3" peak. Finally, a central peak (D'') centred at around 1540 cm^{-1} is used to fit accurately the spectral profile. This peak is the responsible of the dramatic decrease of the G peak intensity, and hence of changing the interpretation of the degree of disorder of the sample.

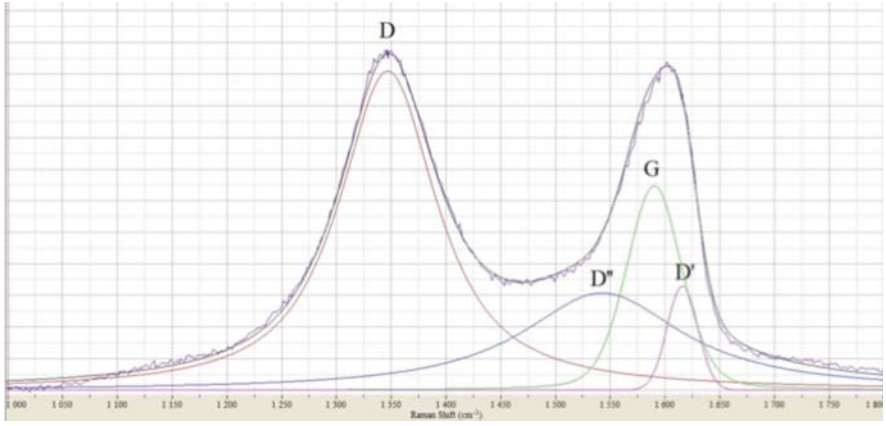

Figure 7. Example of a deconvolution of the Raman spectra of a graphene oxide using 4 peaks.

As said in the Introduction section, the D'' originates from the amorphous fraction of the sample that can be organic molecules, functional groups or amorphous fragments. In our case, according with the XRD and Elemental Analysis results, the "amorphous fraction" comes from the functional groups attached to the graphene surface. So, the characteristics of this band may be dependent of the degree of oxidation, this is, the amount of functional groups attached to the sp^2 structure. As we can see in Figure 8a, the D'' peak position moves to lower wavelengths at higher annealing temperatures, until reaching the 1500 cm^{-1}, that is the value reported for amorphous carbon [30]. So, the elimination of the functional groups seems to rearrange the sp^2 lattice, tending to a more carbonaceous structure. This can be seen in the position of the G peak, as it also has the expected shift in the position in function of the annealing temperature (Fig 8a) in accordance with the literature [4]. Moreover, this effect is not only detected in the basal plane, but also in the c-axis. Figure 8b shows the evolution of the position of the D'' peak of the reduction products with the interlayer distance (functional groups) and also reveals an almost linear tendency, supporting the theory that during the annealing process the functional groups are eliminated and this produces a rearrangement of the sp^2 network, as can be seen in the change in position of the D'' peak. To confirm this, we monitored the change of the I_D/I_G ratios in function of the interlayer distance d_{002} during the annealing process, as can be seen in Figure 9. According to the results

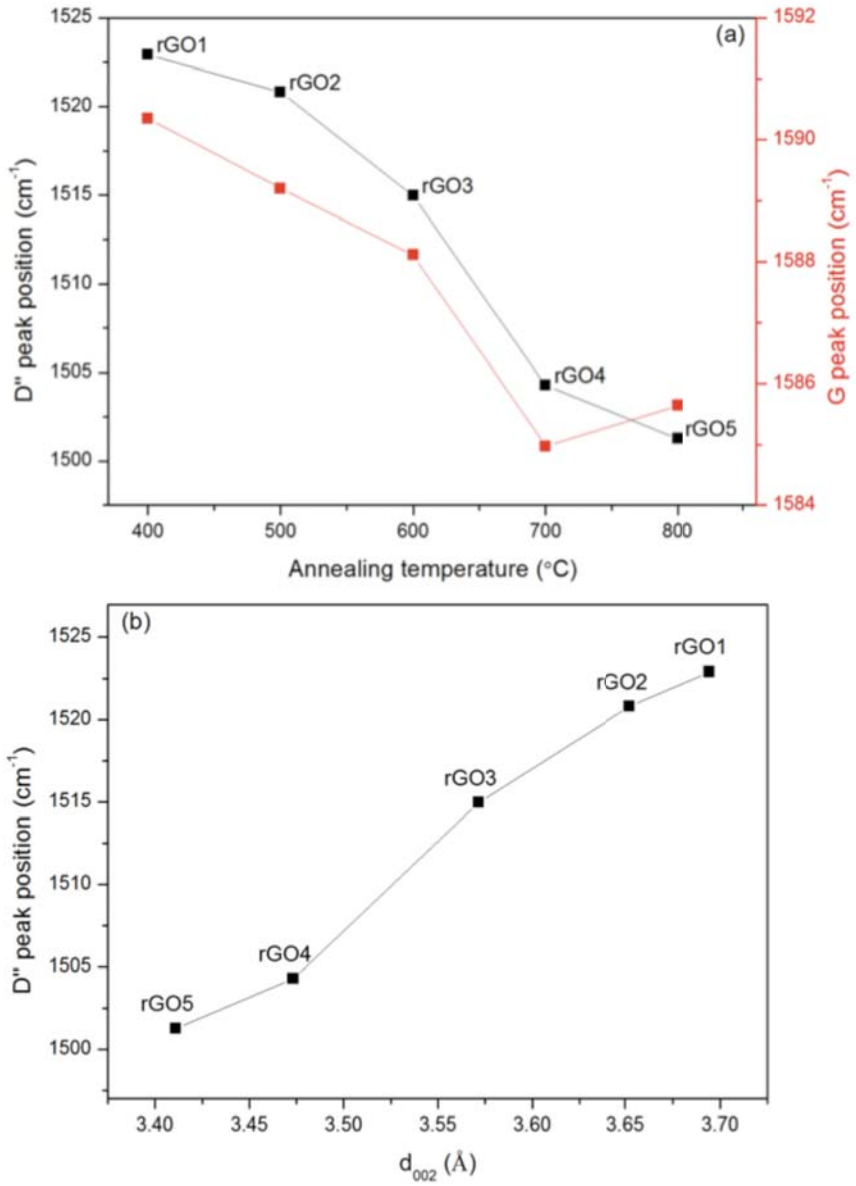

Figure 8. Evolution of the D'' and G peaks position in function of the (a) annealing temperature and (b) position of the D'' peak position in function of the interlayer distance of the rGO.

presented until now, the reduction process eliminates the oxygen functional groups, rearranging the carbon layers and obtaining a more ordered structure. We found that meanwhile for the 4-peak

approximation is observed an important decrease in the I_D/I_G ratio (this is, the G peak gets more intense in relation the D peak) at higher temperatures, for the 2-peak approximation the ratio is almost constant. This means that the 4-peak approximation is more consistent with the reduction process than the simplest 2-peak fitting, as this last strategy seems to overestimate the G peak intensity and is needed to use the D' and D'' to taking into account the effect of the very defective nature of the GO and rGO over the Raman spectra.

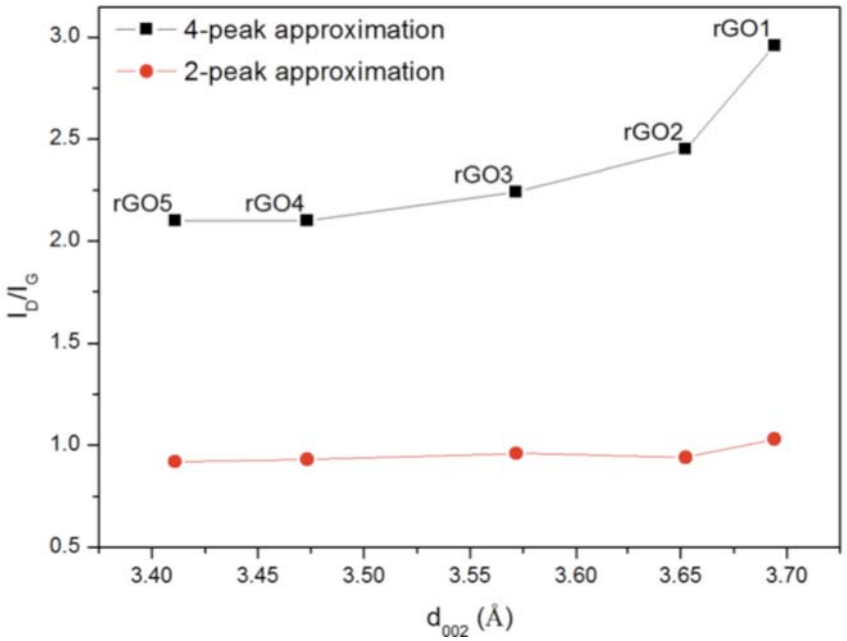

Figure 9. Evolution of the I_D/I_G ratio in function of the interlayer distance for the 4-peak approximation (black squares) and the 2-peak approximation (2-peak circles).

In order to assure that the previous results are consistent, in the following lines we will compare relations used for different types of carbon materials, but not applied for GO and rGO until now.

Tuinstra and Koenig found that there is a linear correlation between the I_D/I_G ratios and the inverse of the crystallite size along basal

planes ($1/L_a$) [7], confirming that with Raman measurements we can obtain the grade of order of a graphite sample. Later it has been found that this relation is not unique and cannot be applied to all type the graphites at once. For example, Cuesta et al., after a systematic study of different samples, found that the original relation underestimate the L_a for defective graphites [24]. In spite of that, it is still applicable but with a different slope for different families of graphites or carbon nanostructures. We applied the Tunistra-Koening correlation to our samples in Figure 10. In there is represented the points obtained from the 4-peak fitting and the 2-peak fitting. We can see that only the 4-peak fitting follows a linear behaviour compatible with the Tunistra-

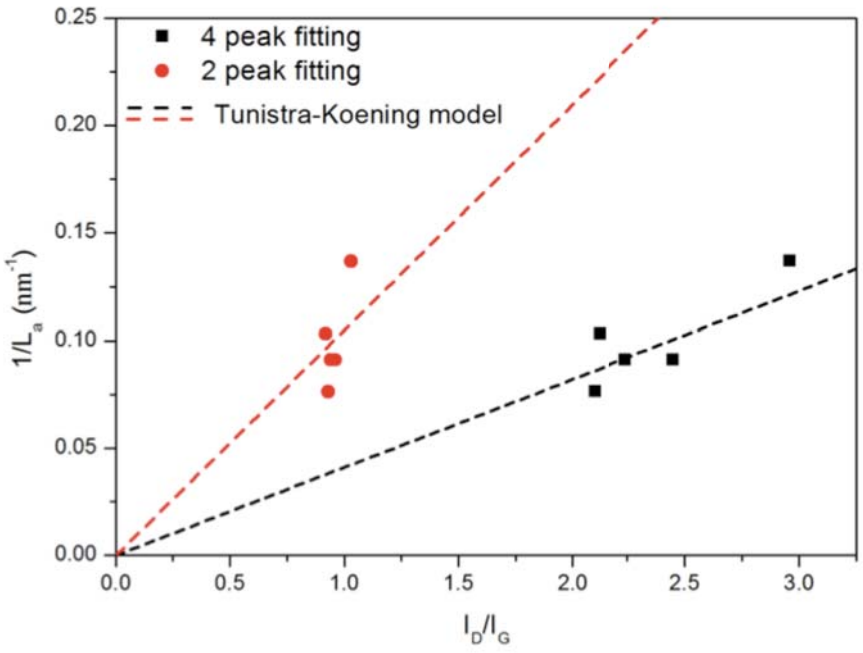

Figure 10. Tuinstra and Koening relations for the data obtained from the 4 peak fitting (black squares) and the 2 peak fitting (red circles).

Koening relation, so this fit may be more adequate for analysing the Raman spectra of the GO and rGO. Also it can be seen that the in the 2-peak approximation we obtain lower I_D/I_G relations, so using this fitting may lead to a misinterpretation of the degree of order of the sample, and hence, its oxidation state.

In order to confirm this result we can analyze other relations. In particular, is possible to compare the percentage of defects (calculated as $\frac{I_D}{(I_D + I_G)}$) obtained from the Raman analysis and parameters measured with the XRD analysis, in particular the crystallite size in the basal plane (as in Tunistra and Koening plots) or the interlayer distance (d_{002}), as is suggested by Cuesta et al [24]. In the case of the basal plane, the points obtained for the 4-peak fitting (Fig. 11a) are at values lower than the curve proposed by Cuesta et al, but are located between the 60% and 80% zone where the majority of disordered carbons are located [24,25]. Meanwhile, with the 2-peak fitting, although the points are closer to this curve, they are located out of this region, around the 50%, that corresponds to the carbon nanofibers region. In the case of the relation with the interlayer distance we obtain a similar result (Fig. 11b). The points obtained with the 4-peak fitting are located in the vertical line of the theoretical evolution that is reserved for the disordered carbons. In spite, with the 2-peak fitting, the points obtained also follows a vertical line but are located in the zone of mid-defective carbons, where the interlayer distance linearly increases with the percentage of defects. These results supports the conclusion obtained using the Tunistra and Koening method, that suggest that using the 2-

peak fitting the G peak is overestimated and hence gives as a result that the oxidation of the sample is lower than really is.

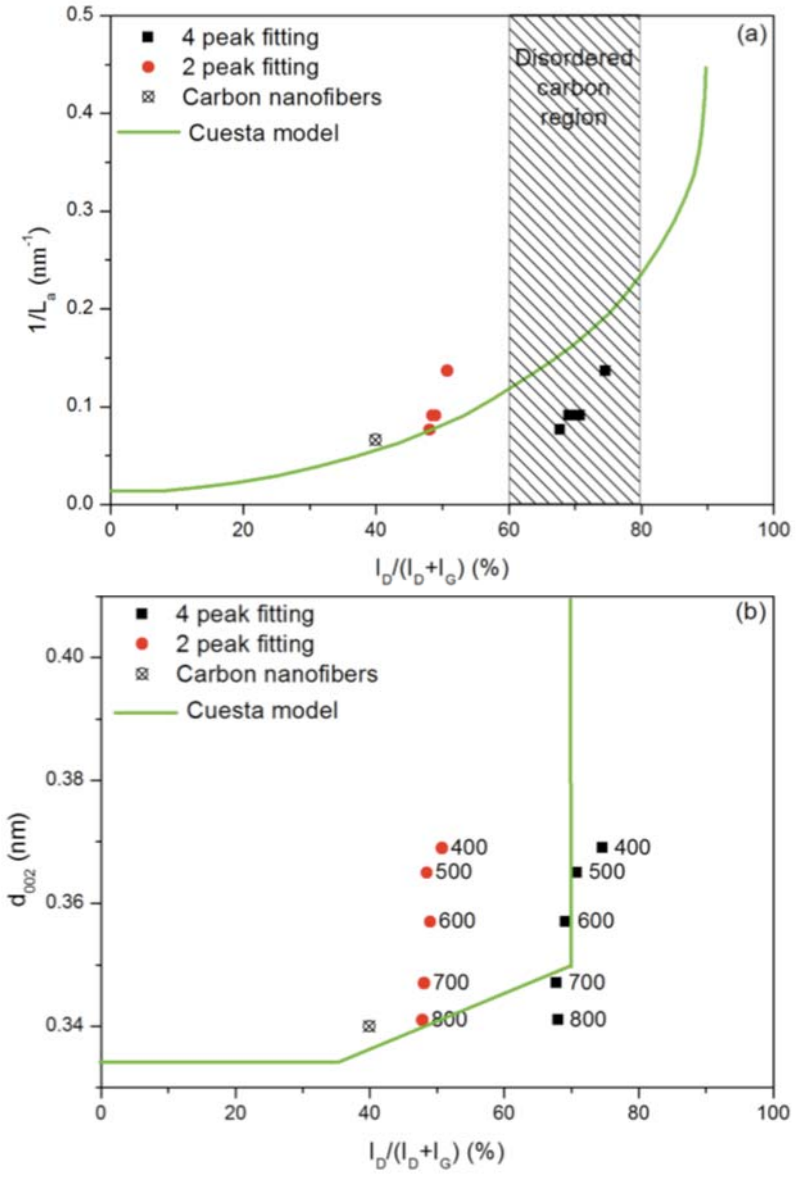

Figure 11. Plots comparing the percentage of defects versus (a) the inverse of crystallite size and (b) the interlayer distance.

5.3. Reduction of graphene oxide by ionic bombardment.

Thermal reduction may be useful for the reduction of material in powder form. But the reduction of this powder will make more difficult its manipulation for create layers of rGO, so is more interesting first deposit a layer of GO and then reduce the sample. This approximation have the drawback that also we depend of the properties of the substrate in order to choose the reduction method. For the thermal reduction, because the high temperatures reached, the substrate may be damaged or destroyed (for example glass or polymer) and other reduction processes may be used. One alternative could be the ionic bombardment. In this technique, the layer of GO is exposed to a plasma of a reducing gas, for example argon. The argon atoms will attack the functional groups over the substrate hopefully leaving the carbon structure intact. Of course, depending the power applied and the exposure time the carbon structure also will be etched.

The samples were synthesised at Grupo Antolín Ingeniería and after proper dispersion were deposited over a SiO_2/Si substrate by the Lagmiur-Blodgett technique. This assures the deposition of a thin layer of material, almost monolayer as can be seen in Figure 12. The control sample was deposited over a marked substrate, so it will be possible to identify always the same analysis region. The analysis was performed exclusively using Raman spectroscopy, as the fastest way to know the grade of reduction after successive plasma treatments.

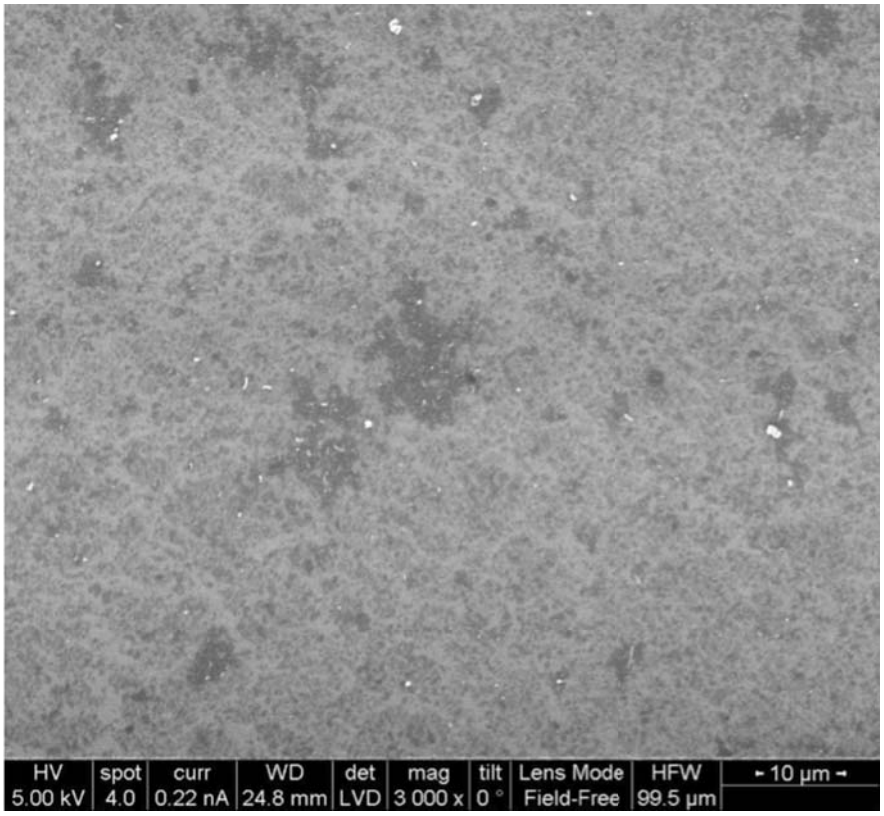

Figure 12. Layer of GO obtained by Lagmiur-Blodgett technique.

As in the case of GO and rGO the signal depends strongly on the amount of material, the Raman analysis will be more difficult. In order to obtain a good signal, has been selected a region with a higher superficial concentration of material that can be seen with a optical microscopy (Fig. 13). By this way, the Raman signal also well be identifiable and with less noise.

After the deposition over the SiO_2/Si substrate the sample is treated with a plasma cleaner using Ar gas and the lowest power. Between Raman meaurement there is a plasma tratment of 30s. This has been done 5 times (30s, 60s, 90s, 120s and 150s) over the same sample.

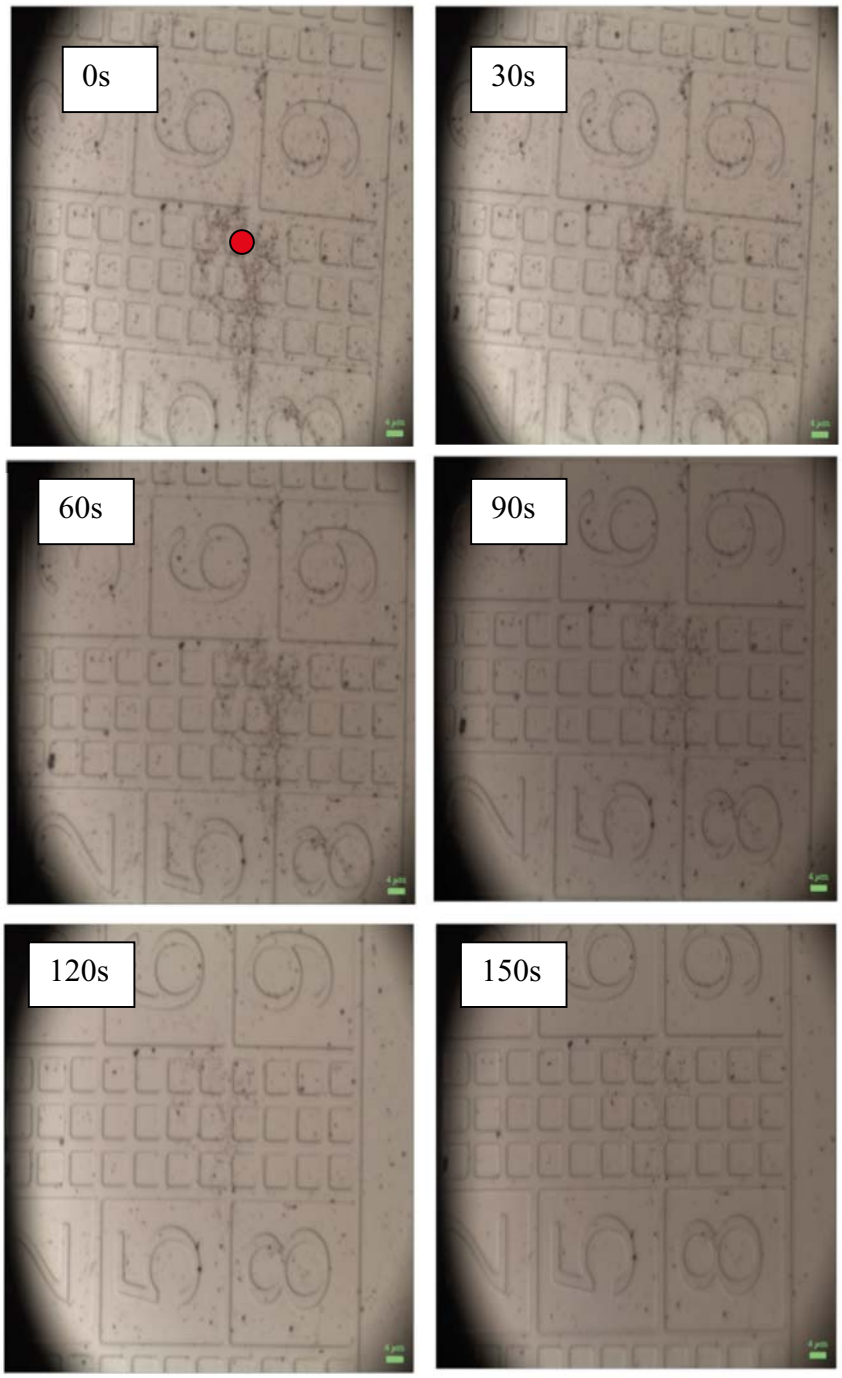

Figure 13. Optical images of successive treatment with Ar plasma of GO depostide by the Lagmiur-Blodgett technique. The red point in the untreated sample points the measurement area used.

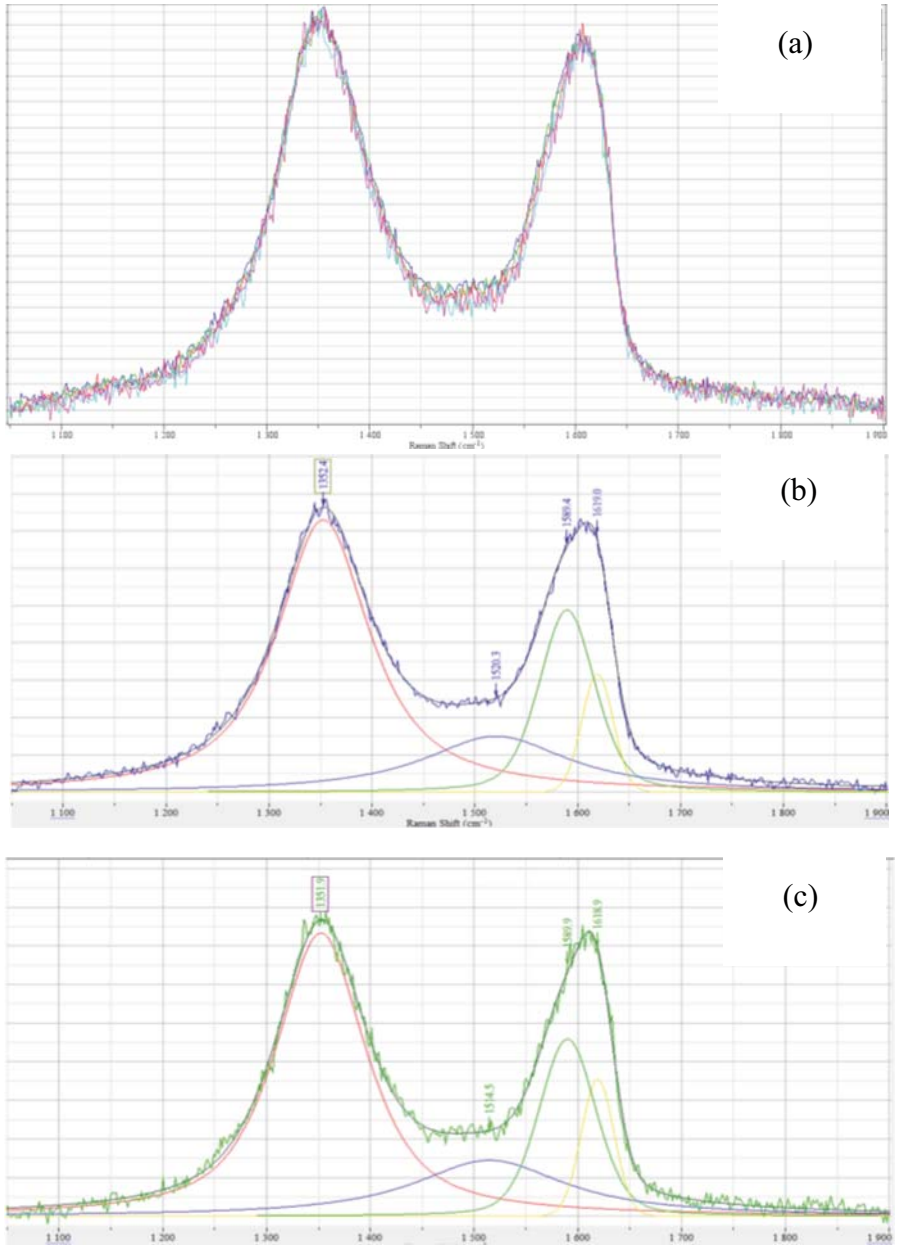

Figure 14. (a) Superposition of the spectra of each treatment process. (b) Adjustment of the Raman spectra of the 30 s treatment and (c) adjustment of the Raman spectra of the treatment of 150s.

One of the first evidences is that the material over the substrate is disappearing for each treatment. Moreover, this also can be seen with the decrease of the Raman signal obtained from the same measurement point. In spite of that is still possible to measure the Raman spectrum for each plasma treatment.

The Raman spectrum of all treatments shows that there is no change after each treatment (Fig. 14). At first sight the ratio between the band do not change. Making the adjustment just explained on the previous section on the 30s sample and 150 s sample also shows that the Raman spectrum do not change at all. There a slight increase of the D' band respect the G band that could indicate a increase of the defect. Also, the D'' is displaced 6 cm^{-1} to lower wavelengths pointing a possible low reduction.

The problem is that using the lowest power the material is destroyed without reaching a proper reduction. In conclusion, the use of a Plasma Cleaner in order to reduce a layer of GO is not useful at all.

5.4. Conclusions

In this chapter have been discussed the Raman analysis of GO. This material have a Raman spectrum different to any other graphitic materials because the defects caused by the oxygen functional groups attached at the basal plane of the graphene layer. We argue that the usual analysis techniques used for graphite cannot be applied to GO. Instead we use a procedure envisioned for activated carbons in general

(chemically similar to GO) that is the addition of a band called D'' originated precisely in the interstitials defects of the oxygen functional groups. Also, we propose that is necessary to use the D' band as being a very defective graphite necessarily has to appear. So, we propose an adjustment of the two main peaks by the use a 4-peak deconvolution (D, G, D' and D''). It was found that the evolution of the D'' and "new" G peaks coincides with the rate of reduction of the sample. Moreover, the D'' displacement is easier to quantify, as moves from 1525 cm^{-1} to 1500 cm^{-1} meanwhile the G peak only moves 10 cm^{-1}, meaning the D'' peak has the potential to be a marker of the reduction state of the rGO. Finally, has been demonstrated that the use of the 4-peak adjustment follows the models proposed by Tuinstra and Koening and Cuesta *et al*. for the evolution of the defects in graphite, meanwhile using the 2-peak approximation fails for GO.

In the second part, it was studied the reduction of a layer of GO using an Ar plasma. It was found that, in spite to use the lowest power available the plasma damage the carbon structure before the reduction take place, meaning that this approximation is not useful for achieve a proper reduction.

References

[1] A.K. Geim, K.S. Novoselov, The rise of graphene., Nat. Mater. 6 (2007) 183–91.

[2] Z. Fan, Q. Zhao, T. Li, J. Yan, Y. Ren, J. Feng, et al., Easy synthesis of porous graphene nanosheets and their use in supercapacitors, Carbon N. Y. 50 (2012) 1699–1703.

[3] X. Wang, L. Zhi, K. Müllen, Transparent, conductive graphene electrodes for dye-sensitized solar cells., Nano Lett. 8 (2008) 323–7.

[4] G. Eda, M. Chhowalla, Chemically derived graphene oxide: towards large-area thin-film electronics and optoelectronics., Adv. Mater. 22 (2010) 2392–415.

[5] K. Andre Mkhoyan, A.W. Contryman, J. Silcox, D. a Stewart, G. Eda, C. Mattevi, et al., Atomic and electronic structure of graphene-oxide., Nano Lett. 9 (2009) 1058–63.

[6] A. Bagri, C. Mattevi, M. Acik, Y.J. Chabal, M. Chhowalla, V.B. Shenoy, Structural evolution during the reduction of chemically derived graphene oxide., Nat. Chem. 2 (2010) 581–7.

[7] J.L. Tuinstra, F., Koenig, Raman spectrum of Graphite, J. Chem. Phys. 53 (1970) 1126 – 1130.

[8] Y. Wang, D.C. Alsmeyer, R.L. McCreery, Raman spectroscopy of carbon materials: structural basis of observed spectra, Chem. Mater. 2 (1990) 557–563.

[9] A.C. Ferrari, J. Robertson, Interpretation of Raman spectra of disordered and amorphous carbon, Phys. Rev. B. 61 (2000) 95–107.

[10] A.C. Ferrari, Raman spectroscopy of graphene and graphite: Disorder, electron–phonon coupling, doping and nonadiabatic effects, Solid State Commun. 143 (2007) 47–57.

[11] C. Thomsen, S. Reich, Double resonant raman scattering in graphite, Phys. Rev. Lett. 85 (2000) 5214–7.

[12] R. Saito, A. Jorio, A.G. Souza Filho, G. Dresselhaus, M.S. Dresselhaus, M.A. Pimenta, Probing Phonon Dispersion Relations of Graphite by Double Resonance Raman Scattering, Phys. Rev. Lett. 88 (2001) 027401.

[13] a. C. Ferrari, J.C. Meyer, V. Scardaci, C. Casiraghi, M. Lazzeri, F. Mauri, et al., Raman Spectrum of Graphene and Graphene Layers, Phys. Rev. Lett. 97 (2006) 1–4.

[14] D. Graf, F. Molitor, K. Ensslin, C. Stampfer, a Jungen, C. Hierold, et al., Spatially resolved Raman spectroscopy of single- and few-layer graphene., Nano Lett. 7 (2007) 238–42.
[15] X. Zhao, Y. Ando, Raman Spectra and X-Ray Diffraction Patterns of carbon nanotubes prepared by hidrogen arc discharge.pdf, Jpn. J. Appl. Phys. 37 (1998) 4846–4849.
[16] J.H. Lehman, M. Terrones, E. Mansfield, K.E. Hurst, V. Meunier, Evaluating the characteristics of multiwall carbon nanotubes, Carbon N. Y. 49 (2011) 2581–2602.
[17] Y. Ouyang, L. Chen, Surface-enhanced Raman scattering studies of few-layer graphene on silver substrate with 514 nm excitation, J. Mol. Struct. 992 (2011) 48–51.
[18] K. Krishnamoorthy, M. Veerapandian, K. Yun, S.-J. Kim, The chemical and structural analysis of graphene oxide with different degrees of oxidation, Carbon N. Y. 53 (2013) 38–49.
[19] I.K. Moon, J. Lee, R.S. Ruoff, H. Lee, Reduced graphene oxide by chemical graphitization., Nat. Commun. 1 (2010) 73.
[20] a. Ferrari, J. Robertson, Resonant Raman spectroscopy of disordered, amorphous, and diamondlike carbon, Phys. Rev. B. 64 (2001) 1–13.
[21] E.H. Martins Ferreira, M.V.O. Moutinho, F. Stavale, M.M. Lucchese, R.B. Capaz, C.A. Achete, et al., Evolution of the Raman spectra from single-, few-, and many-layer graphene with increasing disorder, Phys. Rev. B. 82 (2010) 125429.
[22] M. Cheng, R. Yang, L. Zhang, Z. Shi, W. Yang, D. Wang, et al., Restoration of graphene from graphene oxide by defect repair, Carbon N. Y. 50 (2012) 2581–2587.
[23] R. Vidano, D.B. Fishbach, New Lines in the Raman Spectra of Carbons and Graphite, J. Am. Ceram. Soc. 61 (1978) 13–17.
[24] A. Cuesta, P. Dhamelincourt, J. Laureyns, A. Martínez-Alonso, J.M.D. Tascón, Raman microprobe studies on carbon materials, Carbon N. Y. 32 (1994) 1523–1532.
[25] A. Cuesta, P. Dhamelincourt, J. Laureyns, A. Martínez-Alonso, J.M.D. Tascón, Comparative performance of X-ray diffraction and Raman microprobe techniques for the study of carbon materials, J. Mater. Chem. 8 (1998) 2875–2879.
[26] S. Vollebregt, R. Ishihara, F.D. Tichelaar, Y. Hou, C.I.M. Beenakker, Influence of the growth temperature on the first and second-order Raman band ratios and widths of carbon nanotubes and fibers, Carbon N. Y. 50 (2012) 1561–1565.

[27] T. Jawhari, A. Roid, J. Casado, Raman spectroscopic characterization of some commercially available carbon black materials, Carbon N. Y. 33 (1995) 1561–1565.
[28] S.-K. Sze, N. Siddique, J.J. Sloan, R. Escribano, Raman spectroscopic characterization of carbonaceous aerosols, Atmos. Environ. 35 (2001) 561–568.
[29] S. A., H. Muckenhuber, H. Grothe, R. Niessner, U. Pöschi, Raman microspectroscopy of soot and related carbonaceous materials: Spectral analysis and structural information, Carbon N. Y. 43 (2005) 1731.1742.
[30] J.N. Rouzaud, A. Oberlin, Carbon films: Structure and microtexture (optical and electron microscopy, Raman spectroscopy), Thin Solid Films. 105 (1983) 75–96.
[31] A. Lerf, A. Buchsteiner, J. Pieper, S. Schöttl, I. Dakany, T. Szabo, et al., Hydration behavior and dynamics of water molecules in graphite oxide, J. Phys. Chem. Solids. 67 (2006) 1106–1110.
[32] D. V. Kosynkin, A.L. Higginbotham, A. Sinitskii, J.R. Lomeda, A. Dimiev, B.K. Price, et al., Longitudinal unzipping of carbon nanotubes to form graphene nanoribbons, Nature. 458 (2009) 972–876.
[33] H.-K. Jeong, Y.P. Lee, R.J.W.E. Lahaye, M.-H. Park, K.H. An, I.J. Kim, et al., Evidence of Graphitic AB Stacking Order of Graphite Oxides, J. Am. Chem. Soc. 130 (2008) 1362–1366.
[34] B. Martín-Medina, M.M. Velázquez, F. Rossella, V. Bellani, E. Diez, J.L.G. Fierro, et al., Functionalization of Reduced Graphite Oxide Sheets with a Zwitterionic Surfactant, ChemPhysChem. 13 (2012) 3682–3690.

6. Conclusions and main findings

Here it are presented the conclusions obtained after the end of the thesis:

Electrospray deposition technique:

i) A modified electrospray deposition technique has been developed in order to create thin layers of carbon nanofibers on metal pads.
ii) With this technique there is no need to use micromachined mask like in spray coating.
iii) Have the potential to be used with other materials, like graphene oxide or reduced graphene oxide.

Carbon nanofibers XPS analysis:

i) Extensive literature research on XPS analysis was done and resulted in the proposal of an adjustment routine for C1s and O1s peaks that unifies the different XPS analysis routines.
ii) The analysis of sp^2 and sp^3 bonds signals reveals that the carbon nanofibers have a thin layer of amorphous carbon. Attacking the surface with argon sputtering reveals the true crystallinity of the surface, and shows that the graphiticated

nanofibers have a more crystalline surface than bare carbon nanofibers.

iii) TEM analysis showed that the after the graphitication treatment the graphitic edges closes on itself, exposing only the sp^2 layers.

iv) XPS analysis also shows that in spite of the high temperatures held in the graphitication process there is still 1% of surviving oxygen. Careful analysis of O1s peak reveals that the surviving functional groups are in its majority hydroxyls and carboxylic functional groups.

Carbon nanofiber surface metal decoration:

i) For a correct decoration, is needed that the CNFG were stable in polar solvent. By using a thermal treatment, the borders of the CNFG are again open, exposing the sp^3 bonds, and meaking the nanofibers more reactive. This phenomenon makes the CNFG stable in polar solvents.

ii) The more defective surface of carbon nanofibers (in comparison with crystalline carbon nanotubes) make easier to decorate its surface. The process can be a simple mix of precursors with the nanofibers, only enhanced using an extra ball milling process.

iii) It was found that for Au is needed a complete wet of the surface in order to obtain a good dispersion of nanoclusters. If the concentration of precursor is too low, inhomogeneous dispersion of big Au clusters are obtained.

iv) For Pd, its superior atom mobility over the surface of the carbon nanofiber makes that there is always a homogenous dispersion of Pd over the surface of the nanofiber. Then, for higher concentrations bigger clusters are obtained.

Sensor characterization:

i) Bare carbon nanofibers show responses to NH_3 and NO_2 at even room temperature.

ii) Mesaurement with humidity (50% RH) at room temperature only displaces the baseline but do not change the signal, opening the door for using this nanostructures in sensor applications in the real world.

iii) The addition of Pd clusters over its surface enhance the response for NH_3 meanwhil the addition of Au clusters decrease it, making the first step for increase the selectivity of the nanofibers towards this gas.

iv) At contrary, the response to NO_2 is impaired by both the noble metals.

v) The application of heat improves the response and decreases its response time as the surface is cleaned after the heat treatment. The ideal temperature of operation is around 110ºC.

Raman analysis of graphene oxide:

i) The use of a 4-peak approximation for the adjustment of the two main peaks of graphene oxide is proposed, by adding the less known D'' peak used in materials chemically similar to graphene oxide.

ii) The addition of D'' peak decreases the G peak intensity thus showing that the 2-peak approximation overestimates the crystal quality of graphene oxide.

iii) Analysis of reduced samples show that the relation of the displacement of D'' and the elimination of oxygen is almost linear. Moreover, the G peak position also tends to recover the value found in graphite. With this, the D'' peak have the potential to be a marker for the reduction state of the graphene oxide and its reduction products.

iv) The evolution of the defects analysed with the 4-peak approximation follows better the relations proposed by Tuinstra and Koening and Cuesta *et al.*, demonstrating that this method may be more suitable to apply than the 2-peak approximation used in the literature.

Reduction of GO by ion bombardement:

i) The evolution of the Raman spectra is monitored during successive plasma treatments of the sample.

ii) It was found that the ionic bombardent destroy the thin sample well before the reduction take place, meaning that this method is not useful as a reduction strategy.

Curriculum vitae

In the following lines it will be presented the different works that has been accepted for publications in different jurnals and congresses that has been developed before the end of the thesis.

Accepted papers:

Claramunt S.; Monereo O.; Boix M.; Leghrib R.; Prades J.D.; Cornet A.; Merino P.; Merino C.; Cirera A. (2013) Flexible gas sensor array with an embedded heater based on metal decorated carbon nanofibres. Sensors and Actuators B: Chemical. In Press.

Monereo O.; Claramunt S.; Martínez de Marigota, M.; Boix M.; Leghrib R.; Prades J.D.; Cornet A.; Merino P.; Merino C.; Cirera A. (2013) Flexible sensor based on carbon nanofibers with multifunctional sensing features. Talanta, 109, 239

Martín-García B.; Velázquez M.M.; Rossella F.; Bellani V.; Diez E.; Fierro J.L.G.; Pérez-Hernández J.A.; Hernández-Toro J.; Claramunt S.; Cirera A. (2012) Functionalization of Reduced Graphite Oxide Sheets with a Zwitterionic Surfactant. Chemphyschem, 13, 3682.

Participations in congresses:

Claramunt S.; Monereo O.; Boix M.; Leghrib R.; Prades J.D.; Cornet A.; Merino P.; Merino C.; Cirera A. (2012) Flexible Gas Sensor Array with an Embedded Heater based on Metal Decorated Carbon Nanofibres. Presentation of communication. International Meeting on Chemical Sensors 2012, Nuremberg, Germany.

Claramunt S.; Monereo O.; Leghrib R.; Prades J.D.; Cornet A.; Cirera A. (2012) Fabrication and deposition of Metal-oxide Nanofibres by Electrospinning Method for Sensing Applications. Poster. 2012 MRS Fall Meeting, Boston, United States.

Claramunt S.; Monereo O.; Boix M.; Leghrib R.; Prades J.D.; Cornet A.; Merino P.; Merino C.; Cirera A. (2012) Flexible Gas Sensor Array with an Embedded Heater based on Metal Decorated Carbon Nanofibres. Presentation of communication. 20th Annual International Conference on Composites Engineering, Bejing, China.

Claramunt S.; Leghrib R.; Merino C.; Merino P.; Cornet A.; Cirera A. (2012) Use of the D'' band for the analysis of Raman spectra of graphene oxide. Poster. Graphene Nanoscience: from Dirac Physics to Applications, Granada, Spain.

Monereo O.; Claramunt S.; Vescio G.; Prades J.D.; Cornet A.; Merino P.; Merino C. (2013) Carbon Nanofibres in flexible substrates for sensing applications. Presentation of communication. 21th Annual International Conference on Composite Engineering (ICCE-21), Tenerife, Spain.

Acknowledgements/Agraïments

Ara que estic escrivint aquestes línies, es difícil fer-se a la idea de que s'ha arribat al final d'una etapa. Han estat quatre anys estimulants, en que no he parat d'aprendre coses noves tant en el terreny científic, professional i personal. I aquest coneixement sempre ha vingut acompanyat de totes les persones que m'he anat trobant i han contribuït en major o menor mesura a expandir-lo. M'agradaria expressar el més profund agraïment a totes aquestes persones que m'han ajudat a arribar fins aquí.

Pel que respecta als agraïments personals deixeu-me començar pels meus director de tesi, els Alberts. En especial a l'Albert Cirera, que en el seu moment va confiar en mi i em va fer partícip de la seva recerca. Sota la seva direcció he pogut desenvolupar moltes de les aptituds professionals que tinc i realment ara em sento preparat per els nous reptes que em venen a sobre. A l'Albert Cornet també agrair-li la seva dedicació, sé que no és fàcil compaginar la direcció del departament amb la direcció d'una tesi, però no se com t'ho fas però sempre estaves a les reunions o em podies donar algun consell al passadís. Gracies per tot!

Tampoc no em vull oblidar dels meus companys de laboratori i despatx: Oriol, Giovanni, Núria, Sergio, Xavi, Dani, Jordi, Olga, Bea, Llorenç, Aïda, Alberto, Raduane, Houda, Helena... sembla que fos ahir quan vaig començar i sol érem uns quants estudiants en el grup, deu ni do com ha anat creixent! Ha estat una experiència inoblidable compartir tants bons moments! Igualment, no puc deixar de mencionar a tots els

companys de departament: Julià, Núria F., Lluisos, Sònia, Bernat, Cristina, Javi, Marcel, Marta, Sergi, Oriol, Yonder, Joan Manel, Bernat... hi han masses com per posar-los tots aquí però tots també m'han acompanyat durant el doctorat en infinitat de dinars, cafès, trobades... También enviar un saludo a Bruno, mi primer estudiante de master, fue un placer dirigirte la tesina, creo que los dos aprendimos durante este trayecto.

Ja que aquesta tesi es eminentment de caracterització, tinc que agrair de tot cor la ajuda prestada per el tot el personal de les tècniques de caracterització, tant al personal dels CCiTUB (Eva, Tariq, Sònia, Lluís, Núria, Lorenzo...) com del PCB (Judith, Raül...). Gràcies per tenir tanta paciència amb mi i permetre'm ser un autousuari "hecho y derecho".

También quiero agradecer a los integrantes del departamento de I+D de Grupo Antolín: César, Pilar, Santiago, Erika... gracias por mostrarme el "otro lado" de la investigación en nuestra larga colaboración, espero que en un futuro seguir trabajando con vosotros. También dar las gracias a nuestros compañeros de proyectos de la Universidad de Alicante (Ignacio, Helena,...) y Universidad de Salamanca (Mercedes, David, Bea,...) por la enriquecedora experiencia que me habéis brindado al poder trabajar con vosotros, que espero que continúe en un futuro próximo.

Vull agrair especialment el suport de la meva família, tant del meu germà Albert com dels meus pares, Dani i Isa, no sol durant el període de tesi doctoral, sinó també tota la vida.

I per últim, però no menys important, vull agrair de tot cor el suport de Laia, la meva dona. Podríem dir que has sofert tot el procés que m'ha portat fins aquí, sobretot els últims dies que han estat frenètic. Però com sempre, has estat comprensiva i m'has recolzat en tot moment, afegint "collejes" correctives quan feia falta. Gràcies per ser amb mi.

RC. Resum en llengua oficial

RC1. Introducció

El carboni es pot trobar ordenat en diferents estructures, cada una amb les seves pròpies característiques. En general, els materials de carboni es poden classificat en grafit, diamant, fullerens i carbó amorf. Curiosament la majoria d'estructures ordenades de carboni es poden obtenir a partir de l'estructura bàsica del grafit, es a dir, el grafé [1]. D'aquesta forma, si una fulls de grafé s'enrotlla sobre si mateixa es genera un nanotub de carboni o si es genera una estructura tridimensional apilant els plans s'obté el grafit.

Com s'ha dit, cada tipus de nanoestructura te les seves pròpies propietats que superen les del grafit. Usualment presenten millors característiques tèrmiques, elèctriques o mecàniques [2].

Les aplicacions que es poden trobar per aquestes nanoestructures de carboni semblen no tindre fi. Els nanotubs o nanofibres de carboni ja tenen aplicacions comercials al mercat [3], ja que van ser descoberts abans que el grafé. Ja s'han aplicat en materials compostos [4] per crear, per exemple, bicicletes més lleugeres i ja fa temps que s'estan fent servir com a components de bateries d'ordinadors portàtils per allargar-ne la vida útil [5]. Per la seva banda, les aplicacions basades en grafé no tardaran en aparèixer [6]. Les aplicacions més immediates seran en l'àrea de l'electrònica flexible, ja que es l'entorn natural d'un material amb una alta conductivitat

elèctrica, dúctil i resistent. Però hi han plans de fer-lo servir per fabricar, per exemple, transistors, làsers, moduladors òptics...

Els nanotubs i nanofibres de carboni estan demostrant ser uns bons candidats com a components sensors d'un sensor de gas [7]. A més, son interessant ja que la seva estructura cristal·lina, més senzilla que la dels òxids metàl·lics, els fan una plataforma ideal per analitzar els processos bàsics del sensat de gas. En aquest sentit, s'ha trobat que es necessari que en una estructura perfecta de carboni hi hagi una certa quantitat de defectes perquè la superfície sigui reactiva a certs gasos [8]. A més, si el que es vol es decorar la superfície dels nanotubs amb nanopartícules metàl·liques per millorar-ne la resposta, aquesta generació de defectes és crítica per una bona distribució de les nanopartícules [9].

RC2. Nanofibres de carboni

RC2.1. Anàlisis per Espectroscòpia de Fotoelectrons emesos per Rajos X (XPS).

Les nanofibres de carboni (CNF) síntetitzades per el mètode del catalitzador flotant tenen a la seva superfície moltes impureses generades pel propi mètode de síntesis [10]. Aquestes impureses inclouen níquel, nitrogen i grups funcionals oxigenats. Per eliminar-los les nanofibres es tracten mitjançant un procés de grafitització en que es recouen a uns 2800 ºC en una atmosfera reductora (obtenint CNFG)

[11]. Així, s'eliminen les impureses de la nanofibra i es reordenen els plans cristal·lins. Els anàlisis per XPS confirmen aquest fet, tot i que també revelen dos punts importants:

- Les nanofibres (tant CNF com CNFG) tenen una capa de carboni amorf a la seva superfície. Eliminant aquesta capa, es possible veure que la superfície es cristal·litza després del tractament. Anàlisis posteriors amb Microscòpia Electrònica de Transmissió (TEM) revelen que les vores de la nanofibra es tanquen sobre si mateixes durant la grafitització, exposant majoritàriament els enllaços sp^2.
- Tot i les temperatures a les que s'arriben durant el tractament, a la superfície de les nanofibres hi sobreviu un 1% d'oxigen. D'aquest, la majoria esta en forma de grups hidroxils i carboxílics, mentre que els grups carbonils pateixen la major reducció.

RC2.2. Decoració de les nanofibres de carboni amb nanopartícules metàl·liques

Per tal de variar la selectivitat i sensitivitat dels futurs sensors basats en nanofibres de carboni, aquestes es tenen que decorar amb nanopartícules metàl·liques [12]. Com que l'objectiu és realitzar la decoració mitjançant un procés en líquid primer es té que aconseguir que les CNFG siguin estables en acetona, que és on es farà la mescla

amb el precursor. Mitjançant un escalfament a 400ºC en una atmosfera rica en oxigen es va trobar que s'aconseguien reobrir les vores de la nanofibra, exposant els enllaços sp^3 més reactius, les CNFG es tornen estables solvents polars. Llavors, mesclant el precursor metàl·lic ($AuCl_3$ o $PdCl_2$) amb les nanofibres de carboni seguit d'un tractament tèrmic s'aconsegueix decorar les nanofibres. El rendiment del procés es pot millorar realitzant la mescla en un molí rotatori ja que augmenta l'adhesió de precursor a la nanofibra. A més, augmentant o reduint la concentració de precursor de les nanofibres es pot controlar la dispersió i mida de les nanopartícules metàl·liques que es generen.

RC2.3. Fabricació del sensor i anàlisi de la resposta de les nanofibres de carboni a diferents gasos.

L'objectiu es fabricar un sensor de gas flexible fent ús amb les nanofibres de carboni (decorades o no) com a capa sensora. Com a substrat s'ha escollit el kapton mentre que els pads del sensor s'han fabricat mitjançant impressió inkjet. Per el dipòsit de les nanofibres de carboni s'ha fet servir una forma modificada d'electrospray. Per això, per una banda s'han connectat els elèctrodes del sensor a una font negativa per focalitzar el camp elèctric sobre la zona d'interès, evitant la utilització de màscares. Per una altre banda, s'ha escalfat el substrat mitjançant una placa calefactora prèviament aïllada elèctricament. Amb aquest sistema, es possible generar capes de nanofibres de cartboni homogènies, primes i en relativament poc temps.

Una vegada fabricat el sensor, s'ha estudiat la resposta de les nanofibres a NH_3 i NO_2. Les CNFG sense decorar mostren resposta als dos gasos inclús a temperatura ambient i amb poc efecte d'enverinament de la superfície. Per el cas del NH_3, l'adició del Pd fa que augmenti la resposta mentre que l'Au la disminueix, obrint la porta a la possibilitat de modificar la selectivitat de les nanofibres. Per una altre banda, tant el Pd com l'Au fa que la resposta al NO_2 disminueixi dràsticament. La utilització de calor per netejar la superfície de les nanofibres de carboni millora les propietats del sensor, augmentant la resposta als gasos i disminuint tant el temps de resposta com el de recuperació.

R3. Anàlisis de grafé oxidat i grafé oxidat reduït.

R3.1. Anàlisis Raman de grafé oxidat i del seu procés de reducció tèrmica

L'espectre Raman del grafé oxidat es semblant al del grafit, però diferent ja que els pics son més amples [13]. Això pot suggerir que no hi ha un eixamplament sinó que en un pic pot haver la contribució de dos o més pics. Matemàticament, l'espectre Raman del grafé oxidat accepta un pic al voltant de 1500 cm^{-1} que millora l'ajust de l'espectre. Aquest pic ha estat proposat per materials químicament similars al grafé oxidat com poden ser cendres o carbó activat tèrmicament [14,15]. Per aquest motiu es pensa que la estratègia de fer servir

únicament dos pics per definir l'espectre Raman pot ser un error. Aquí és proposa la utilització de quatre pics: D, G, D' i D''. Aquest pics defineixen el espectre Raman d'un material carbonós amb molts defectes com pot ser el òxid de grafé.

Després d'analitzar els espectres Raman d'un grafé oxidat i la seva reducció tèrmica a diferents temperatures es pot veure que el desplaçament del pic D'' degut a aquesta reducció (millora de l'estructura carbonosa) té una dependència lineal amb la quantitat d'oxigen a la mostra. Per una altre banda, el seu desplaçament es major que el desplaçament del pic G, cosa que fa que el pic D'' un bon candidat com a mesura del estat d'oxidació de la mostra.

Per una altre banda, s'ha comparat els defectes mesurats per el pic G obtingut per el mètode dels 4 pics i el obtingut per el mètode dels 2 pics. S'ha trobat que per el mètode dels 4 pics l'evolució dels defectes segueix molt bé els models proposats per Tuinstra i Koening i per Cuesta *et al.*, mentre que pel mètode del 2 pics els defectes estan subestimats.

R3.2. Anàlisis de la reducció de grafé oxidat per bombardeig iònic

S'ha estudiat la estratègia de reduir capes de grafé oxidat amb plasma d'argó (bombardeig iònic). Les capes de grafé oxidat s'han fabricat mitjançant la tècnica de Lagmiur-Blodgett per assegurar el gruix mínim [16]. El atac amb ions d'argó s'ha realitzat dins d'un netejador de

plasma a la mínima potència, realitzant atacs successius de 30 s. En cada procés s'ha analitzat el espectre Raman d'una zona en particular. S'ha trobat que el atac amb plasma es massa agressiu tot i ser a la mínima potència ja que elimina el material abans de realitzar la reducció, no observant cap canvi en els espectres Raman. Mentre, les imatges òptiques mostren clarament una desaparició del material visible (principalment agregats).

Referències

[1] A K. Geim, K.S. Novoselov, The rise of graphene., Nat. Mater. 6 (2007) 183–91.
[2] M.H. Al-Saleh, U. Sundararaj, A review of vapor grown carbon nanofiber/polymer conductive composites, Carbon N. Y. 47 (2009) 2–22.
[3] M.F.L. De Volder, S.H. Tawfick, R.H. Baughmann, A.J. Hart, Carbon Nanotubes: Present and Future Commercial Applications, Science (80-.). 339 (2013) 535–539.
[4] O. Breuer, U. Sundararaj, Big Returns From Small Fibers: A Review of Polymer/Carbon Nanotube Composites, Polym. Compos. 25 (2004) 630–645.
[5] K. Evanoff, J. Khan, A. a Balandin, A. Magasinsky, W.J. Ready, T.F. Fuller, et al., Towards Ultrathick Battery Electrodes: Aligned Carbon Nanotube–Enabled Architecture, Adv. Mater. 24 (2012) 533–537.
[6] K.S. Novoselov, V.I. Fal'ko, L. Colombo, P.R. Gellert, M.G. Schwab, K. Kim, A roadmap for graphene, Nature. 490 (2012) 192–200.
[7] E. Llobet, Gas sensors using carbon nanomaterials: A review, Sensors Actuators B Chem. 179 (2013) 32–45.
[8] R. Ionescu, E.H. Espinosa, E. Sotter, E. Llobet, X. Vilanova, X. Correig, et al., Oxygen functionalisation of MWNT and their use as gas sensitive thick-film layers, Sensors Actuators B Chem. 113 (2006) 36–46.
[9] R. Ionescu, E.H. Espinosa, R. Leghrib, a. Felten, J.J. Pireaux, R. Erni, et al., Novel hybrid materials for gas sensing applications made of metal-decorated MWCNTs dispersed on nano-particle metal oxides, Sensors Actuators B Chem. 131 (2008) 174–182.
[10] I. Martin-Gullon, J. Vera-Agullo, J.A. Conesa, J.L. González, C. Merino, Differences between carbon nanofibers produced using Fe and Ni catalysts in a floating catalyst reactor, Carbon N. Y. 44 (2006) 1572–1580.
[11] M. Weisenberger, I. Martin-Gullon, J. Vera-Agullo, H. Varela-Rizo, C. Merino, R. Andrews, et al., The effect of graphitization temperature on the structure of helical-ribbon carbon nanofibers, Carbon N. Y. 47 (2009) 2211–2218.
[12] E.H. Espinosa, R. Ionescu, C. Bittencourt, a. Felten, R. Erni, G. Van Tendeloo, et al., Metal-decorated multi-wall carbon nanotubes for low temperature gas sensing, Thin Solid Films. 515 (2007) 8322–8327.
[13] D. a Dikin, S. Stankovich, E.J. Zimney, R.D. Piner, G.H.B. Dommett, G. Evmenenko, et al., Preparation and

characterization of graphene oxide paper., Nature. 448 (2007) 457–60.

[14] A. Cuesta, P. Dhamelincourt, J. Laureyns, A. Martínez-Alonso, J.M.D. Tascón, Raman microprobe studies on carbon materials, Carbon N. Y. 32 (1994) 1523–1532.

[15] T. Jawhari, A. Roid, J. Casado, Raman spectroscopic characterization of some commercially available carbon black materials, Carbon N. Y. 33 (1995) 1561–1565.

[16] B. Martín-Medina, M.M. Velázquez, F. Rossella, V. Bellani, E. Diez, J.L.G. Fierro, et al., Functionalization of Reduced Graphite Oxide Sheets with a Zwitterionic Surfactant, ChemPhysChem. 13 (2012) 3682–3690.